博士論文

Modeling and Assimilating Frozen Soil Hydrology

(凍土水文過程のモデル化と同化)

HUIYI BAO

(包　慧漪)

A Dissertation Submitted to the University of Tokyo
In Partial Fulfillment of the Requirements for the Ph. D. Degree

Department of Civil Engineering
The University of Tokyo

September 2016

ACKNOWLEDGMENTS

First of all, I would like to express my sincere gratitude to Prof. Toshio Koike for accepting me as his student. He helped me to found my basis from zero to state of the art, guide me to discover pleasure and value in my journey of science exploration and offered me all the possible support. His profound knowledge and professional suggestions led the direction of my research and shaped my thought on this research work. Every personal meeting with him indeed filled me with courage and wisdom. Moreover, I am impressed and inspired by his personal charisma, constant passion, astounding patience, indomitable willpower and international outlook. I never saw such an excellent scientist and admirable supervisor before that I am very proud of being one of his students and what I learned from him will be endless benefit throughout my life.

I would like to thank my committee members: Prof. Masaru Mizoguchi, Prof. Taikan Oki, Prof. Yukiko Hirabashi, Prof. Kei Yoshimura and Prof. Akiyuki Kawasaki for their insightful and encouraging comments. Also, I should extend my thanks to all the civil engineering staffs for sharing your knowledge in the PhD courses.

I am also going to take this opportunity to appreciate two excellent Chinese scientist: Prof. Kun Yang and Prof. LeiWang. Thank you for sharing your vision, knowledges, source code and giving me constructive suggestions for the study, paper writing and revision.

Being a member of the REEL family and having a good time in Todai would be an enjoyable and unforgettable memory in my mind. Thank you, all of former and current laboratory staffs and students. Especially, I would like to thank Dr. Maheswor Sherestha for helping me on my learning of hydrology, physics of WEB-DHM and teach me how to do model development study patiently, Dr. Hideyuki Tsutsui, Dr. Mohamed Rasmy, Dr. Yohei Sawada for providing help on Radiative transfer modeling study. Mr. Peter Lawford is very helpful by giving WEB-DHM and Fortran training and debugging programing problem and spending hours at my desk screening the codes. I am very grateful to him for his genuine friendship and inspired opinion.

Ms. Seto Rie (my tutor), Mr. Panduka, Neluwala, Mr. Asif Nasser, Dr. Weiqiang Ma, Mr. Katsunori Tamagawa, Mr. Ralph Achierto, Dr Patricia Ann Jaranilla-Sanchez, Mr. Kinya Toride, Mr. Martin Gomez Gracia, Ms. Menglu qin and Ms. Wenxin Lin. Thank you for your friendship and fruitful discussions on my research as well as life in Japan.

I also wish to express my heartfelt gratitude to my host family, Mr. and Mrs Amano for their generosity and hospitality, and kind concern on my life in Japan. I would extend my thanks to Ms. Akiko and Ms. Ayoko for supporting the host family program.

My thanks go to all staffs at the EDITORIA office, who had ever help me directly or indirectly, also, to the teachers of Japanese language course, staffs of Foreign Students Office and Administration Office.

I would like acknowledge to the China Scholarship Council for providing scholarship to support my three-year life in Japan. I am grateful to the Japan-China friendship center and the Japan Student Services Organization for offering me comfortable and economical dormitory.

Finally, I would like to thank my dependable fiancé, Changxiong Wang, who supports me to study abroad, accompanies me on my way home almost every night on the phone and makes my life so sweet. Without his comfort and encouragement, I may lose myself, confidence, courage to face the life and study alone in Japan. I would like to delicate this thesis to my fiancé and my family for their love, patience, and understanding.

ABSTRACT

Frozen soil is widely distributed in high latitude Arctic and Antarctic region, and mountainous region in low latitude, which takes up 35% total land area of earth. It plays an important role in the cryosphere hydrology, climate change, ecosystem and social economy, which are closely tied to human life. It is crucially important to understand frozen soil processes and its impacts, to simulate the frozen soil processes, and to project the future variation of frozen soil. Although previous studies have achieved advance progresses in frozen soil modeling, the frozen soil processes are still defectively represented in most of land surface models and hydrological models. Therefore, it is necessary to introduce frozen soil processes into hydrological and land surface modeling, to make use of satellite data for enhancing large-scale observation of frozen soil, and to reproduce hydrological and thermal processes of frozen soil.

An enthalpy-based frozen soil model was developed for the simulation of water and energy transfer in cold regions. To simulate the soil freezing/thawing processes stably and efficiently, a three-step algorithm was applied to solve the non-linear governing equations: 1) a thermal diffusion equation was implemented to simulate the heat conduction between soil layers; 2) a freezing/thawing scheme used a critical temperature criterion to judge the phase status, and introduced enthalpy and total water mass into the derived Clapeyron equation to represent ice formation/melt and corresponding latent heat release/absorption; and 3) a water flow scheme was employed to describe the liquid movement within frozen soil. In addition, a parameterization set of hydraulic and thermal properties was updated by considering the frozen soil effect.

The performance of the frozen soil model was validated at point scale in a typical mountainous permafrost basin of China. An ice profile initialization method is proposed for permafrost modeling. Results show that the model can achieve a convergent solution at a time step of hourly and a surface layer thickness of centimeters that are typically used in current land surface models. The three-step frozen soil algorithm we developed can solve highly non-linear energy and mass equations of frozen soil stably and reduce the computation time for greater efficiency. The simulated profiles of soil temperature, liquid water content, ice content and thawing front depth are in good agreement with the observations and the characteristics of

permafrost. The model is capable of continuously reproducing the diurnal and seasonal freeze-thaw cycle, simulating heat - water transfer within frozen soil and predicting streamflow in permafrost basin, which can be widely applied in simulating hydrological processes of cold regions.

Passive microwave remote sensing have outstanding advantages for monitoring the ground freezing and thawing processes, because of ability of penetration and strong sensitivity to soil water. We clarified the frozen soil radiative transfer mechanism that spectral gradient of frozen soil is negative, that is, brightness temperature (Tb) of low frequency (6GHz) is relative higher than Tb in high frequency (36GHz). This characteristic is regarded as an indicator of frozen soil and widely adopted in most of current frozen soil mapping algorithms. Although this phenomenon was qualitatively explained as the volume scatter darkening within frozen soil like that recognized for microwave emission as is snow, the complete physical mechanism for frozen soil radiative transfer processes is still not clear and quantitative simulation is still defective. By contrast, for soils that contain liquid water, the spectral gradient is positive because the Debye process has a greater darken effect at low frequency than high frequency and the Tb is relative high than that of frozen soil due to its high physical temperature.

We tried to clarify the mechanism of frozen soil radiation transfer processes by developing a frozen soil radiative transfer model. The radiative transfer processes of frozen soil are described as two separate processes: 1) soil emission transfers within frozen soil: In cold season, water absorption is so weak that the penetration depth becomes deep. Emission from deep soil and the volume scattering effect of soil particles is considered in this RTM. However when frozen soil thaws in warmer season, the penetration depth is so shallow because of water absorption that the radiation from deep soil can be neglected. 2) Soil radiation passes through soil-air boundary: the difference of dielectric constant between frozen soil and air is small, because of low water content, which means the transmissivity of air-soil boundary is high and surface scattering of frozen soil is very weak. While the dielectric constant of wet soil and air is large, which in turn causes strong surface scattering in air-soil boundary.

This frozen soil RTM employed a multiple parallel-layer soil structure, similar as frozen soil physical model. Soil properties are assumed homogeneous within each layer and soil particles are assumed as sphere. An atmosphere RTM 4 stream fast model was modified for representing the soil emission transfer from bottom to top soil layer. A dense media radiative transfer model QCA-CP was adopted to calculate the extinction coefficient and single scattering albedo of each soil layer. Surface scattering is also considered by implementing

Advanced Integral Equation Model (AIEM). In addition, roughness and shadow effects are also taken into account.

By inputting simulated frozen soil profile information into this frozen soil RTM, the Tb of different frequencies can be simulated. And an validation is conducted by comparing the simulated Tb with the AMSR-E Tb. Results show that this RTM can predict Tb of frozen soil from 6 GHz to 36 GHz with good accuracy and the phenomenon of negative spectral gradient are also successfully reproduced, which has not been achieved in previous studies. According to simulation and AMSR-E observation, it is proved that volume scattering dominates the radiative transfer process in frozen season and the negative spectral gradient is attributed to the strong scattering in higher frequency. In turn, it is also proved that the frozen soil radiative transfer mechanism we proposed does correspond to the reality and can explain the phenomenon of microwave radiation transfer in frozen. Moreover, the modeling algorithm coupled volume scattering and surface scattering processes can reproduce the radiation transfer processes within frozen soil and reflect the radiative characteristics of freeze- thaw cycle. Therefore, it is demonstrated that the frozen soil RTM offers a realistic and quantitative understanding for frozen soil radiative transfer mechanism and has a good capability of simulating the radiative transfer processes in frozen soil at frequencies from 6GHz to 36 GHz.

CONTENTS

ACKNOWLEDGMENTS ii

ABSTRACT i

CONTENTS iv

1. INTRODUCTION 1

1.1 Background 1

1.2 Review of Previous Studies and Problem statements 6

1.2.1 Frozen Soil Modeling 6

1.2.2 Satellite Remote Sensing on Frozen soil 9

1.2.3 Frozen Soil State Initialization 11

1.3 Objectives 12

1.4 Study Framework 13

1.5 Outline of the Dissertation 13

2. DEVELOPMENT OF AN ENTHALPY BASED FROZEN SOIL MODEL 15

2.1 Introduction 15

2.2 Physics of Frozen Soil 16

2.2.1 Impact factors of frozen soil (What Controls Permafrost?) 16

2.2.2 Properties of frozen soil 18

2.2.3 Frozen Ground Surface Energy and Mass Balance 20

2.2.4 Heat–Water Transfer and Phase Change within Frozen Soil 22

2.3 Model Structure 24

2.4 Frozen Soil Algorithm 26

2.4.1 Thermal Diffusion 26
2.4.2 Phase Change 30
2.4.3 Liquid Water Flow 33
2.5 Parameter estimation for frozen soil 36
2.5.1 Thermal Properties 36
2.5.2 Hydraulic Properties 38
2.6 Summary 38
3. VALIDATION OF FROZEN SOIL MODEL IN A PERMAFROST BASIN 40
3.1 Site and dataset 40
3.2 Model initialization and calibration 42
3.3 Results and Analysis 44
3.3.1 Soil temperature 44
3.3.2 Volumetric liquid water content and ice content 46
3.3.3 Evolution of frozen soil 49
3.3.4 River Discharge 51
3.4 Discussion 55
3.4.1 Diurnal Variation 55
3.4.2 Sensitivity to soil depth 57
3.4.3 Sensitivity to soil layer thickness 58
3.4.4 Sensitivity to time step 59
3.5 Summary 60
4. PASSIVE MICROWAVE REMOTE SENSING OF FROZEN SOIL 62
4.1 Introduction 62
4.2 Dielectric Constant of Frozen Soil 63
4.2.2 Dielectric model of soils 67
4.2.3 Dielectric model of frozen soil and its improvement 70
4.3 Radiative transfer theory in frozen soil 72
4.3.1 Radiative characteristics of frozen soil 72

4.3.2 Mechanism of radiative transfer in frozen soil 75
4.4 Development of multiple-layer RTM for frozen soil 78
4.4.1 Model structure 78
4.4.2 Frozen Soil RTM Algorithm 80
4.5 Validation of the multiple-layer RTM for frozen soil 83
4.5.1 Site introduction 83
4.5.2 Frozen soil state variables simulation and parameter calibration 85
4.5.3 Result and analysis 91
4.6 Summary 94
5. INITIALIZATION OF FROZEN SOIL PROFILE FOR FROZEN SOIL MODELING 96
5.1 Introduction 96
5.2 Soil Profile Initialization method 97
5.2.1 Penetration depth 97
5.2.2 Sensitivity study to soil temperature and moisture initialization 99
5.2.3 Initialization method design 103
5.3 Application Soil Profile Initialization method 105
5.4 Summary 110
6. CONCLUSIONS 112
6.1 Conclusions 112
6.2 Suggestions to future study 113
APPENDIX 118
REFERENCES 125

1. INTRODUCTION

1.1 Background

Frozen soil is ground including rock, soil at or below the freezing point of water 0°C. According the duration of frozen state, frozen soil can be classified to 3 types: permafrost, seasonal frozen soil and short-term frozen soil. Permafrost is perennially frozen ground that have remained at or below 0°C for at least two consecutive years, while seasonally frozen ground refers to ground that freezes in cold seasons and thaws completely in summer [*Subcommittee*, 1988] and short-term frozen soil only freezes for few hours to less than one month.

The vertical structure of frozen soil depends on the soil temperature. As shown in Figure 1.1, permafrost is bounded on top by the active layer and on bottom by the permafrost base. The active layer is the surface layer of soil that thaws in summer and refreezes in winter. The location of permafrost base is determined by an energy balance between cooling from the surface and warming from the interior geothermal heat. Temperatures at active layers reflect diurnal and seasonal variability in air temperature. The temperatures at the depth of zero annual amplitude reflect climate conditions at the end of 20^{th} century, while permafrost temperature at 400-800 meters depth represent the climate just after the end of last ice age, at the Holocene optimum about 8000 years ago [*Haeberli*, 2000; *Osterkamp and Romanovsky,* 1999].

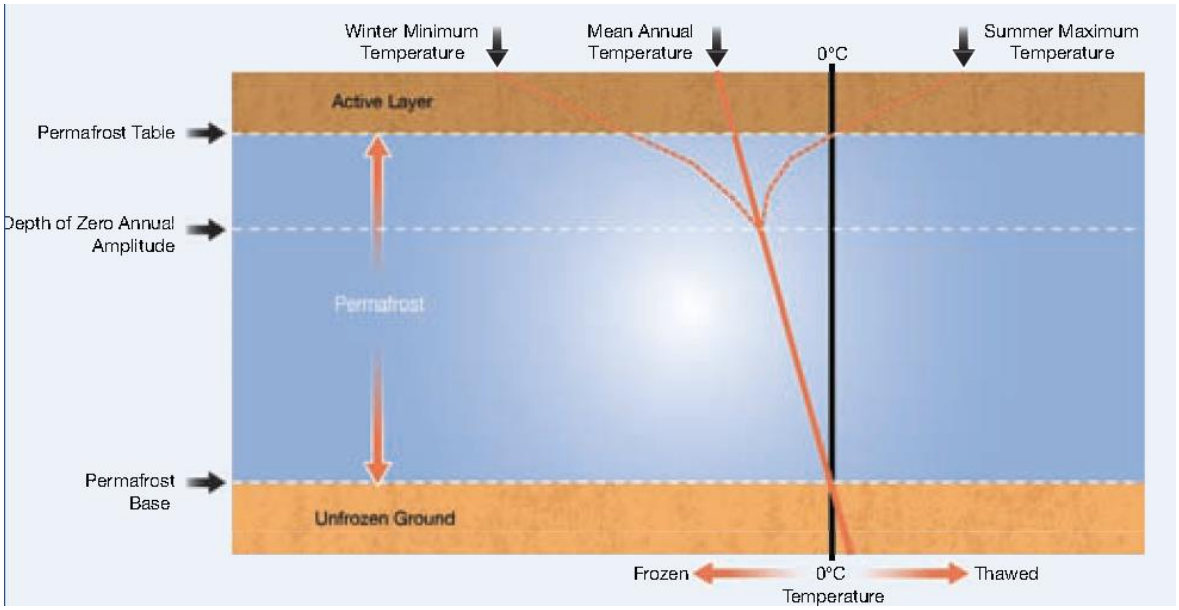

Figure 1.1. The vertical structure of permafrost is defined by temperature. [*Schaefer et al.*, 2012].

Frozen soil is widely distributed in high latitude Arctic and Antarctic region, and mountainous region in low latitude, which takes up 35% total land area of earth. Permafrost regions occupy about 24% of the exposed land area in the Northern Hemisphere [T Zhang et al., 1999], which mainly locates in Russia, Canada, China, Alaska and so on. Seasonally frozen ground takes up 25% of total continents, which exists in the place higher than 24°N or 24°S of all the continents. Between 22°~24°N (°S), there are vast areas of short-term frozen soil occurring temporarily. As shown in Figure 1.2, permafrost regions can be classified into zones based on the fraction of land area that contains permafrost. Continuous permafrost zones have permafrost underlying 90-100% of the land area; discontinuous permafrost zones have 50-90%; and sporadic permafrost 10-50%. Isolated patches refer to regions where permafrost underlies less than 10% of the land area[Schaefer et al., 2012].

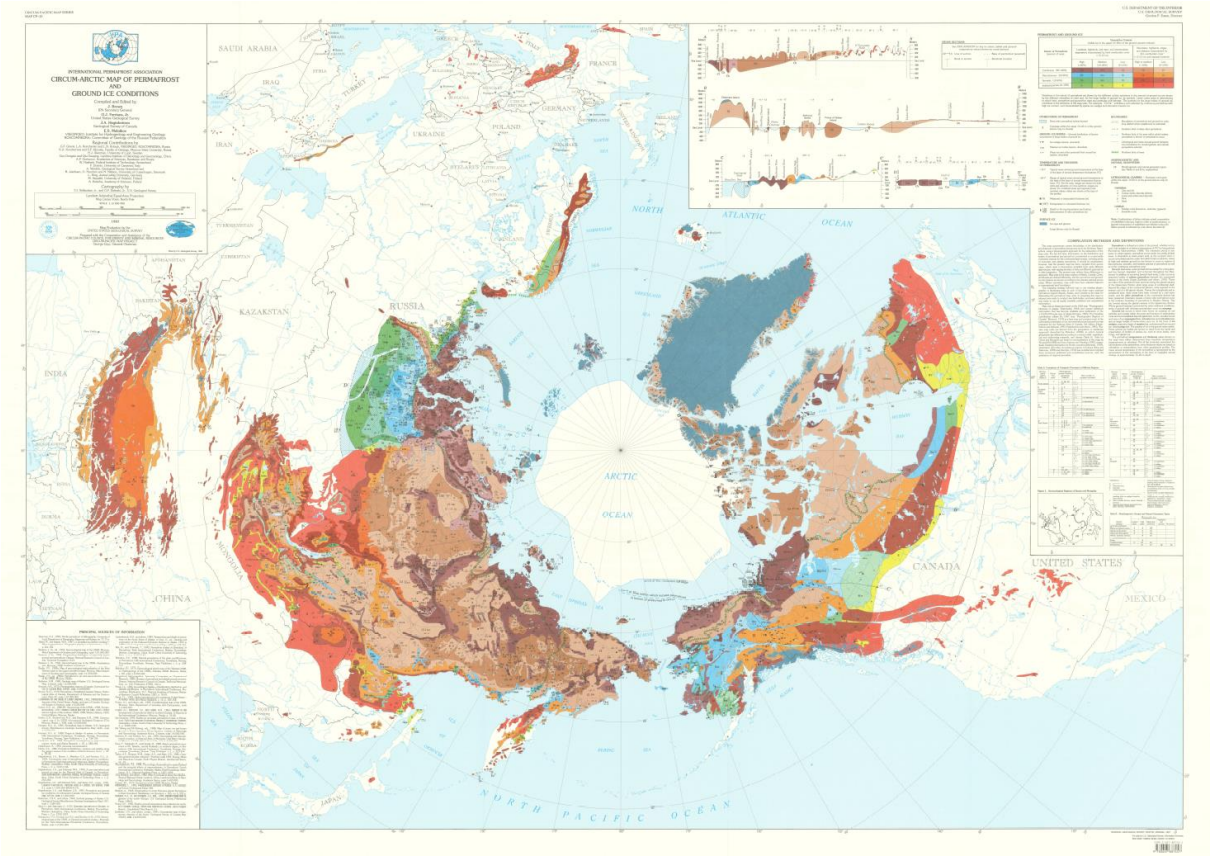

Figure 1.2. Circum-Arctic map of permafrost [*J. Brown et al.*, 1997]

Frozen soil plays an important role in the hydrology of cold regions. The coexistence of ice and liquid water changes the distribution of water and energy in soil by modulating the soil hydraulic and thermal properties. Pore blockage by ice greatly decreases the permeability and infiltration capacity of frozen soil, and prohibits rainfall and snowmelt infiltrating into deep soil, which in turn generally create high soil moisture contents in the thawed active layer [*Cherkauer and Lettenmaier*, 1999a; *Poutou et al.*, 2004; *Yanlin Zhang et al.*, 2013]. The water phase transition also alters soil water potential, which influences water evaporation and redistribution in the soil [*Stähli et al.*, 1999; *Yinsheng Zhang et al.*, 2003b]. The underlying impervious frozen soil generally encourages the generation of large runoff , which may result in severe flash floods along with landslides and debris flow after heavy rainfall or snowmelt events [*Flerchinger and Saxton*, 1989; *Victor Koren et al.*, 2014; *Storey*, 1955]. The freeze-thaw cycle of soil strongly controls not only the timing of spring runoff, but also the total amount of soil water conserved in winter that is available for runoff generation and evapotranspiration in subsequent spring and summer. In the thermal aspect, different from the unfrozen soil, frozen soil has high thermal conductivity and low heat capacity, which allow heat reach to deeper soil and influence heat flux transfer in soil. What's more, a large amount of latent heat is released or absorbed during

freezing and thawing processes, which can change the distribution of energy and soil temperature.

As part of the lower boundary of the atmosphere, frozen ground is strongly connected with the atmosphere. Frozen soil processes significantly influence water and heat fluxes between the atmospheric boundary layer and the land surface. At diurnal scale, the depths of seasonal frost and thaw penetration are driven by the diurnal cycle of soil surface heat flux. If the daily net heat flux into ground is negative, the freezing front advances; if it is positive, the freezing front retreats and a thawing front may advance into the soil. Although the diurnal cycle may only penetrate top few centimeters, it can drive the season freezing front as deep as 2-3m [*Williams and Smith*, 1991]. On a seasonal timescale, soil freezing delays the winter cooling and thawing delays the summer warming of the land surface because of the latent heat related to the liquid–ice phase shift [*Poutou et al.*, 2004]. Over long timescales, the shrink or expansion of permafrost is a key response to climate change. By tracking historical changes in permafrost, the paleoclimate and its variations can be reproduced [*Grab*, 2002; *Ono and Irino*, 2004; *Sidorchuk et al.*, 2001]. Changes in permafrost temperature, thickness, timing, duration, and extent can be good indicators of climate change [*V Romanovsky et al., 2002*]. According to the Intergovernmental Panel on Climate Change (IPCC) fifth assessment report, there is high confidence that permafrost temperatures have increased up to 3°C in Northern Alaska (1980s–mid-2000s) (Figure 1.3) and up to 2°C in Russian European North (1971–2010) as a result of the increased Arctic warming [*Stocker et al.*, 2014]. Several studies suggest that a warmer permafrost and deeper active layers in the arctic region and Qinghai-Tibet plateau are mainly in response to increased air temperature and change of snowfall [*Christiansen et al.*, 2010; *S L Smith et al.*, 2012; *Q Wu and Zhang*, 2010]. Permafrost has been identified as one of six cryosphere indicators of global climate change within the international framework of the WMO Global Climate Observing System[*Jerry Brown et al.*, 2008]. However, in most of continental scale hydrological models and global land surface models, heat-water transfer within frozen soil and freeze-thaw cycle are not well described [*V. Koren et al.*, 1999; *Y. Zhang and Lu*, 2002], which may have significant impact on regional or global climate and hydrological processes.

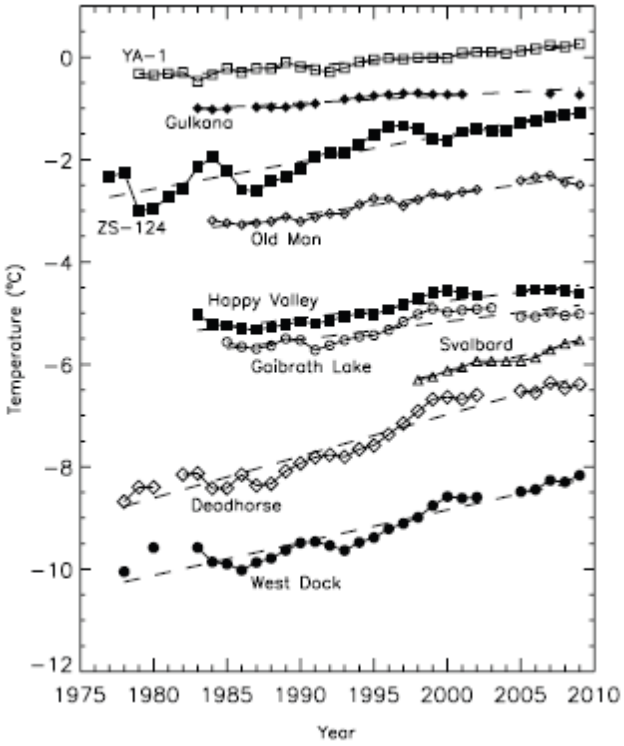

Figure 1.3: Mean annual ground temperatures at depths between 10 and 20m for boreholes throughout the circumpolar northern permafrost regions[*V E Romanovsky et al.*, 2010]

Through carbon budgets, frozen soil also can act back to climate system. Frozen organic soils store a vast amount of carbon as peat or methane. As heat from the atmosphere penetrates into the permafrost, it may release greenhouse gases into the atmosphere, which exerts a positive climate feedback and may exacerbate global warming and permafrost thaw (Figure 1.4) [*Laurion et al.*, 2010; *Schuur et al.*, 2009; *Zimov et al.*, 2006].

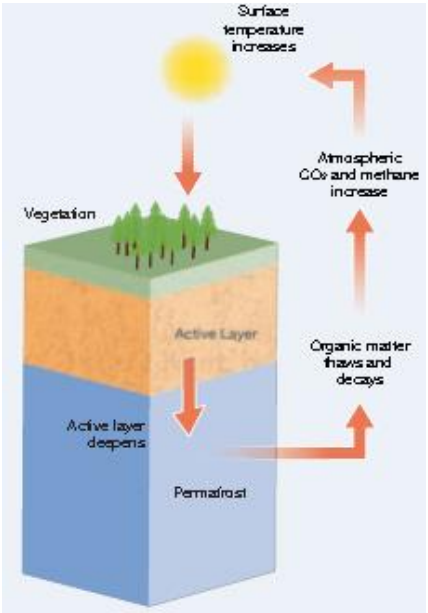

Figure 1.4：Permafrost carbon feedback [*Schaefer et al.*, 2012]

In terms of ecosystems, permafrost degradation may disturb ecosystems and change species composition, altering wildlife habitat and migration. The number reduction of lakes and wetlands in permafrost region may alter wildlife habitats and migration, particularly for migratory birds [*S L Smith et al.*, 2005b]. Change of permafrost in Tibet tends to decrease species diversity and the primary productivity of vegetation [*YANG et al.*, 2010]. Permafrost degradation also may cause fires in boreal forests, thermal erosion and thermokarst, which may rapidly or slowly change ecosystems.

From a social and economic viewpoint, permafrost thawing can damage or even destroy buildings, transport lines, pipelines, and coastlines, thus putting human infrastructure at high risk because of the structural weakness of unstable thawing ground [*Schaefer et al.*, 2012]. The coastline of Arctic, Alaska and Siberia with ice-rich sediment are found most vulnerable to coastal erosion of permafrost [*Lantuit et al.*, 2011], and similar erosion occurs along riverbeds and lake shores throughout permafrost regions [*Jones et al.*, 2011]. Awareness and attention need to be raised that increasing temperature, widely expected throughout the next century, may especially threat constructions in permafrost regions.

Frozen soil has a huge impact on cryosphere hydrology, climate change, ecosystem and social economy, which are closely tied to human life. Therefore, it is crucially important to understand frozen soil processes and its impacts, to monitor the change of frozen soil, to simulate the frozen soil processes, and to project the future variation of frozen soil in high and cold regions [*L Wang et al.*, 2010; *X Zhang et al.*, 2007a]. To clarify the interaction between frozen soil and climate change and to address the potential ecological, social, and economic impacts of permafrost, it is highly essential to introduce frozen soil processes into hydrological and land surface modeling, to make use of satellite data for enhancing large-scale observation of frozen soil, and to reproduce hydrological and thermal processes of frozen soil.

1.2 Review of Previous Studies and Problem statements

1.2.1 Frozen Soil Modeling

Significant progress has been achieved over recent decades in both empirical and physical modeling of ground freezing and thawing, and coupling these processes to hydrological and land surface models. Many semi-empirical models have been developed to predict the spatial variation of permafrost and contributed to permafrost-climate relation[*Riseborough et al.*, 2008]. The TTOP-approach (Temperature at the Top Of Permafrost) is a common modeling

scheme for semi-empirical models which delivers a mean annual ground temperature (MAGT) and identifies permafrost by MAGT ≤ 0°C [*Gisnås et al.*, 2013]. A semi-empirical permafrost model CryoGrid 1 based on the TTOP approach was employed to map the North Atlantic Permafrost region at a spatial resolution of 1 km at continental scales [*Westermann et al.*, 2015]. Another semi-empirical model, GIPL (Geophysical Institute Permafrost Lab model), has been widely applied in Alaska, the Russian Arctic and the Qinghai–Tibet Plateau [*D Luo et al.*, 2014; *Panda et al.*, 2014]. Although the agreement with measured temperature is promising, the physical understanding is still limited and the parameters highly depend on the knowledge of thermal ground conditions from field observations.

Several physic-based models are developed to simulate freezing and thawing processes over a short time scale and have a high computation cost. In hydrological modeling in cold regions, the effects of ice on soil water flux and runoff generation are considered in distributed hydrological models; for example, the SHAWDHM model[*Yanlin Zhang et al.*, 2013], the GEOtop model [*Rigon et al.*, 2006], the Water and Energy Budget-based Distributed Hydrological Model (WEB-DHM) [*L Wang et al.*, 2010], the Cold Regions Hydrological Model [*Pomeroy et al.*, 2007], and the variable infiltration capacity (VIC) Model[*Cherkauer and Lettenmaier*, 1999b; *Z Zhang et al.*, 2000]. Frozen soil schemes have been introduced into a large variety of land surface models for use in modeling land surface processes [*Jafarov and Schaefer*, 2016; *Luo*, 2009; *Li and Koike*, 2003; *Slater et al.*, 1998; *Flerchinger and Saxton*, 1989]. In the project for intercomparison of Land-Surface Parameterization Scheme (PILPS) Phase2(d) experiment, the frozen soil simulation ability of 21 land surface schemes (Table 1.1) was evaluated using observed vertical profiles of soil temperature and moisture at Valai, Russia[*L F Luo et al.*, 2003]. The study shows that the models with frozen soil parameterization produce more reliable estimates of soil moisture and temperature profiles than those without a frozen scheme [*L F Luo et al.*, 2003]. The Community Land Model (CLM) is a commonly used land surface model, which has an explicit frozen soil scheme, assuming that phase freezing or thawing only occur at a fixed freezing temperature, and treating thermal diffusion and phase change separately [*Niu and Yang*, 2006]. However, the phase change simulation in the CLM can be artificially stretched, leading to inaccurate temperature dynamics, and it has been suggested that enthalpy formulation should be included in heat equations [*Nicolsky et al*, 2007]. In addition, although the significance of ground freezing-thawing cycle in global and regional climate simulation have been recognized[*B Chen et al.*, 2014; *Kurylyk et al.*, 2014], the frozen soil processes are still defectively represented in most of climate models [*V. Koren et al.*, 1999; *Y. Zhang and Lu*, 2002]. The insufficient physical understanding and high computational

demand still strongly limit the wide use of physics based frozen soil models in permafrost and associated hydrological and climate research [*Sun*, 2005].

Table 1.1: Evaluated land surface schemes in PILPS (2d). Thermal schemes: ZS = zero storage, FR: force and restore method and HC: heat conduction. Frozen schemes: No, without water phase change scheme; Yes: with water phase change scheme [L F Luo et al., 2003].

	Model	Contact(s)	Soil temperature	Frozen soil?
1	AMBETI	H. Braden	HC	Yes
2	BASE	A. Slater C. Desborough A. Pitman	HC	Yes
3	BATS	Z. L. Yang R. E. Dickinson	FR	No
4	BUCKET	C. A. Schlosser	ZS	No
5	CLASS	D. Verseghy	HC	Yes
6	CROCUS	P. Etchevers	HC	No
7	CSIRO	E. Kowalczyk	HC	Yes
8	IAP94	Y. Dai	HC	Yes
9	ISBA	F. Habets J. Noilhan	FR	Yes
10	MAPS	T. Smirnova	HC	No
11	MOSES	P. Cox	HC	Yes
12	NCEP	K. Mitchell Q. Duan	HC	Yes
13	PLACE	A. Boone, P. Wetzel	HC	No
14	SECHIBA2	P. de Rosnay J. Polcher	HC	No
15	SLAM	C. Desborough	HC	Yes
16	SPS	J. Kim	HC	Yes
17	SPONSOR	A. B. Shmakin	HC	Yes
18	SSiB	Y. Xue C. A. Schlosser	FR	No
19	SWAP	Y. M. Gusev O. N. Nasonova	FR/ZS	Yes
20	UGAMP	N. Gedney	HC	No
21	UKMO	P. Cox	HC	No

Currently, the most common problems in frozen soil modeling are unstable simulation and heavy computational cost due to the highly non-linear relationship in soil temperature, soil moisture and ice content caused by the substantial latent heat associated with the phase change. Thus, how to deal with this highly nonlinear relationship between these three variables in frozen soil is the key focus of frozen soil model development. Although shortening the time step duration may produce a mild and continuous energy change, a heavy computational cost is unavoidable with this approach [*Flerchinger and Saxton*, 1989]. Another approach is to pre-estimate ice content by numerical iteration, but even a small error in this estimate may produce substantial errors in the calculation of temperature and moisture as well as to the energy balance, owing to the great amount of latent heat release [*Q Li et al.*, 2009a]. Consequently, this may make it difficult for the model to reach convergence or even cause a failure to obtain any final solution. However, permafrost has the characteristics of large thermal inertia of the frozen

ground and long time periods required for any apparent change. Thus, long term stability and efficiency are crucially important for frozen soil modeling.

1.2.2 Satellite Remote Sensing on Frozen soil

Currently, there are mainly two ways for frozen soil observation. One is ground survey or observation, like soil temperature, active thickness measurements and sample drilling. Another one is satellite based remote sensing. Frozen soil usually locates in cold, mountainous or uninhabited regions, where there are few weather stations. Even there are stations, not all the stations are well equipped for frozen soil observation and only spatially sparse dataset can be obtained in the vast cold region, which cannot satisfy the spatial and temporal requirement of continuous frozen soil monitoring. Satellite based remote sensing, which can obtain regional or global multi-spectral information in repeat, periodic and fast way, become an indispensable means for permafrost and seasonal frozen soil monitoring.

Satellite remote sensing techniques have been applied in detecting frozen ground extend, land surface changes and near surface soil freeze/thaw status. Since permafrost and seasonal frozen soil are underground phenomena which are not detectable from satellite imagery, almost all the visible and infrared remote sensing researches focus on indirectly identifying frozen soil-related landscape and periglacial features such as palsas, peat plateaus, rock glaciers, thaw lakes and ice-wedge polygon. By mapping changes of thermokarst ponds and lake in permafrost region near Alaska and Siberia through high resolution IKONOS imagery, a dramatic change were revealed due to taliks expansion under recent climate conditions[*L C Smith et al.*, 2005a; *Yoshikawa and Hinzman*, 2003]. Some researchers tried to connect spectral characteristics to the ground truth data by using spectral classification algorithm and map the frozen/ unfrozen ground [*Duguay et al.*, 2005].

Passive microwave remote sensing have outstanding advantages over visible and infrared ones for monitoring the ground freezing and thawing processes, because of less atmosphere effects, ability of vegetation and soil penetration, high sensitivity to soil water, high revisit frequency and all-weather working ability. What's more, passive microwave data are available to monitor the long term variation of frozen soil at global, continental, or regional scales due to continuous series of microwave radiometers, such as AMSR2 (2012-now), AMSR-E (Advanced Microwave Scanning Radiometer-EOS,2002-2011), SSM/I (Special Sensor Microwave/imager, 1987- now), SMMR (Scanning Multichannel Microwave Radiometer,

1978-1987). However, the coarse spatial resolution of radiometers (5km-50km) limits the passive microwave remote sensing to large scale applications.

Significance advances have been made in the mapping of the freeze-thaw state by using passive microwave imagery [*Chang and Cao*, 1996; *Jin et al.*, 2009; *N V Smith et al.*, 2004; *T Zhang and Armstrong*, 2001]. Most of classification methods were developed based on freeze indicator method proposed by Zuerndorfer and England [1992], which judge the frozen status by two criteria-the negative spectral gradient of 10, 18 and 37 GHz, and low 37 GHz brightness temperature threshold. England [1991] and Judge [1997] explained that the spectral gradient of frozen soil is negative because the higher frequency, the more heterogeneities within the frozen soil is, and the stronger the volume scattering effect is. Generally, for thawed wet soil, the spectral gradient is positive because the Debye process has a greater darkening effect at 10 GHz than 37GHz. 37GHz is used as a cutoff brightness temperature because it is more strongly correlated with low thermodynamic temperature of frozen soil than 10 and 18 GHz are[*T Zhang and Armstrong*, 2001]. Recently, researchers contribute to the improvement of frozen soil classification algorithm by considering the presence of snow, cold rainfall, deserts and lakes [*Duguay et al.*, 2005; *Jin et al.*, 2009; *T Zhang et al.*, 2003a]. Although the classification accuracy of classification results were validated as high as 70%-80%, the results mainly depends on the threshold setting, which need to be changed with different regions and determined by empirical knowledge of researchers. The threshold and index design are different from different methods, however, they did not provide a clear physical explanation as to the reason for using new index or cutoff value.

Only qualitatively identifying the ground freeze-thaw status are insufficient for investigating the microwave radiative transfer mechanism of frozen soil and describing the radiative characteristics of freeze-thaw cycle quantitatively. However, there are only few quantitative studies on radiative transfer simulation and retrieval of frozen soil based on the microwave radiative transfer theory. England gave a theoretical description to volume scattering in frozen soil and an explanation for negative spectral gradient by using a simple one-order radiative transfer model (RTM) considering volume scattering effect[*A England et al.*, 1991; *A W England*, 1976]. Liou tried to couple a one-order water-heat soil model with a surface radiative transfer model without considering volume scattering [*Y-A Liou and England*, 1996]. After those researches, there has been almost no recent progress made in radiative characteristics of frozen soil and transfer processes mechanism[*L Zhang*, 2010]. In the previous studies, it has not been reported that any RTMs have successfully reproduced the negative spectral gradient

of frozen soil and radiative transfer processes inside of frozen soil considering volume scattering effect.

1.2.3 Frozen Soil State Initialization and assimilation

Initialization is a common problem for land surface modeling. It is extremely difficult for frozen soil state initialization, because of the three dimension structure of frozen soil and scarce soil observation. The coverages of frozen soil measurement sites are very limited, and the measurements are not comprehensive and standardized. Generally continuous soil temperature, moisture and ice content profile are not available, which are key parameters for frozen soil numerical modeling. In recent studies of frozen soil modeling, tens or hundreds of year spin-up simulation with repeat year forcing were conducted to generate proper vertical soil state [*Lawrence et al.*, 2011; *Lawrence et al.*, 2008; *Yanlin Zhang et al.*, 2013], however great bias could be introduced due to the uncertainty in precipitation data and high computation cost have to be paid. Moreover, spin-up simulation is a virtual running which assume that there is no interannual variation in forcing data, so the spin-up result only provides a roughly approximation of soil state, not a realistic soil state.

Satellite based microwave radiometers can regularly provide long term, spatial-continuous ground information in regional, continental or global scale. Microwave radiation is very sensitive to both soil temperature and liquid water. As we all know, frozen soil is characterized as low soil temperature and low water content. Another unique advantage of passive microwave remote sensing is that in very dry situation, microwave penetration depth becomes deeper, which means that the deep soil information is obtainable. Assimilating the passive microwave remote sensing data into the initial state of frozen soil numerical model system could be a potential solution for initialization problems. Data assimilation technique has been widely applied in atmospheric, oceanic and land surface models. However very few data assimilation studies on frozen soil modeling have been published so far and studies on this field are still in its early stage. England et al. [2006] proposed an investigation that assimilating 1.4 or 6.9 GHz brightness into the SVAT model to monitor active layer thickness and soil moisture in arctic tundra. Jin Rui and LiXin [2009] tried to improve the estimation of hydrothermal state variables in the active layer of frozen ground by assimilating in situ and SSM/I 19GHz data into the SHAW model, but the result of the 19GHz data assimilation is not as good as that from assimilating soil observation directly due to the poor frozen soil RTM. Jafarov et al. [2014] assimilated measured ground temperature to optimize snow thermal conductivities for

improving ground surface temperature simulation, while they neglected the consideration of optimizing snow albedo. However, these studies either assimilated in situ soil observation or was only able to optimize ground surface states. The microwave satellite data assimilation into frozen soil profile state have not been successfully realized. Therefore, how to get proper vertical soil profile by assimilating microwave remote sensed observation instead of ground observation is a new topic and a challenge for optimizing frozen soil initial state and improving frozen soil modeling performance.

1.3 Objectives

The Objective of this study is to enhance the capability of simulating frozen soil processes in land surface models and hydrological models based on satellite remote sensing technique, thus monitoring and forecasting the response of permafrost and seasonal frozen soil to climate change, and providing an efficient diagnostic tool for water resource management and climate change adaptation in cold region.

Currently, the most common problems in frozen soil modeling are unstable simulation and heavy computational cost due to the highly non-linear relationship in soil temperature, soil moisture and ice content caused by the substantial latent heat associated with the phase change. The insufficient physical understanding and high computational demand still strongly limit the wide application of frozen soil models in permafrost and associated hydrological and climate research. Another issue is that good initial condition is extremely important for model forecast. But it is especially difficult for frozen soil modeling to obtain initial soil profile in the place without soil observation. Passive microwave remote sensing, as one of important observation methods for frozen soil research in regional or global scale, has achieved advances in mapping soil freeze-thaw states. However, there are only few quantitative studies on radiative characteristics of frozen soil, transfer processes mechanism and numerical simulation of microwave radiative transfer in frozen soil.

To address the problems mentioned above, we set up 3 goals as follows:

1. To develop a new frozen soil model by considering not only physical realism, but also computational stability and efficiency to obtain a better understanding of frozen soil physics and reproduce the hydrological and thermal processes of frozen soil.

2. To develop a multi-layer radiative transfer model considering volume scattering to simulate radiative transfer process inside frozen soil quantitatively

3. To obtain initial conditions of soil profile for physical modeling by taking advantage of passive microwave satellite observation.

1.4 Study Framework

The study framework of this thesis is shown in Figure 1.5. Firstly, developing a frozen soil model based on the land surface scheme HydroSiB2 with coupled water and energy budgets and then frozen soil temperature, moisture and ice profile can be obtained through simulation. Secondly, investigating on radiative characteristics of frozen soil, transfer processes mechanism and numerical simulation of microwave radiative transfer in frozen soil. By introducing the frozen soil states into the RTM, radiative transfer processes and brightness temperature out of soil could be reproduced. Thirdly, by comparing predicted brightness temperature and observed brightness temperature from a satellite based microwave radiometer, the observed brightness temperature could be assimilated into the initial state of frozen soil model and the optimum initial soil condition can drive the model to get promising forecast.

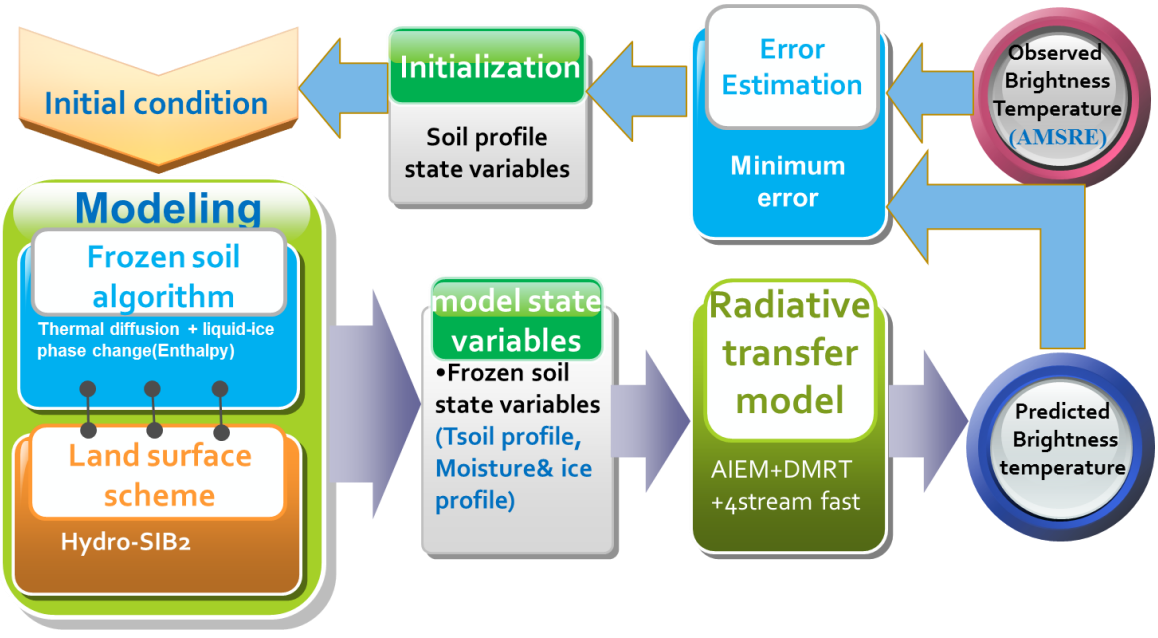

Figure 1.5 study framework of modeling and assimilating of frozen soil hydrology

1.5 Outline of the Dissertation

The dissertation mainly comprises three parts: Chapter 2 and Chapter 3 concentrate on the development of frozen soil model and its validation, chapter 4 covers a microwave radiative transfer model of frozen soil and chapter 5 presents an assimilation method for frozen soil profile initialization.

Chapter 2 briefly introduces the physics of frozen soil at first, then focus on the frozen soil modeling. A three-step frozen soil algorithm is proposed including thermal diffusion scheme, freezing/thawing scheme and soil moisture transport scheme, and a multi-layer, enthalpy-based frozen soil model is developed to represent the freeze-thaw and heat–water flow in frozen soil. In addition, a parameterization set for frozen soil is updated to approximate realistic changes in hydraulic and thermal properties.

Chapter 3 describes the validation of the frozen soil model in a permafrost basin. The model was first tested at point scale by comparing soil temperature, ice, liquid water content, and thaw depth with observations at a permafrost station in the upper reach of the basin. Then, we validated the simulated hourly river discharge through frozen - thaw periods by using discharge measured at a basin outlet. In addition, sensitivity studies are conducted to verify the accuracy and robustness with a certain wide range of soil depth, layer thickness and time step.

Chapter 4 investigates on the radiative transfer processes and the RTM development for frozen soil. The dielectric constant of frozen soil and its model are present, firstly. Then we give explanation for the mechanism of microwave radiative transfer process in frozen soil. Next, a multilayer RTM for frozen soil was developed considering both surface scattering and volume scattering. Finally, this frozen soil RTM is assessed by applying to a seasonal frozen soil region on Tibet Plateau and comparing with the AMSR-E brightness temperature.

Chapter 5 proposed a soil profile initialization method by assimilating the passive microwave satellite data into the frozen soil modeling. Firstly, the penetration depth of microwave are estimated for different frequency. Then sensitivity studies on soil temperature initialization is conducted. Next, the assimilation methods are proposed. Finally, an experiment is conducted to test this method in the seasonal frozen site.

Finally, Chapter 6 summarizes the main achievement of this study and gives a conclusion for this thesis.

2. DEVELOPMENT OF AN ENTHALPY BASED FROZEN SOIL MODEL

2.1 Introduction

This study investigated a new frozen soil algorithm using the concept of enthalpy and developed a frozen soil model based on a land surface scheme, as well as updated the parameterization of the thermal and hydraulic properties. The motivation of this development is not only to represent the physical realism of frozen soil processes in the land surface scheme, but also to improve computational stability and iteration efficiency of modeling; furthermore, to improve the streamflow prediction capabilities and applicability of hydrological model in cold region river basins, such as the Arctic or Tibet plateau.

Lei Wang et al. [2009b] developed a water and energy budget land surface scheme called Hydro-SiB2 by modifying the Simple Biosphere Model 2 (SiB2) [Sellers et al., 1996] with a more detailed description of soil water flow. The scheme can realistically simulate land surface and hydrological processes and has shown consistent accuracy in the estimation of radiation, turbulent fluxes between the atmosphere and the land surface, CO_2 fluxes and the soil moisture profile. However, the heat transfer processes in Hydro-SiB2 are too simple to represent heat flow through soil column and freeze-thaw cycles of frozen soil. Only ground surface temperature T_g and deep soil temperature T_d are roughly described without specific depth by an empirical approach force-restore method, which simply utilize the concept of amplitude damping of soil temperature and assuming T_d is at somewhere annual temperature wave can penetrate. In addition, freezing and thawing effect on hydraulic and thermal properties were not considered and water only can exist in liquid state.

Based on the Hydro-SiB2 land surface scheme, we developed a frozen soil model with coupled water and energy budgets to obtain a better understanding of frozen soil physics and reproduce the frozen soil processes. A new physical system inside the frozen soil model consists of vertical profiles extending from the atmosphere, vegetation, snow, soil, and aquifers, which allow the description of vertical water and heat transport, and liquid-ice phase shift in the soil–

vegetation–atmosphere transfer system, lateral water flow along a hillslope, and runoff generation.

2.2 Physics of Frozen Soil

To model frozen soil, knowledge of physics of frozen soil and the seasonal evolution of active layer is crucial for gaining a better understanding of the hydrological processes of permafrost, for capturing the physical characteristics of frozen soil, and reflecting the physical reality in algorithms and models.

2.2.1 Impact factors of frozen soil (What Controls Permafrost?)

Any location with annual average air temperatures below freezing can form permafrost [*Humlum*, 1998; *Stocker‐Mittaz et al.*, 2002]. Cold climate and subfreezing air temperature for long period are hallmarks of frozen soil presence. Nonetheless, frozen soil may form in regions with mean annual air temperature as high as 2°C or not be present where annual average air temperature is as low as -20°C due to local factors [*Jorgenson et al.*, 2010]. Essentially, the presence of permafrost are controlled by six factors [*Ferrians and Hobson*, 1973]: air temperature, snow cover, vegetation cover, geological factors, hydrological factors, and topographic factors.

(1)Air temperature: Air temperature is the dominant control on global permafrost distribution and the thickness of permafrost, especially the mean annual air temperature. High air temperatures can cause warmer permafrost, even the thawing of permafrost. The active layer thickness is also up to the summer air temperature and higher summer air temperatures result in deeper active layers [*Q Wu et al.*, 2015; *Q Wu and Zhang*, 2010].

(2) Snow cover: Overlying snow also has an important impact on frozen ground. The major component of snow is air, which has a low thermal conductivity, making it a very effective insulator. Snow duration, timing and thickness can greatly influence the heat exchange between ground and atmosphere, especially an early snow remains throughout the winter can result in shallower frost depth than a late snowfall. Snow also can reduce the amount of solar energy reaching the ground by reflecting most of radiation back to atmosphere because of its high

albedo. In turn, freezing and thawing processes of soil have implications for snow accumulation /ablation.

(3) Vegetation cover: Vegetation such as lichen, mosses and larch can block solar radiation partly and have good ground-insulting abilities to prevent the permafrost from thawing [*Briggs et al.*, 2014]. Similarly, the surface organic matters such as peat are seasonally dependent insulator. They are good conductors of heat in frozen autumn and winter, and turn to poor conductors of energy in drier summer. The effects of surface vegetation and organic soil matter often result in large variability in active layer thickness within the space of a few meters [*Humlum*, 1997]. Shading by vegetation reduces the sunlight absorbed by the soil, resulting in shallower active layers than bare exposed soil. The presence of organic matter in the soil tends to result in shallower active layers. In discontinuous permafrost, shading by surface vegetation and the insulating effect of thick organic soil or peat are often required for permafrost to exist [*Shur and Jorgenson*, 2007].

(4) Hydrology: Hydrological factors such as soil moisture and proximity to water bodies can greatly affect ground thermal regimes. Liquid water has a higher specific heat capacity and ice has a higher thermal conductivity. Warmer rainfall can bring energy to frozen ground directly. Generally, wetter soil in summer results in deeper frost depth in winter and shallower active layers. Moreover, when soil water freezes or melts, significant amount of latent heat is released into or absorbed from surrounding soil materials, which strongly slows down the dropping and rising of soil temperature. Finally, lake and river can cause the formation of discrete unfrozen zones in permafrost regions (taliks) [*Mackay*, 1997]. Also, stream through or over ground can effectively maintain ground in unfrozen conditions.

(5) Geology: geological properties of soil materials determine the porosities, bulk density and soil texture, which influence the hydrological and thermal properties of frozen soil. Soil bulk density and quarts content have a large effect on thermal conductivity. Large soil particle size may result in large porosity and high permeability. At same temperature, unfrozen water content increases with the increasing of particle size (clay> loam>sand) [*Xu et al.*, 2001].

(6) Topography: Elevation, slope and orientation of slope control the presence of frozen soil in mountainous regions. Air temperature drops with elevation raising. At high elevations, permafrost can exist at latitudes where it does not normally occur, for example permafrost in Tibet Plateau. Slope and aspect also affect frozen soil distribution by controlling the amount of solar energy received by the ground. Usually, a north-facing, shaded slope may develop permafrost, while a nearby south-facing, sunlit slope may not [*Ferrians and Hobson*, 1973;

Haeberli et al., 2010]. In continuous permafrost zone, frozen soil would be thicker and colder under north-facing slopes than that under south-facing slopes[*Duguay et al.*, 2005].

2.2.2 Properties of frozen soil

Frozen soil is composed of solid matrix, ice, liquid water and gas component (including air and water vapor). Frozen soil structure and constitutes can be simplified as Figure 2.1. The amount of each constitutes are usually expressed by the ratio of each volume to unit volume soil. Soil porosity ϕ is the proportion of pore spaces in a volume of soil, which decreases with depth due to compaction and biological activity near the surface. However, it is considered as constant in most hydrological analysis. Pores among grains can hold liquid water, ice, water vapor and air. Soil porosity can be described as follows:

$$\phi = 1 - \theta_d = \theta_l + \theta_i + \theta_a \tag{2.1}$$

where θ_l, θ_i, θ_a and θ_d are the volumetric liquid water content, volumetric ice content, volumetric air content and volumetric soil grains.

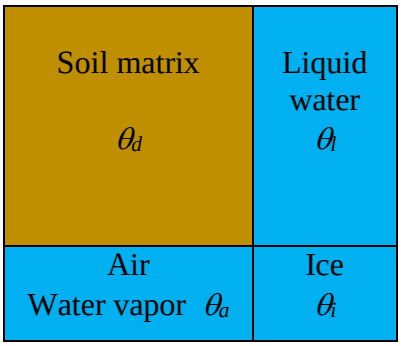

Figure 2.1. Simplified frozen soil structure and its constitutes

Saturated soil moisture is the maximum liquid water content pores can contain in a volume soil. For normal soil, it is equal to soil porosity. However, when frozen soil get saturated, water only can fill the pore space which has not been taken by ice. Thus, saturated water content θ_s and wetness S of frozen soil are defined as:

$$\theta_s = \phi - \theta_i \tag{2.2}$$

$$S = \frac{\theta_l}{\phi - \theta_i} \tag{2.3}$$

Frozen soil has relatively low hydraulic conductivity, compared to normal soil. Ice forms in the spaces between soil particles and ice content can control infiltration. At low ice contents, liquid water will continue to flow unhindered, but as the ice content increases, the open channels narrow, and liquid water movement is restricted [*Cherkauer and Lettenmaier,* 1999a]. Another explanation is that available unfrozen liquid water decreases as temperature drops below 0°C [*Burt and Williams*, 1976]. Low temperature also has impact on water potential by increasing viscosity and decreasing surface tension. However, there is still neither comprehensive theory nor enough accurate measurements to clarify the influence of ice on matric potential. Generally, the effect of ice on hydraulic properties for frozen soil are considered by using some empirical methods [*Cosby et al.*, 1984; *Kulik*, 1978; *O'Neill and Miller*, 1985].

Ice in frozen soil makes its thermal properties distinct from normal soil, higher thermal conductivity and lower heat capacity, which change the dynamics of soil heat transfer and indirectly influence surface heat fluxes between land and atmosphere. Because thermal conductivities of ice (2.2 W m^{-1} K^{-1}) is four times higher than the liquid water thermal conductivity (0.57 W m^{-1} K^{-1}), frozen soil will have a higher thermal conductivity than soil with an equivalent content of liquid water. Moreover, the specific heat capacity of water is 4.195 J K^{-1} g^{-1}, while that of ice is 2.1 JK^{-1} g^{-1}, suggesting that a soil containing a high ice content has lower heat capacity than a soil with an equivalent content of liquid water. The thermal properties of each constituent are shown in table 2.1.

Table 2.1 Heat capacity and thermal conductivity of frozen soil constituents

constituents	**Heat Capacity (J/g/℃)**	**Heat Conductivity (W/m/K)**
Water at 20 °C	4.195	0.57
Ice	2.1	2.2
Quartz sand	0.85	7.7
Still air at 20 °C	1.030	0.023

Until now there has been no theory comprehensive enough to predict the thermal conductivity of frozen soil, but various empirical methods based on field measurements for computing thermal conductivity have been developed [*Sun*, 2005]. While the volumetric heat capacity of frozen soil C_v are generally calculated according to the linear contribution of each constituents:

$$C_v = \sum_i c_i \rho_i \theta_i = c_d \rho_d + c_l \rho_l \theta_l + c_i \rho_i \theta_i \tag{2.4}$$

where C_d, C_l, and C_i represent the specific heat capacity of dry soil, liquid water, and ice. ρ_d is the bulk density of a dry soil; and ρ_l (1000 kg m^{-3}) and ρ_i (920 kg m^{-3}) are the densities of liquid water and ice. The mass of air is so small that its contribution to soil heat capacity can be neglected.

Another thermal measurement called enthalpy is also used in this study, which can describe total thermodynamic potential energy of frozen soil system. At a constant pressure, enthalpy H is energy absorbed or released to change temperature from defined reference point T_f to a certain temperature T. Generally T_f is set as 0K or 273.15K. In our study, we set 273.15K as T_f. Frozen soil is a mixture of several constituents, so we assume that each constitute has same temperature and the enthalpy of each constitutes is defined as:

$$\begin{aligned}
&\text{Soil matrix}: && H_d = c_d T \theta_d \rho_d \\
&\text{Liquid water}: && H_l = c_l T \theta_l \rho_l \\
&\text{Ice}: && H_i = c_i T \theta_i \rho_i - L_{il} \theta_i \rho_i \\
&\text{Water vapor}: && H_v = c_v T \theta_v \rho_v + L_{lv} \theta_v \rho_v .
\end{aligned} \tag{2.5}$$

Then the volumetric enthalpy of frozen soil is the sum over all the contribution of constitutes.

$$H_{soil} = \sum_{j=i,l,d,v} c_j \theta_j \rho_j (T - 273.15) - L_i \theta_i \rho_i + L_v \theta_v \rho_v \tag{2.6}$$

Where L_{il} is specific latent heat of fusion for ice (0.3336×10^6J/kg), L_{lv} is specific latent heat of vaporization (2.5104×10^6J/kg), L_{iv} is specific latent heat of sublimation(2.884×10^6J/kg),($L_{iv} = L_{il} + L_{lv}$).

2.2.3 Frozen Ground Surface Energy and Mass Balance

Energy and water exchange between the frozen ground surface and atmosphere plays an important role in the hydrology and climate of cold regions. For ground surface energy budget (see Figure 2.2), solar radiation is the main heat source including short wave (SW_{ng}) and long wave (LW_{ng}) radiations, while precipitation also can brought heat (G_{pr}) to soil through infiltration and conduction. Turbulent latent heat (lE_g) is absorbed or released by ground corresponding to evapotranspiration or condensation. Sensible heat (H_g) is driven by ground-

air temperature gradient through conduction or convection. Ground heat flux (G_0) can travels down or up the soil profile through conduction to heat or cool the soil and change the phase of soil water.

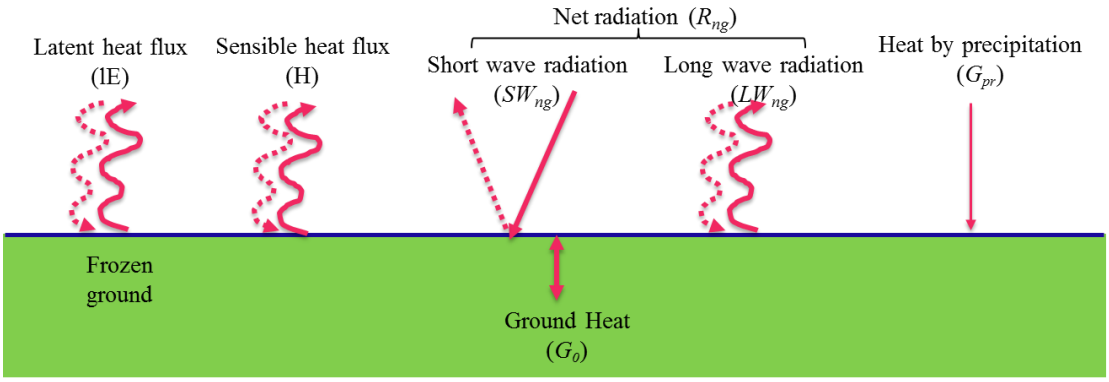

Figure 2.2. Surface energy budget of frozen ground

$$R_{ng} + G_{pr} = G_0 + H_g + lE_g \tag{2.7}$$

where R_{ng} is the net radiation flux (W m^{-2}), which is the sum of net short wave and long wave radiation ($R_{ng}=SW_{ng}+LW_{ng}$); G_{pr} is the sensible heat brought by precipitation (W m^{-2}); G_0 is the ground heat flux (W m^{-2}), which change the internal energy of frozen soil and melt ice (freeze soil water); H_g and lE_g represent the sensible heat flux and the latent heat flux of the ground surface (W m^{-2}), respectively.

Surface mass balance (see Figure 2.3) controls the total amount and rate of infiltrated water into ground. For soil, precipitation (P) is the main water resource including rainfall and snowfall. Once water arrives at the ground surface, water may start to infiltrate. If the rate of rainfall or snowmelt exceeds infiltration capacity, water may start to pond over ground. If snowfall occurs, snowmelt would contribute to soil water infiltration. Excessive water over ground may be driven to flow along slope and becomes to surface runoff (R_{off}). Water on the ground also can be brought back to atmosphere through evaporation (E_g) and transpiration (E_c), even sublimation of snowcover (E_s).

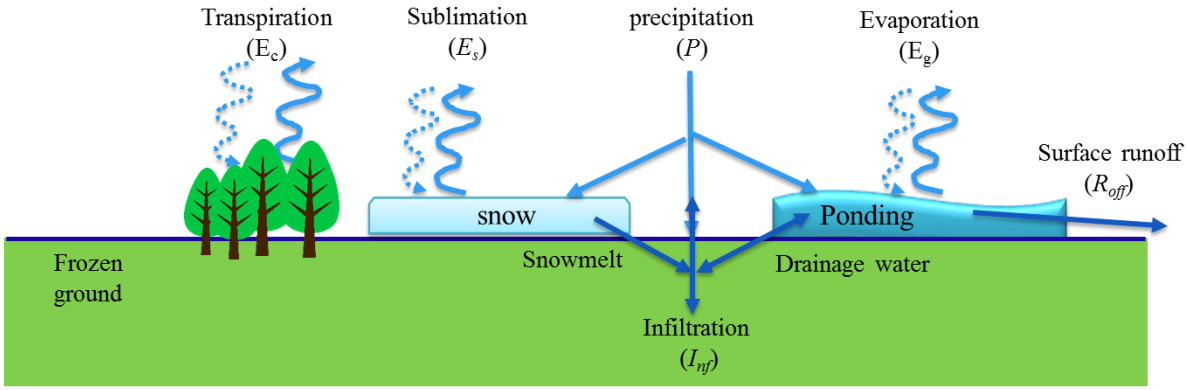

Figure 2.3. Surface water budget of frozen ground

$$P = E_c + E_g + E_s + R_{off} + I_{nf} \tag{2.8}$$

where P is the precipitation rate (m s^{-1}), which is the sum of rainfall and snowfall; E_c, E_g and E_s are the vegetation transpiration rate (m s^{-1}); ground evaporation rate (m s^{-1}) and sublimation rate of snow, respectively; R_{off} is the surface runoff (m s^{-1}); I_{nf} represents the water infiltration rate from surface to soil (m s^{-1}).

2.2.4 Heat–Water Transfer and Phase Change within Frozen Soil

Heat and water transfer processes in frozen soil can be described by an energy conservation equation and a mass balance equation proposed by Zhao et al. [1997], which considered the movement of all phases of water (liquid, ice and vapor) and their phase transitions.

Liquid water could be redistributed in porous soil according to water potential and gravity. Phase change between liquid and ice, or liquid and vapor also control the liquid water content in frozen soil:

$$\text{Liquid: } \frac{\partial \theta_l}{\partial t} = -\frac{\partial u_l}{\partial Z} + \frac{M_{il} - M_{lv}}{\rho_l} . \tag{2.9}$$

In case of ice, it does not move. Only freeze/melt and sublimation / desublimation correspond to the change of ice volume:

$$\text{Ice: } \frac{\partial \theta_i}{\partial t} = -\frac{M_{iv} + M_{il}}{\rho_i} . \tag{2.10}$$

In case of vapor, it not only can diffuse according to its concentration gradient, but also has phase change with ice and liquid water:

$$\text{Vapor: } \frac{\partial \theta_v}{\partial t} = \frac{M_{iv} + M_{lv}}{\rho_v} + \frac{\partial}{\partial Z}(D_{eff} \frac{\partial \rho_v}{\partial Z}). \tag{2.11}$$

The total water mass conservation equation (2.12) of frozen soil can be obtained by organizing equation (2.9)-(2.11).

$$\frac{\partial \theta_i}{\partial t} + \frac{\partial \theta_l}{\partial t} + \frac{\partial \theta_v}{\partial t} = -\frac{M_{iv} + M_{il}}{\rho_i} - \frac{\partial u_l}{\partial Z} + \frac{M_{il} - M_{lv}}{\rho_l} + \frac{M_{iv} + M_{lv}}{\rho_v} + \frac{\partial}{\partial Z}(D_{eff} \frac{\partial \rho_v}{\partial Z}) \tag{2.12}$$

In equations (2.9) - (2.12), the subscripts *i, l, v* indicate ice, liquid and vapor, respectively; the M_{il}, M_{lv}, and M_{iv} are rates of phase change between ice and liquid, liquid and vapor, and ice and vapor (kg s^{-1}). D_{eff} is the effective diffusivity of vapor in soil voids; Z and t denote depth in soil and time.

On the other hand, the energy balance of frozen soil can be explained by the equation 2.13. The internal energy or temperature (the first term on the left side) of frozen soil and liquid-ice-vapor phase change (the left terms on the left side) of water mainly depend on the heat conduction (the first term on the right side) and heat convection arises from liquid movement (the second term on the right side). According to magnitude analysis, the heat transfer due to vapor diffusion driven by temperature gradient and concentration gradient are too small to consider for normal soils, which also can be reasonable neglected for frozen soils [*SUN*, 2005].

$$\frac{\partial C_v T}{\partial t} + L_{il} M_{il} + L_{lv} M_{lv} + L_{iv} M_{iv} = \frac{\partial}{\partial Z}(K_{eff} \frac{\partial T}{\partial Z}) - \rho_l c_l \frac{\partial u_l T}{\partial Z} \tag{2.13}$$

where C_v is average volumetric heat capacity of frozen soil and K_{eff} is the effective heat conductivity; u_l represents liquid water fluxes.

As we all know that temperature changes discontinuously during water phase change, as shown in Figure 2.4. Before the soil starts freezing, the soil temperature changes continuously and linearly with energy losing, and water content almost remains constant. Once freezing begins, the decrease of the soil temperature slows down and remains around freezing point, despite its continuous energy loss, while simultaneously ice grows rapidly and liquid content drops dramatically with little temperature change. During phase transitions, a large amount of extra latent heat releases into the surroundings materials, and resists rapid soil cooling, which involves a highly nonlinear relationship between ice content, soil temperature, and liquid water in frozen soil [*Q Li et al.*, 2009a; *Q Li et al.*, 2010].

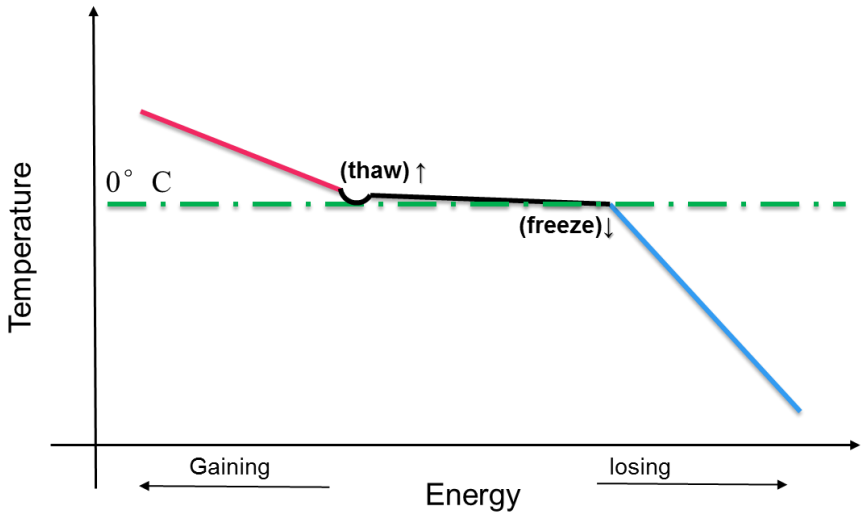

Figure 2.4. Discontinuous temperature variation during freeze or thaw

Generally, a large number of iteration procedures are required to solve the highly nonlinear mass and energy equations [*Hansson et al.*, 2004; *Zarba et al.*, 1990; *X Zhang et al.*, 2007b]. However, the large magnitude of internal energy loss and the great amount of latent heat release against each other may cause that the simulated soil temperatures oscillate around freezing points and fail to reach convergent solutions at heavy computational cost. To avoid this problem, some explicit approaches assume that soil temperatures are fixed as 0°C during water phase change, which does not agree with the reality. According to many observations, liquid water may coexist with ice in frozen soil, when soil temperature is much lower than 0°C [*Q Li et al.*, 2010]. Freezing/thawing is a continuous process without fixed freezing temperature and temperature only depends on the energy state of soil system. Therefore, how to reproduce the physical realism of freeze-thaw process of frozen soil and solve the highly nonlinear mass and energy equations stably and efficiently are the main task and challenge for this frozen soil modeling study.

2.3 Model Structure

This study focuses on the development of the frozen soil model to represent heat-water transfer and phase change in frozen soil. In this motivation, the land surface scheme Hydro-SiB2 is used as a base model to describe land surface mass–energy budget and soil water flow in the development of frozen soil model.

In consideration of both frozen soil physical realism and computational efficiency, the frozen soil algorithm was designed as three schemes: thermal diffusion scheme, freezing/thawing scheme and soil moisture transport scheme, which solve the thermal diffusion, liquid–ice phase change and water diffusion, respectively separately. At each time step: firstly, soil temperature through the soil column is solved by the thermal diffusion scheme prior to the treatment of the phase change. Secondly, the freezing/thawing processes are simulated and soil temperature, liquid soil moisture, and ice content are calculated simultaneously, according to the phase change simulation in the freezing/ thawing scheme. Subsequently, soil hydraulic properties are adjusted using updated soil temperature, liquid water, and ice contents. Next, the liquid water flux flow through the soil layers and the vertical soil moisture profile, lateral runoff, and exchange with groundwater are computed using updated hydraulic properties. Finally, soil thermal properties for the next time step calculation are estimated from the redistribution of soil moisture and ice.

A multiple-layer soil structure is employed to represent heat and water fluxes through the frozen soil column (Figure 2.5). The surface layer was defined as shallow as 5 cm, because variables close to the surface are very sensitive to the atmospheric diurnal forcing. The underlying soil between the surface layer and the groundwater layer is uniformly divided into several layers, the thickness of which can be specified by users. The heat and water budget of the uppermost soil layer is affected by the net radiation, sensible heat, latent heat fluxes, precipitation and evaporation derived from the land surface model. The energy distribution inside the soil column is controlled by the heat conduction between layers and the phase change inside each individual layer. The water distribution within the soil is driven by the liquid water movement and liquid–ice phase change.

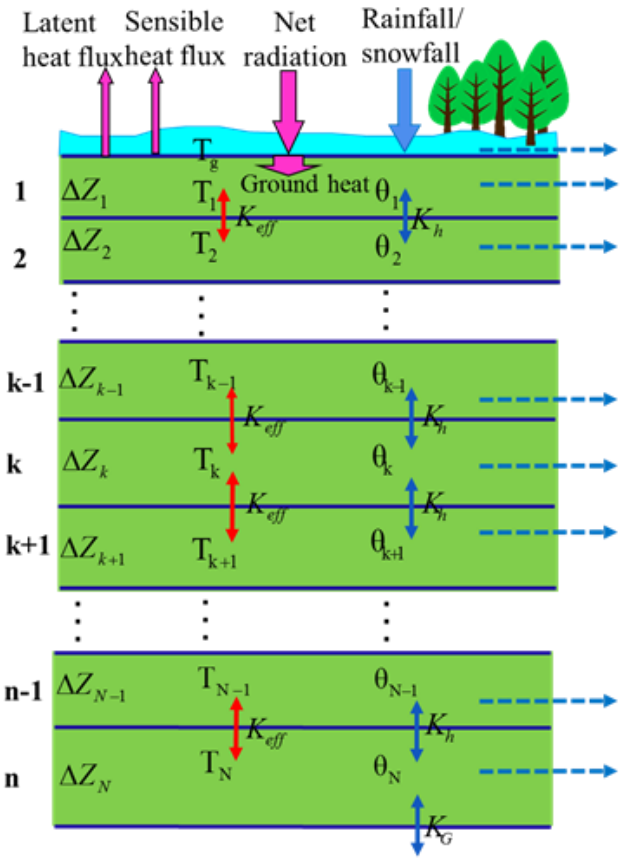

Figure 2.5. Structure of the numerical discretization for the heat and water fluxes of the numerical frozen soil model. Number of soil layer is *k*, ranged from 1 to n. Soil temperature and soil moisture of each layer are *T* and θ, respectively. Heat conductivity and hydraulic conductivity are K_{eff} and K_h, respectively.

2.4 Frozen Soil Algorithm

A three-step scheme is adopted to obtain a stable numerical solution of this non-linear equation. In the first step, all available coming energy passes through vegetation and reaches the ground surface and heat is diffused into the soil. In the second step, the phase change of soil water is treated as a continuous process without a fixed freezing point. The third step describes liquid water movement through frozen soil pores. When no phase change occurs (e.g. during summer or in extreme dry soil), the second step is not implemented.

2.4.1 Thermal Diffusion

A general energy governing equation for heat flux through the soil column can be written as:

$$C_v \frac{\partial T}{\partial t} - L_i \rho_i \frac{\partial \theta_i}{\partial t} = \frac{\partial}{\partial z}\left(K_{eff} \frac{\partial T}{\partial z} \right) - \rho_l c_l \frac{\partial q_l T}{\partial z} \quad , \tag{2.14}$$

where C_v is the soil volumetric heat capacity (J m^{-3} K^{-1}); K_{eff} is the effective soil thermal conductivity (W m^{-1} K^{-1}); T is the soil temperature (°C); ρ_i and ρ_l represent the density of ice and liquid water (kg m^{-3}), respectively; L_i is the specific latent heat of fusion (J kg^{-1}); θ_i is the volumetric ice content of the layer (m^3 m^{-3}); q_l is the liquid water flow rate (m s^{-1}); c_l is the specific heat capacity of liquid water (J kg^{-1} K^{-1}); and t and z respectively represent the time (s) and the vertical depth (m) with downward as positive. The first term is the heat storage change with time. The second term corresponds to the latent heat due to freezing or thawing. The term $\frac{\partial}{\partial z}\left(k_{eff} \frac{\partial T}{\partial z} \right)$ refers to the vertical conductive heat. The final term is the convective heat arises from liquid movement. In frozen soil, water moves slowly and the amount of water is limited, so the convective heat is quite small. According to magnitude analysis, the convective heat term ($-\rho_w c_l \frac{\partial q_l T}{\partial z}$) in soil is two orders of magnitude less than the value of the conduction term when soil is in the dry or frozen condition [*Li et al*, 2009]. Hence, in this frozen soil study, the heat contribution from liquid flow inside the soil can be reasonably neglected. However, the contribution of convective heat from rainfall infiltration is important for soil surface and is reserved.

At the first step, all available coming energy reaches ground surface and heat is passed into the soil. We obtained a simplified thermal diffusion equation by assuming no conversion between ice and liquid water at the current time step:

$$C_v \frac{\partial T}{\partial t} = \frac{\partial}{\partial z}\left(k_{eff} \frac{\partial T}{\partial z} \right). \tag{2.15}$$

The thermal diffusion equation (Equation 2.15) is numerically posed as implicit finite difference approximations. In the following equations, the subscripts t and k indicate the time step and the layer number, respectively. Here, ΔZ_k and Z_k denote the thickness and center depth of each layer, respectively.

For the surface layer (k = 1):

$$C_{v(k)}\Delta Z_k(T_k^{t+1}-T_k^t)=\left(G_0^{t+1}-K_{eff(k)}\frac{T_k^{t+1}-T_{k+1}^{t+1}}{Z_{k+1}-Z_k}\right)\Delta t\,. \tag{2.16a}$$

For the inner layer (k = 2 to k = N−1):

$$C_{v(k)}\Delta Z_k(T_k^{t+1}-T_k^t)=\left(K_{eff(k-1)}\frac{T_{k-1}^{t+1}-T_k^{t+1}}{Z_k-Z_{k-1}}-K_{eff(k)}\frac{T_k^{t+1}-T_{k+1}^{t+1}}{Z_{k+1}-Z_k}\right)\Delta t\,. \tag{2.16b}$$

The bottom layer (k = N):

$$C_{v(k)}\Delta Z_k(T_k^{t+1}-T_k^t)=\left(K_{eff(k-1)}\frac{T_{k-1}^{t+1}-T_k^{t+1}}{Z_k-Z_{k-1}}-0\right)\Delta t\,. \tag{2.16c}$$

In all cases, K_{eff} is the effective soil thermal conductivity between soil layers (W m^{-1} K^{-1}), defined as the average thermal conductivity, K_t, of two neighboring layers by the inverse distance weighting method:

$$K_{eff}=\frac{K_{t(k)}\Delta Z_{k+1}+K_{t(k+1)}\Delta Z_k}{2(Z_{k+1}-Z_k)}\,. \tag{2.17}$$

By reorganizing Equations (2.16a)–(2.16c), we obtain a tridiagonal linear equation system with soil temperature of all the layers as unknowns that can be solved using an implicit backward numerical scheme.

The heat content of soil is mainly affected by the net short- and long-wave radiation, latent and sensible heat fluxes at the surface, heat conduction between sublayers, ground heat storage, and latent heat from the phase change of water. The boundary conditions and initial condition are critical for the numerical solution of Equation (2.15). The ground heat fluxes in upper boundary (equation 2.18a-2.18b) are influenced by the vegetation and ground surface. The insulating effect of surface vegetation is considered, which usually prevents the permafrost from thawing [*Briggs et al.*, 2014]. Vegetation and ground heat are mainly derived from the two stream radiation model and the surface energy balance, consisting of net radiation, latent heat, and sensible heat fluxes, which can be written as:

$$C_c\frac{\partial T_c}{\partial t}=R_{nc}-H_c-lE_c \tag{2.18a}$$

$$G_0^{t+1}=R_{ng}-H_g-lE_g \tag{2.18b}$$

$$G_n=0 \tag{2.18c}$$

where G_0^{t+1} is the ground heat flux (W m^{-2}); C_c is vegetation heat capacity; the vegetation and the ground is subscripted as c and g; and R_{ng}, R_{nc}, H_g, H_c, lE_g and lE_c represent the net radiation flux, the sensible heat flux, and the latent heat flux of the ground surface and canopy (W m^{-2}), respectively. For the lower boundary conditions, it is assumed that there is no heat flux from the deeper soil (equation 2.18c) affecting the temperature of the boundary layer, because the available incoming energy decreases with depth as it travels down the soil profile and the temperature gradient between deep soil layers is close to zero. The depth of the lower boundary can be estimated by the soil depth sensitivity study presented in Section 3.4.

G_0^{t+1} is defined as the sum of the heat flux through the soil at the depth of $\frac{1}{2}z_1$ and the heat storage change between the surface and $\frac{1}{2}z_1$:

$$G_0^{t+1} = G(0.5z_1) + \Delta S(0-0.5z_1). \tag{2.19}$$

$G(0.5\overline{z_1})$ is the heat flux at the depth of $\frac{1}{2}z_1$, which can be expressed by from T_g and T_1:

$$G(0.5\overline{z_1}) = K_{t(1)}\frac{(T_g^{\,t} + \Delta T_g - T_1^{\,t} - \Delta T_1)}{z_1} \tag{2.20}$$

$\Delta S(0-0.5\overline{z_1})$ is the heat storage change between the surface and $\frac{1}{2}z_1$, and $\overline{\Delta T}$ is the temperature change between the surface to $\frac{1}{2}z_1$

$$\Delta S(0-0.5z_1) = \frac{0.5C_{v(1)}z_1\overline{\Delta T}}{\Delta t} \tag{2.21}$$

$\overline{\Delta T}$ is defined as:

$$\Delta\overline{T} = (1-w)\Delta T_g + w\Delta T_1 \tag{2.22}$$

where w is a weight number, $w \approx 0.25$, $\Delta T_g = T_g^{t+1} - T_g^t, \Delta T_1 = T_1^{t+1} - T_1^t$

Thus, equation (2.19) can be written as:

$$G_0^{t+1} = \left[\frac{K_{t(1)}}{z_1} + \frac{0.5C_{v(1)}(1-w)z_1}{\Delta t}\right]\Delta T_g + \left[-\frac{K_{t(1)}}{z_1} + \frac{0.5C_{v(1)}wz_1}{\Delta t}\right]\Delta T_1 + K_{t(1)}\frac{(T_g^{\,t} - T_1^{\,t})}{z_1} \tag{2.23}$$

If we set $A = \frac{K_{t(1)}}{z_1}$, $C = \frac{K_{t(1)}}{z_1} + \frac{0.5C_{v(1)}(1-w)z_1}{\Delta t}$ and $D = \frac{K_{t(1)}}{z_1} - \frac{0.5C_{v(1)}wz_1}{\Delta t}$, then equation (2.23) can be simplified as:

$$G_0^{t+1} = C\Delta T_g - DT_1^{t+1} + DT_1^t + A(T_g^t - T_1^t) \tag{2.24}$$

Finally, introducing the above G_0^{t+1} to equation (2.18b), then ground surface energy balance can be expressed by T_g and T_1 :

$$\left[C_{v(1)} + \frac{\partial H_g}{\partial T_g} + \frac{\partial lE_g}{\partial T_g} - \frac{\partial R_{ng}}{\partial T_g}\right]\Delta T_g$$
$$= DT_1^{t+1} + (\frac{\partial R_{ng}}{\partial T_c} - \frac{\partial H_g}{\partial T_c} - \frac{\partial lE_g}{\partial T_c})\Delta T_c - DT_1^t - A(T_g^t - T_1^t) + R_{ng} - H_g - lE_g \ . \tag{2.25}$$

2.4.2 Phase Change

Before the soil starts freezing (thawing), the soil system changes continuously and linearly under the atmospheric forcing, which can be simply represented by the thermal diffusion scheme in the previous section. Once freezing (thawing) begins, the phase transition processes involve in the highly nonlinear relationship between soil temperature, ice content and liquid content, which is caused by the release of latent heat (detail in section 2.2.4). This highly non-linear system makes it difficult for a numerical algorithm to reach convergence at a typical time step of land hydrological modeling (hourly).

Instead of solving temperature and ice content profile explicitly, this new scheme introduces two new variables: enthalpy and total water mass to express soil temperature, liquid water content, and ice content. Enthalpy not only can retains energy conservation, but also can represent the continuous and slow energy change of the whole soil system, compared with the discontinuous changes of temperature and the dramatically changing ice content during the freezing/thawing process. The volumetric enthalpy H_{soil} is defined as a thermodynamic energy potential that consists of the internal energy of the system and the potential energy for phase change:

$$H_{soil} = C_v(T - 273.15) - L_i\theta_i\rho_i \ . \tag{2.26}$$

In addition, total water mass m is employed to maintain water mass conservation in the liquid–ice phase change, defined as:

$$m = \rho_l\theta_l + \rho_i\theta_i \ . \tag{2.27}$$

Introduction of enthalpy and total water mass offers a simple way to represent the phase transition processes and solve highly non-linear differential equations.

Another characteristic of frozen soil is that at subfreezing temperatures not all the liquid water transforms to ice and partial water remains in liquid form, adhering to soil particles. This freezing point depression of capillary bound water is related to the soil water potential exerted by surface tension, expressed by the Clausius–Clapeyron equation[*Clapeyron*, 1834; *Clausius*, 1850]:

$$\frac{dP}{dT} = \frac{P - P_0}{T - T_0} = \frac{L_i}{T_0 \Delta v} \tag{2.28a}$$

where P is the water pressure in soil (Pa, d$P=\rho_l g\, \psi_m$) and Δv is the specific volume change of ice-liquid phase transition (m^3/kg) which is $v_i - v_l = \frac{1}{\rho_i} - \frac{1}{\rho_l} = 0.09 \times 10^{-3}$ m^3/kg. The absolute point (T_0, P_0) is (273.15K, 101325 Pa). Based on the assumption that ice was formed under ordinary atmospheric pressure while osmotic pressure of water is zero[*Fagerlund*, 1973; *Hansson et al.*, 2004], this generalized Clausius–Clapeyron equation (2.28a) can be reformed, as follow:

$$\psi_m(\theta_l) = \frac{L_i (T - T_f)}{0.09 g T_f}, \tag{2.28b}$$

where ψ_m is soil water head (m), T_f is 273.15 K, $T-T_f$ is the freezing point depression, and g is the gravitational constant (9.8 N/kg). This expression is also called the water freezing depression equation which is widely applied in describing freezing point depression of water due to pressure change during phase transition. In the unsaturated frozen soil, because $\psi_m(\theta_l)$ is a function of unfrozen liquid water, an important relationship between θ_i, θ_l, and T is obtained by extending the derived Clapeyron equation (equation 2.28b):

$$T = \frac{0.09 g T_f \psi_m(\theta_l)(1 + c_k \theta_i)^2}{L_i} + T_f, \tag{2.29}$$

where c_k is an adjustable constant, accounting for the increased interface between soil particles and liquid water owing to the increased number of ice crystals. This equation connects the soil

temperature to the amount of unfrozen soil moisture, which is widely used to calculate the unfrozen liquid water content for frozen soil.

To solve the nonlinear phase change system efficiently and stably, we designed numerical approximations of Equations (2.26), (2.27) and (2.29) and an iteration scheme for solving them. The solutions of three unknowns (i.e., liquid water content, ice water content and soil temperature) are obtained through the following procedures for each layer independently.

In the first step, we assumed no freezing and thawing during thermal diffusion and that the soil is thawed. Namely, $\theta_i = 0$, all the water is in liquid form $\theta_l = m/\rho_l$ and soil temperature $T = H/C + T_f$. A critical temperature *T** is proposed to identify the phase state of each soil layer. *T** is defined as follows:

$$T^* = \frac{0.09 g T_f \psi_m(\theta_l)}{L_i} + T_f . \tag{2.30}$$

If $T \geq T^*$, then our assumption of thawed soil is correct and the solution of *T* from the first step is true, $\theta_i = 0$, $\theta_l = m/\rho_l$.

If $T < T^*$, the soil layer is definitely in a frozen state. In this case, θ_i, θ_l and *T* are solved iteratively by using *H*, *m* and the derived Clapeyron equation. In the following iteration steps, a superscript *t* indicates the time step and a subscript *n* indicates the iteration step:

(1) Initialization of *H* and *m*: $H = C_v(T^{t+1} - 273.15) - L_i \theta_i^t \rho_i$, $m = \rho_l \theta_l^t + \rho_i \theta_i^t$. Once *H* and *m* are set, energy and water mass conservations are maintained by *H* and *m* through all the iteration steps during a single time step.

(2) Initialize the soil state as unfrozen soil: $\theta_{i(0)} = 0, \theta_{l(0)} = m/\rho_l$, $T_0 = H/C + T_f$.

(3) Solve Equation (2.29) using the Newton iteration method and define a function $f(T_n)$ as follows: $f(T_n) = \frac{0.09 g T_f \psi_m(\theta_l)(1 + c_k \theta_i)^2}{L_i} + T_f - T$. (2.31)

An approximation of soil temperature T_{n+1} for the $n+1$-th iteration step is $T_{n+1} = T_n - \frac{f(T_n)}{f'(T_n)}$,

$$f'(T_n) = \frac{0.09 g T_f \psi_m(\theta_l)(1+c_k\theta_i)^2}{L_i}\left[\frac{b\rho_i}{\theta_l\rho_l} + \frac{2c_k}{1+c_k\theta_i}\right]\frac{C}{L_i\rho_i} - 1.$$

(4) Update ice content and soil moisture: $\theta_{i(n+1)} = \left(C_v T_{n+1} - H\right)/L_i\rho_i$,

$\theta_{l(n+1)} = \left(m - \rho_i\theta_{i(n+1)}\right)/\rho_l$ according to T_{n+1}.

(5) Return to Step (3) until the increment of T reaches an extremely small value. Thus, sufficiently accurate θ_i, θ_l and T are obtained in this new freezing/thawing scheme.

It should be noted that *Li et al.* [2009] introduced the two variables enthalpy and total water mass for the solution of soil freezing/thawing processes. They used an explicit algorithm with iterations to solve the full energy and water mass governing equations for all the layers and each time step. In the present algorithm, if ice does not exist in any soil layers (e.g. during summer), then no iteration is needed in this integration time step, which can reduce the number of iterations and improve the efficiency of computation. What's more, this scheme treats the freezing/thawing process as continuous process, without a fixed freezing point, and allows the coexistence of water and ice.

2.4.3 Liquid Water Flow

After freezing and thawing processes, if the ice does not fill the soil pores completely then liquid water will continue to flow through the soil. Four types of water flow processes were described in the vertical soil moisture profile model component, including vertical flow, overland flow, lateral flow, and ground water flow. A more detailed description of the dynamic hydrology model can be found in *Wang et al.* [2009].

The conservation of liquid flow through a frozen or unfrozen, unsaturated vertical soil profile is expressed as a one-dimensional Richards' equation [*Richards*, 1931]

$$\frac{\partial\theta_l}{\partial t} = -\frac{\partial q_{vertical}}{\partial z} + E, \tag{2.32}$$

where θ_l is the liquid water content, E is the evaporation or transpiration, and z is the depth from the soil surface (m). The soil water flux in the vertical direction, $q_{vertical}$ ($m^3\ s^{-1}\ m^{-2}$), is described by Darcy's law [*Darcy*, 1856]:

$$q_{vertical} = -K_h(\theta_l, T)[\frac{\partial \psi(\theta_l, \theta_i)}{\partial z} - 1], \tag{2.33}$$

where K_h is the hydraulic conductivity ($m\ s^{-1}$) and ψ is the soil matric potential (m). Liquid water movement is limited by the impermeability of ice and the low surface tension of cold water. In the unsaturated frozen soil, the ice effect on K_h and ψ should be considered and expressed as functions of not only liquid water, but also of ice content and soil temperature. The parameterization of hydraulic properties is given in Section 2.5.2 in detail.

Instead of solving soil moisture directly, this numerical algorithm firstly solves water fluxes $q_{k,k+1}$ between soil layers, then obtains the soil moisture of each layer [*Wang et al.*, 2009b].

$$q_{k,k+1} = K_{h(k,k+1)}[\frac{\Delta \psi(\theta_l)}{\Delta \theta_l} \frac{(\theta_{l(k)} - \theta_{l(k+1)})}{z_{k+1} - z_k} + 1] \tag{2.34}$$

For the surface layer:

$$\theta_{l(1)}^{t+1} = \theta_{l(1)}^{t} + \frac{q_1^{t+1} - q_{1,2}^{t+1} - E_g / \rho_w}{\Delta z_1} \Delta t\ . \tag{2.35a}$$

For the root zone layer:

$$\theta_{l(k)}^{t+1} = \theta_{l(k)}{}^{t} + \frac{q_{k-1,k}^{t+1} - q_{k,k+1}^{t+1} - E_{ct} / \rho_w}{\Delta z_k} \Delta t\ . \tag{2.35b}$$

The deep zone layer:

$$\theta_{l(k)}^{t+1} = \theta_{l(k)}{}^{t} + \frac{q_{k-1,k}^{t+1} - q_{k,k+1}^{t+1}}{\Delta z_k} \Delta t\ . \tag{2.35c}$$

E_g and E_{ct} are ground surface evaporation and canopy transpiration, respectively. Inserting Equations (2.35a)–(2.35c) into Equation (2.34) and then reorganizing Equation (2.34), we obtain the following equation among $q_{k-1,k}^{t+1}$, $q_{k,k+1}^{t+1}$ and $q_{k+1,k+2}^{t+1}$ between soil layers:

$$A_k q_{k-1,k} + B_k q_{k,k+1} + C_k q_{k+1,k+2} = D_k, \tag{2.36}$$

where A_k, B_k, C_k and D_k are the known coefficients and functions of $\theta_{l(k)}$, $\theta_{l(k+1)}$ at the previous time step. Water fluxes at the current time step can be solved using this tridiagonal equation system. After the solution of water fluxes, the soil moisture of each layer can be easily obtained from Equations (2.35a)–(2.35c).

For the upper boundary conditions, the input water from the surface layer mainly depends on direct rainfall, canopy drainage, snow melting, and surface runoff:

$$q_1 = D_d + D_c - E_{gi} - R_{off}, \tag{2.37}$$

where D_d is the direct rainfall rate (m s^{-1}), D_c is the canopy drainage rate (m s^{-1}), E_{gi} is the evaporation rate of ground interception, and R_{off} is the surface runoff.

This submodel also allows soil water flow laterally along the hillslope. Inside the unsaturated zone, interflow occurs as a result of gravity when soil moisture θ_l exceeds the field capacity θ_f [*Wang et al.*, 2009b] as follows:

$$q_{sub} = K_h \sin\beta, \quad \theta_l > \theta_f, \tag{2.38}$$

where q_{sub} is the lateral interflow rate (m^3 s^{-1} m^{-1}) and β is the slope of a grid cell. The total interflow of a grid cell is the summation of q_{sub} from all the sublayers.

In this model, the aquifer layer is a crucial connection between the unsaturated zone and the river, which allows discharge or recharge among the unsaturated soil zone, groundwater layer, and river. All the grid cells in one flow interval share the same groundwater level. The groundwater flows here are treated as steady flow using Darcy's law [*Wang et al.*, 2009b].

After the vertical infiltration, the infiltration excess (Horton overland flow) and saturated excess (Dunne overland flow) can be obtained at the upper boundaries of the unsaturated zone to generate surface runoff. When water intercepted over ground, M_{gw}, is greater than the detention capacity, M_{gwmax}, surface flow will flow downslope, and can be described as a steady constant sheet flow using Manning's equation[*Manning et al.,* 1890]:

$$q_{sfc} = \frac{1}{n_s}(\sin\beta)^{1/2}(M_{gw} - M_{gwmax})^{5/3}, \tag{2.39}$$

where q_{sfc} is the surface runoff interflow rate ($m^3\ s^{-1}\ m^{-1}$) and n_s is Manning's roughness parameter.

2.5 Parameter estimation for frozen soil

2.5.1 Thermal Properties

Ice changes the dynamics of soil thermal fluxes through the dependence of soil thermal properties (thermal conductivity and volumetric heat capacity) on soil liquid water and ice content. The thermal conductivity of liquid water is 0.57 W m^{-1} K^{-1}; whereas, the value for ice is 2.2 W m^{-1} K^{-1}, four times higher than the liquid water thermal conductivity. Increasing ice content of soil raises its thermal conductivity. Soil of 1400 kg m^{-3} bulk density with 40% ice content has a thermal conductivity about 1.14 times higher than that of the same soil with 40% water content. Until now there has been no theory comprehensive enough to predict the thermal conductivity of frozen soil, but various empirical methods based on field measurements for computing thermal conductivity have been developed [*Sun,* 2005]. The method of Johansen [*Johansen*, 1977] is recommended by Farouki [*Farouki*, 1986] and Peters-Lidard et al. [*Peters-Lidard et al.*, 1998]. Yang [*K Yang et al.*, 2005] modified the method by merging this formula with a global soil data task formula and improved its performance in the freezing situation. In our study of frozen soil, we modify the method of Yang by embedding the ice part of the formulas by *Vafai and Whitaker* [*Vafai and Whitaker*, 1986]:

$$K_t = K_{dry} + K_{wet} + K_{ice}, \tag{2.40}$$

$$K_{ice} = \theta_i K_i = \theta_i \times 2.2, \tag{2.40a}$$

$$K_{dry} = (0.135\rho_d + 64.7)/(2700 - 0.947\rho_d), \tag{2.40b}$$

$$K_{wet} = (K_{sat} - K_{dry})\exp[f(1-1/w)], \tag{2.40c}$$

$$K_{sat} = 0.5^{\theta_s}(7.7^{q_c}2.0^{1-q_c})^{1-\theta_s}, \tag{2.40d}$$

where K_t is the thermal conductivity of frozen soil (W m^{-1} K^{-1}) computed using the sum of the thermal conductivity of dry soil, wet soil, and ice (K_{dry}, K_{wet}, and K_{ice}, respectively); K_i , K_{sat} are the thermal conductivity of ice and saturated soil, respectively; θ_s . w is the effective wetness of soil, defined as the ratio of liquid water to saturated soil moisture; ρ_d is the bulk density of a dry soil; f is a coefficient with a value of 0.36; and q_c is the quartz content in dry soils.

Moreover, the specific heat capacity of water is 4.195 J K^{-1} g^{-1}, while that of ice is 2.1 JK^{-1} g^{-1}, suggesting that a soil containing a high ice content has lower heat capacity than a soil with an equivalent content of liquid water. The volumetric heat capacity C_v is computed as a sum over the specific heat capacities of the soil constituents (J m^{-3} K^{-1}), using the following equations:

$$C_v = \sum_i c_i \rho_i \theta_i = c_d \rho_d + c_l \rho_l \theta_l + c_i \rho_i \theta_i, \tag{2.41}$$

$$C_d \rho_d = (0.076 + 0.748\rho_d / \rho_l) \times 10^6, \tag{2.41a}$$

$$C_l \rho_l = 4195 \times 10^3, \tag{2.41b}$$

$$C_i \rho_i = 2100 \times 920, \tag{2.41c}$$

where C_d, C_l, and C_i represent the specific heat capacity of dry soil, liquid water, and ice (JK^{-1} Kg^{-1}); ρ_d is the bulk density of a dry soil; and ρ_l (1000 kg m^{-3}) and ρ_i (920 kg m^{-3}) are

the densities of liquid water and ice.

2.5.2 Hydraulic Properties

Ice in frozen soil not only affects thermal processes, it also affects hydrological processes by modulating hydraulic properties such as permeability, hydraulic conductivity, and saturated soil moisture. The impermeable frozen soil generally prevents rainfall and snowmelt from infiltrating into deep soil, which may influence runoff generation and groundwater recharge. We used the method proposed by Wang et al. [*L Wang et al.*, 2010]. The soil water hydraulic conductivity K_h and ground water hydraulic conductivity K_G of each layer are described by adding a freezing factor for considering viscosity rise with temperature drop and the presence of ice:

$$K_{h(ice)} = f_{ice} K_{h(k)} = \exp(-10(T_f - T_k)) K_s \Theta^{\frac{1}{2}} [1-(1-\Theta^{1/m})^m]^2, \tag{2.42}$$

$$K_{G(ice)} = f_{ice} K_G = \exp(-10(T_f - T_N)) K_G, \tag{2.43}$$

$$\psi = \frac{[1/\Theta^{1/m} - 1]^{1/n}}{\alpha} \text{ and } \Theta = \frac{\theta_l - \theta_r}{\phi - \theta_i - \theta_r}, \tag{2.44}$$

$$\theta_s = \phi - \theta_i, \tag{2.45}$$

where θ_r is residual water content; ϕ is the soil porosity; K_s is the saturated hydraulic conductivity α, n, and m are empirical parameters in Van Genuchten's equation [*Van Genuchten*, 1980]; and T_k and T_N are soil temperatures at the k^{th} layer and bottom soil layer, respectively. Eventually, by using these updated hydraulic properties, the vertical soil moisture profile, lateral runoff, and exchange with ground water are computed in the original hydrological module.

2.6 Summary

For deep understanding of the hydrological processes and the physical characteristics of frozen soil, the physics of frozen soil is introduced firstly including the 6 impact factors of frozen soil, hydraulic and thermal characteristics, ground surface energy and mass balance,

heat-water transfer and phase change processes within frozen soil through the complete energy and mass balance equations. Note that freezing/ thawing involves a highly nonlinear relationship between ice content, soil temperature and liquid water, and is a continuous process with no fixed freezing point.

A multi-layer, enthalpy-based frozen soil model was developed to represent the phase change and heat–water flow in frozen soil based on the modified one-dimensional land surface scheme. In order to improve the robustness and efficiency of frozen soil modeling, we proposed a critical temperature criterion to judge the phase state, and introduced enthalpy and total water mass into the derived Clapeyron equation to simulate the freezing/thawing process. This frozen soil scheme offers a simple method for solving highly non-linear equations stably and reduces the computation time for greater efficiency. Furthermore, freezing/thawing is treated as a continuous process, without a fixed freezing point, and allows the coexistence of water and ice.

The frozen soil algorithm presented in this study includes four main parts: 1) a land surface scheme to describe the energy and mass exchange between the frozen ground and the atmosphere, 2) a heat diffusion scheme implementing the thermal diffusion equation to describe heat conduction between soil layers, 3) a freezing/thawing scheme to represent ice formation/melt, corresponding latent heat release/absorption and temperature adjustment, and 4) a water flow scheme to describe the liquid movement in frozen soil and exchange with aquifers. Additionally, a parameterization set for frozen soil is updated to approximate realistic changes in hydraulic and thermal properties owing to the presence of ice and unfrozen soil water.

3. VALIDATION OF FROZEN SOIL MODEL IN A PERMAFROST BASIN

3.1 Site and dataset

Binggou Watershed is a high mountainous drainage watershed of the Qilian Mountains in a typical cold region of northwestern China (Figure 3.1). This watershed is in the upper reaches of the Heihe River Basin. Its area is as small as 30.4 km^2, but its elevation is very high, varies from 3440 to 4400 m. Above 4000 m elevation, permafrost dominates with a subzero temperature period as long as 9 months per year; however, below 4000 m, permafrost is distributed discontinuously with subzero temperatures for 7 months of the year (October–April) [*Z Yang et al.*, 1993]. The annual mean air temperature is as cold as −7°C in the headstream area and the annual mean precipitation is about 686 mm, of which 26% is snowfall from October to April. On average, the seasonal snow depth is about 0.5 m and reaches a maximum of 0.8–1.0 m [*Z Yang et al.*, 1993].

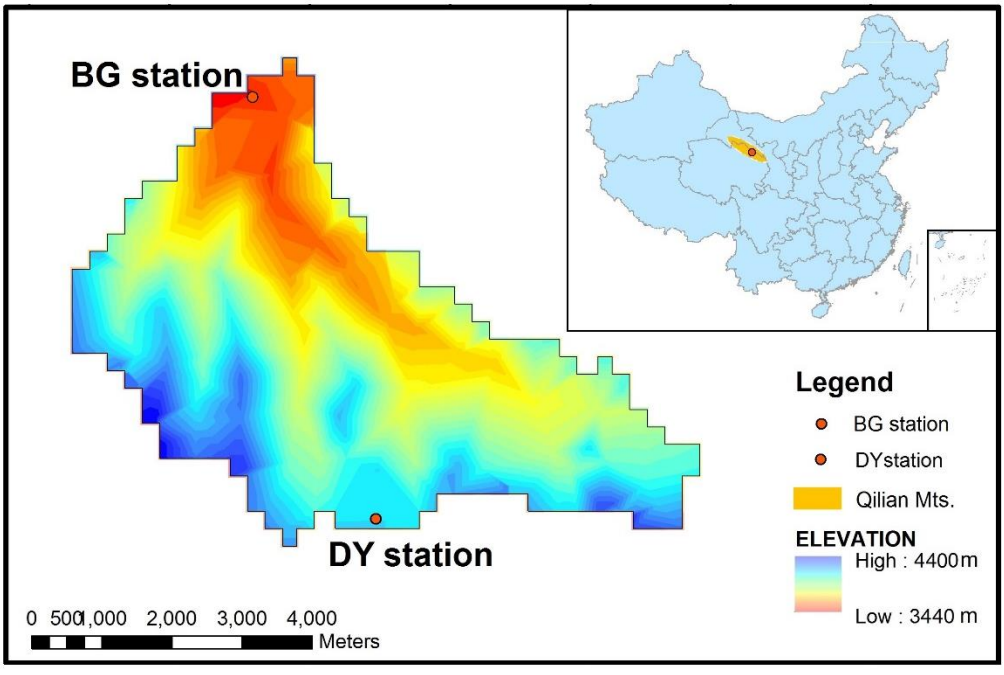

Figure 3.1. Map of the DY station and BG station at Binggou basin in Qilian Mountains of China.

The model was tested in this Binggou basin using comprehensive observation datasets from the Water Allied Telemetry Experimental Research (WATER) project [*X Li et al.*, 2009b]. A well-equipped automatic weather station, Dadongshu-Yakou (DY, 38° 01′ N, 100° 14′ E, 4146.8 m altitude), is located at a flat highland (Figure 3.2(a)) in the upper reaches of the Binggou basin. Another water gauge station, Binggou (BG, 38° 04′ N, 100° 13′ E, 3449.4 m altitude), is located at the basin outlet (Figure 3.2(b)), equipped with a cup-type current meter.

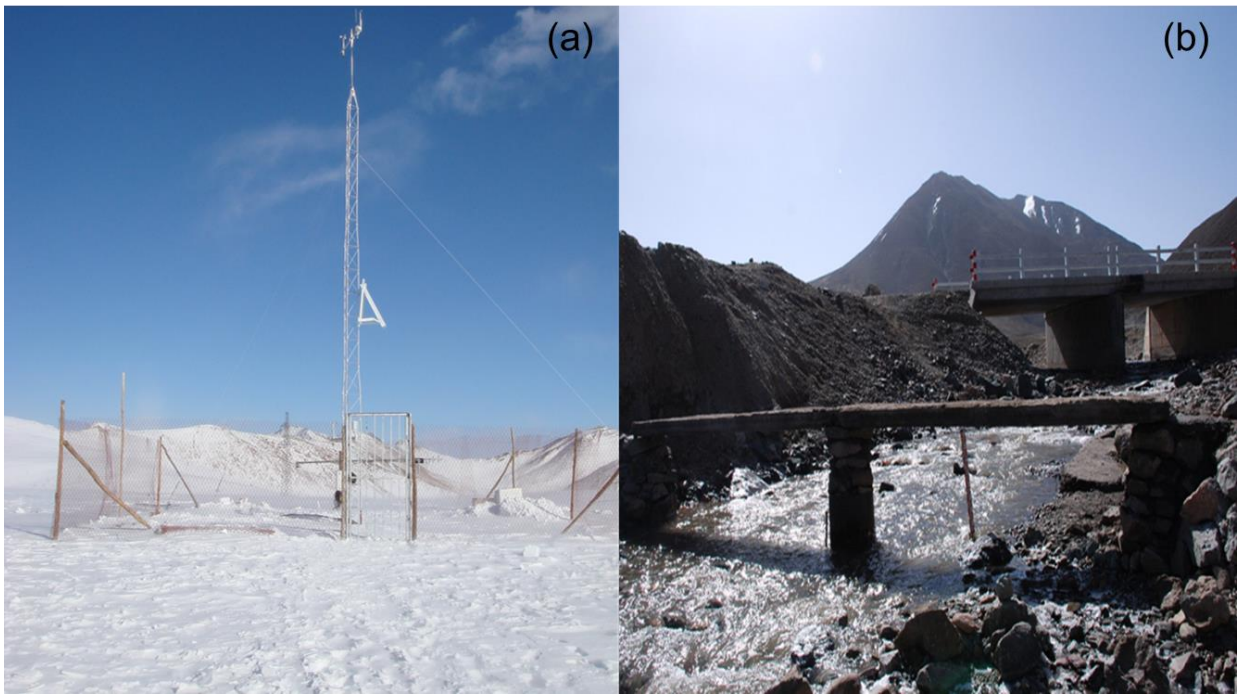

Figure 3.2. DY station (a) and BG station (b) at Binggou basin in Qilian Mountains of China [*J Wang et al.*, 2008a; *J Wang et al.*, 2008b].

Measurements of meteorological forcing data and snow depth from 21 November 2007 to 16 July 2009 were collected from the DY station with an automatic weather station and an ultrasonic snow depth sensor. The soil water content and soil temperature are measured at six depths: 5, 10, 20, 40, 80, and 120 cm every 10 min. Hourly data series for the DY station including precipitation, air temperature, relative humidity, wind speed, and the downward long- and short-wave radiation, were used as the forcing data to run the model for the whole watershed, because this Binggou basin is small enough to treat its weather states as homogenous. Since the BG station started its observation from 2008, we can obtain the discharge data from Jan 17 2008 to July 16 2009 for model validation with the frequency of 1-3 times per day.

In this watershed, from 3500 to 4000 m, the land is covered by alpine meadow; whereas, the area higher than 4000 m is alpine desert with little vegetation. The land cover type was reclassified as broadleaf shrubs with bare soil in the SiB2 classification system. The dynamic

vegetation parameters including Leaf Area Index (LAI) and Fraction of Photosynthetically Active Radiation (FPAR) were obtained from the Level 4 MODIS (Moderate Resolution Imaging Spectroradiometer) global LAI and FPAR product. The subgrid topography of this grid was described by a 50 m DEM.

3.2 Model initialization and calibration

To optimally estimate the model parameters and set up the initial conditions, a point scale optimization procedure was carried out based on either field observations [*X Li et al.*, 2009b] or parameters calibrated in the same basin by Wang et al. [2010]. Calibration was applied on the summer (1 July–31 August 2008) of the first year. The calibrated parameters are applied in both the frozen soil model and Hydro-SiB2. The thicknesses of soil layers were uniformly set to 10 cm, except 5cm for surface layer. The soil column was divided into 40 layers and the lower boundary condition was placed at 4 m depth.

As for morphological and physiological properties of vegetation static parameters, the heights of the canopy top and canopy bottom, the root depth, leaf length, and canopy cover fraction were given as 0.05, 0.005, 0.25, 0.03, and 0.2 m, respectively. The soil properties, including soil pore size, residual soil moisture, sand content, bulk density, soil reflectance of visible radiation, and surface emissivity, were obtained using the values recommended by Wang et al. [*L Wang et al.*, 2010] and Sun [*SUN*, 2005]. The Van Genuchten parameters α and n, which control soil hydraulic conductivity, were calibrated based on a comparison between the simulated and observed soil moisture during the summer season. The original FAO values were retained for the other hydraulic properties [*FAO*, 2003].

The initial soil temperature and liquid water content of each layer were given by interpolating the observed soil temperature and liquid water content at six depths using the inverse distance weighting method. The initial snow water equivalent of snow pack on the ground was assigned by calculating from the observed snow depth with the assumption of an average snow density of 0.2 g cm^{-3}.

Because ice content measurements were unavailable, it was not possible to obtain the initial soil ice content profile from observations. However, initial ice contents are critical parameters for simulation in permafrost areas in which ice is present all year round. Ice not only affects initial thermal and hydraulic properties, but also determines how much water will be passed to

soil after melting and how much energy will be needed for melting in the next warm season. More ice in a certain layer means that water is prohibited from infiltrating further down, which leads to low soil moisture in sublayers. As a result, melting event may subsequently be postponed because more energy is needed. Different initial ice contents can therefore lead to considerable differences in soil moisture results and the freezing/thawing simulation. Obtaining a realistic initial ice profile is a major challenge for permafrost modeling.

To solve this problem, we conducted a 20-year spin-up simulation with repeat year forcing (21 November 2007–20 November 2008), with the assumption that there is no ice present in the beginning. Figure 3.2 shows the ice content results of this 20-year simulation. Ice grows gradually from zero to permafrost formation and shallow soil reaches freezing/thawing equilibrium. According to the soil temperature and soil moisture observations, the soil at 80 cm thawed in the warm season and was frozen for the whole year at 120 cm. Therefore, it is reasonable that the ice profile should be confined to the location of the permafrost table (between 80 and 120 cm in the warm season). In this study, the results of the 13th year matched the above requirements and the ice profile in the 13th year was thus selected.

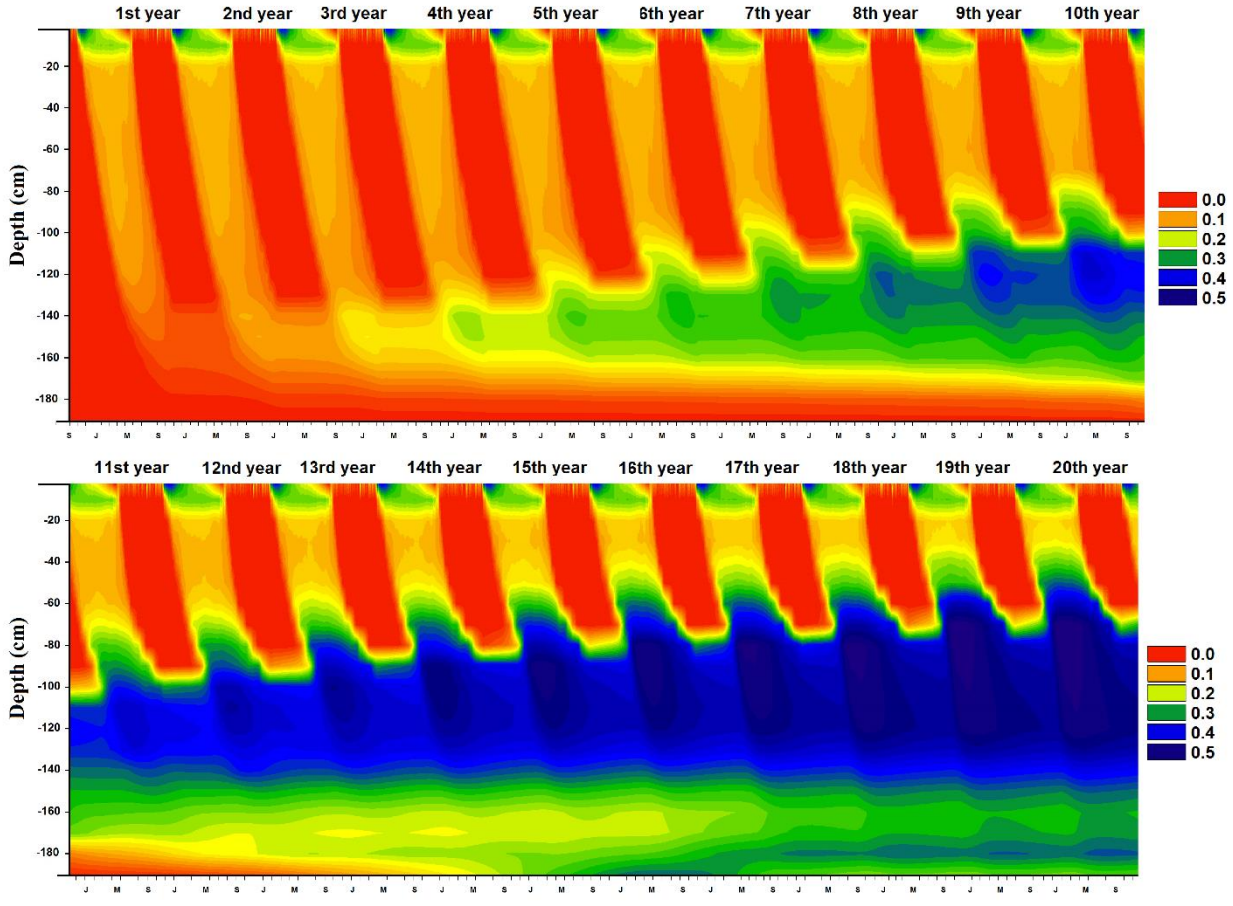

Figure 3.2. Volumetric ice content profile of the 20-year spin-up simulation.

For seasonally frozen soil, simulation can start from summer without considering ice content initialization. However, ice content initialization is unavoidable for permafrost and difficult to set properly. The number of years that are needed for spin-up simulation depends on the study object. Shallow permafrost can be formed in tens of years, while deep permafrost formation may take longer time. In permafrost, the ice table raises up and descends down in conjunction with freezing and thawing processes. The height range of the ice table can be judged from soil temperature and moisture observations. By matching the permafrost table heights between spin-up results and observations in thawing and freezing periods, the initial ice content can be determined. This is therefore a potential method for obtaining a suitable ice initial condition for permafrost modeling in the absence of ice observations.

3.3 Results and Analysis

The model was run at hourly time steps with 1.5 years of forcing data from 21 November 2007 to 16 July 2009 to evaluate the model's performance. Three simulation cases were run at point scale at the DY station: the first set of simulations from the modified land surface scheme without frozen scheme (Hydro-SiB2), the second from the Hydro-SiB2 with the enabled thermal diffusion scheme (UNFROZEN), and the third from the frozen soil model developed based on Hydro-SiB2 with both thermal diffusion scheme and the freezing/thawing scheme (FROZEN). The same calibrated parameters were applied to these three simulations. The models were calibrated in the first year and the results were validated across the full one-and-a-half-year period. The simulated numerical results were compared with the observational soil temperature, liquid water content, and thaw depth measured at the DY station. Furthermore, simulated hourly discharge through frozen and thaw periods are validated by using the measured flow rate at the BG station from Jan 17 2008 to July 16 2009.

3.3.1 Soil temperature

Figure 3.3 presents a comparison of the soil temperature at six depths between the frozen soil model results and observational data at the DY station. To show the performance of the thermal diffusion scheme and the freezing/thawing scheme separately, we first compare the UNFROZEN and FROZEN simulation results. It is clear that the large difference between UNFROZEN and FROZEN appears in the freezing and thawing seasons. Without considering the liquid–ice phase change, UNFROZEN can simulate temperature as successfully as

FROZEN in the completely thawed season. However, it produces early warming in the freezing season and early cooling in the thawing season. Use of the thermal diffusion scheme alone is not enough to represent the characteristics of frozen soil when the liquid–ice phase shift occurs.

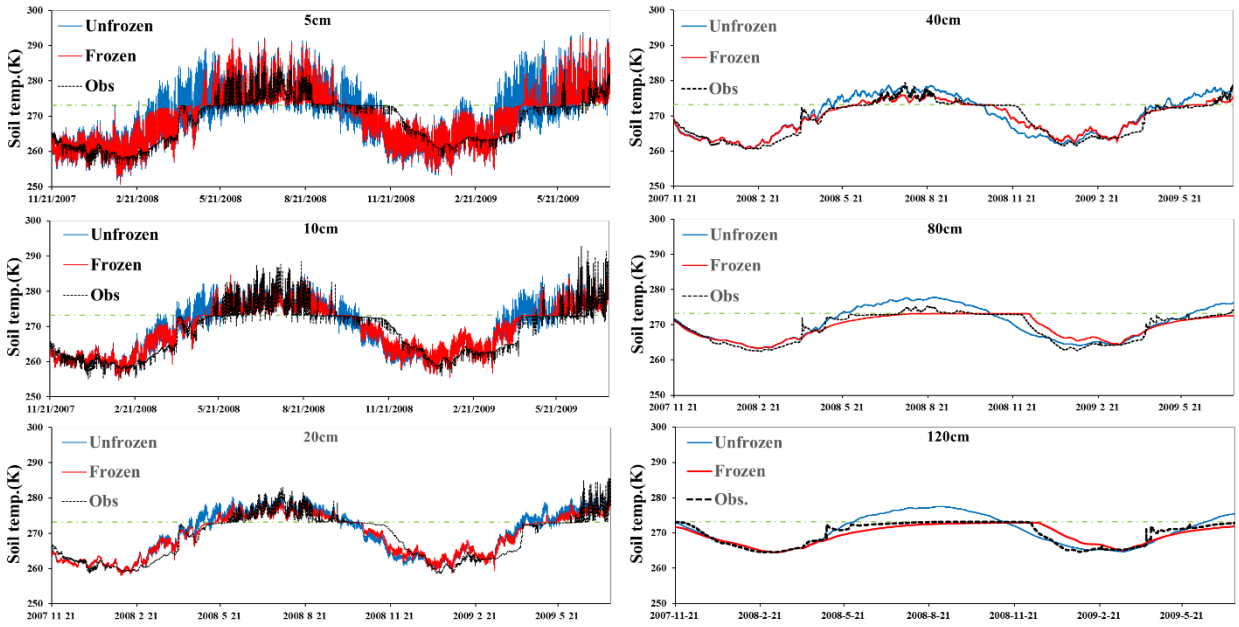

Figure 3.3. Comparison of observed and simulated soil temperature at six soil depths at the DY station (2007–2009). Obs. (black dash) denotes observation data. UNFROZEN (blue solid) denotes results from Hydro-SiB2 with the thermal diffusion scheme only. FROZEN (red solid) denotes results from the frozen soil model with both the thermal diffusion and freezing/thawing schemes. The green dotted line denotes 273.15 K.

In contrast, the results produced by FROZEN are for the most part in good agreement with the observed datasets in magnitude and trend variation. In the freezing and thawing seasons, FROZEN delays the summer warming and winter cooling, and soil temperature is maintained at around 0°C. Figure 3.3 indicates another phenomenon of soil temperature: diurnal variation and annual variation can be seen in the shallow soil (5, 10, 20 cm) and deep soil (40, 80, 120 cm), respectively. The time lag and amplitude damping of temperature become more pronounced with increasing depth and are also well described by the simulation. For the surface 5 cm layer, the simulated soil temperature at 2.5 cm is validated against the observed soil temperature measured at 5 cm. This may contribute to the large diurnal variations of simulated soil temperature in the surface layer. Another potential explanation is snow underestimation in winter. Snow cover above frozen ground can reflect energy and attenuate the diurnal variation of soil. However, the snow scheme in this model, originating from SiB2, is too simple to describe these snow processes accurately [*Shrestha et al.*, 2012]. Although there are some

discrepancies, it is clear from Figure 3.3 that the frozen soil model can predict soil temperatures within a certain depth of frozen soil with good accuracy.

3.3.2 Volumetric liquid water content and ice content

Soil moisture validations made in this study are limited to the liquid water content only because no ice content measurements were available. The simulation results of soil moisture from the frozen soil model are compared with the observations and the soil moisture calculated from the modified one-dimensional land surface scheme (Hydro-SiB2) without considering frozen soil processes (Figure 3.4). The simulations with and without the frozen soil scheme are almost the same for shallow soil during the summer season, in which shallow soil was thawed completely and water in soil mainly originates from rainfall. In contrast, in both the freezing and thawing seasons, Hydro-SiB2 tends to give more liquid water than FROZEN, because of the snow melt caused by early warming of soil and the lack of consideration of freezing water in soil. The comparisons between the observations and frozen soil scheme predictions show that the frozen soil model does reasonably well in representing the soil moisture during the frozen season, thawed season, and freezing season. The most noticeable differences between simulated and observed soil moisture occurred when soil started thawing in spring. Soil moisture increased early in the shallow soil layer (5, 10, and 20 cm), as shown in Figure 3.4. We speculate that the early start of snow melt on the ground caused the early start of soil thawing. The snow scheme used in this model substantially underestimated the amount of snow and melted it quickly. Snow covered the ground surface in winter and its early melt in spring may release snowmelt water to soil and expose the frozen soil to solar energy. In addition, the large peaks of soil moisture at 20 and 40 cm are possibly as a result of macropores, which caused the peak at 10 cm to disappear in the sublayers. Although some discrepancies occurred between observed and simulated soil moisture, the basic features of frozen soil clearly show that in summer the soil moisture variation of active layers are mainly driven by rainfall and in freezing/thawing seasons the liquid water contents dropped or raised rapidly as a result of the freezing and thawing processes, and in winter the frozen soil remains dry. Overall, the frozen soil model was found to simulate soil moisture more successfully than Hydro-SiB2.

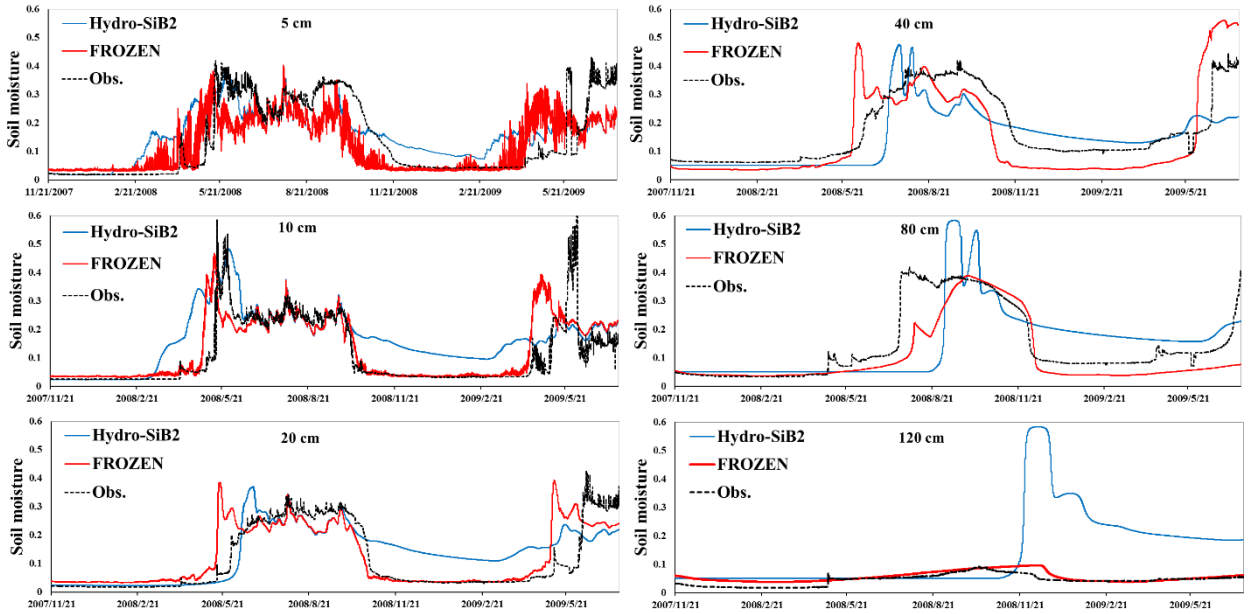

Figure 3.4. Comparison of observed and simulated soil liquid water content at six soil depths at the DY station (2007–2009). Obs. (black dash) denotes observation data. Hydro-SiB2 (blue solid) denotes results from the modified one-dimensional land surface scheme. FROZEN (red solid) denotes results from the frozen soil model with both the thermal diffusion and freezing/thawing schemes.

The simulated liquid water content, ice content, and total water content are shown in Figure 3.5. A large amount of ice coexisted with a little unfrozen liquid water in the winter season from November to May in frozen soil. Note that even when ice contents reached the maximum of 0.55, 0.03 unfrozen liquid water content still remained present as adsorbed films surrounding soil particles. Regardless of the water phase, considerable water storage can be seen from the total water content in frozen soil all year round (Figure 3.5). With the spring thaw, the ice content rapidly dropped to zero while peaks in liquid water content appeared. When ice melted completely, the ice content became zero and total water content equaled the liquid water content. As winter began, ice was regenerated and liquid water diminished. In the deep soil, there was no diurnal variation of soil moisture, but a slow seasonal change with time lag was apparent.

To quantitatively evaluate the the performance of the frozen soil model, we compare the root mean square error (RMSE) and absolute bias (BIAS) (equation 3.1 and 3.2) between observed and simulated temperature and liquid water content from the frozen soil model with those from Hydro-SiB2 without the frozen soil scheme (Table 3.1):

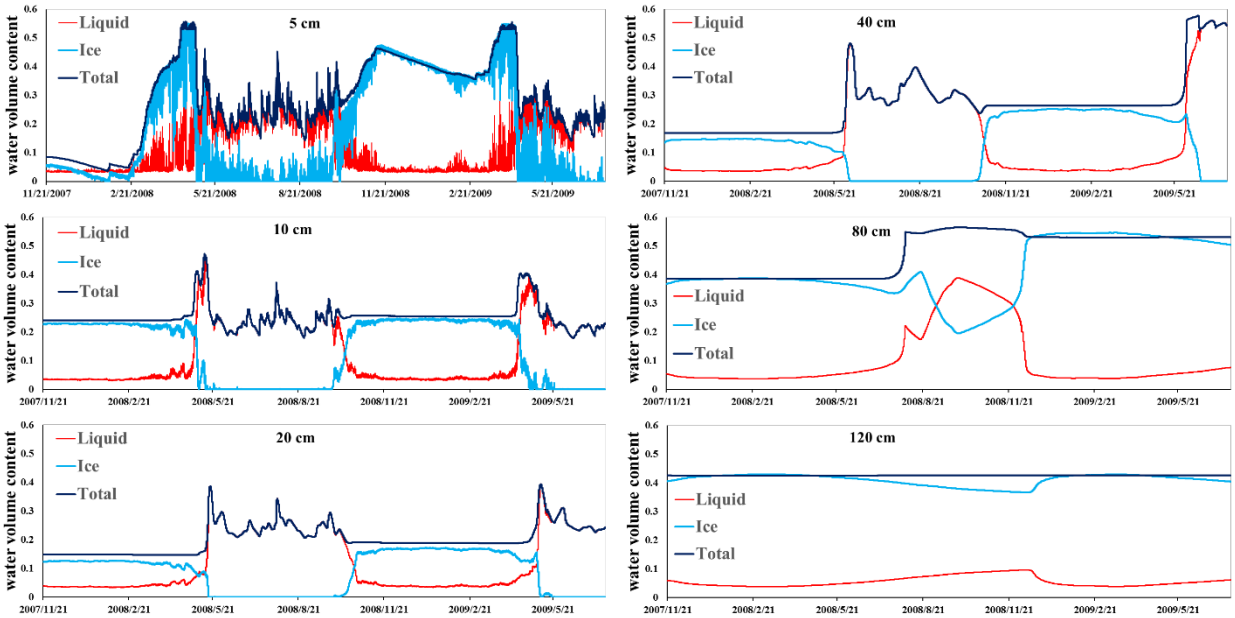

Figure 3.5. Simulated liquid water content (red), ice content (light blue), and total water content (dark blue) at six soil depths at the DY station (2007–2009).

$$RMSE = \sqrt{\frac{\sum_{i=1}^{N}(V_{sim} - V_{obs})^2}{N}} \tag{3.1}$$

$$BIAS = \frac{\sum_{i=1}^{N}(V_{sim} - V_{obs})}{N} \quad . \tag{3.2}$$

Here V_{sim} and V_{obs} are the simulated and observed series; N is the number of observation.

Table 3.1. Error statistics of the frozen soil model and Hydro-SiB2 at six depths at the DY station

Soil depth	Temperature (K)				Liquid water content (m^3 m^{-3})			
	Frozen		Unfrozen		Frozen		Unfrozen	
	RMSE	BIAS	RMSE	BIAS	RMSE	BIAS	RMSE	BIAS
5 cm	4.329	0.449	5.507	0.661	0.089	−0.016	0.089	0.019
10 cm	3.012	0.620	3.623	0.901	0.079	0.015	0.097	0.053
20 cm	2.175	0.543	3.640	0.841	0.070	0.012	0.074	0.026
40 cm	1.408	0.235	2.336	0.824	0.093	−0.025	0.078	−0.025
80 cm	1.355	0.205	1.890	0.984	0.075	−0.039	0.112	0.005
120 cm	1.386	−0.220	1.931	0.707	0.015	0.011	0.158	0.096

Table 3.1 shows that the RMSE and BIAS of frozen soil modeling are apparently less than those of Hydro-SiB2 modeling without frozen soil scheme at all six depths. Overall, the frozen

soil model produces more realistic estimates of both soil moisture and temperature profiles than the model without a frozen soil scheme and can predict the heat and water transfer processes in permafrost region with a reliable accuracy.

3.3.3 Evolution of frozen soil

The permafrost freezing and thawing evolutions are clearly illustrated by mapping the soil liquid water, ice content, and soil temperature contours (Figure 3.6). When the soil temperature dropped to 0°C, freezing began from the soil surface, the freezing front deepened into the soil, ice formed, and the ice content rose rapidly. All soil layers were completely frozen for up to 5 months at the DY station. During the frozen period, soil remained in a state of negative temperature and low liquid water content. Thawing from the surface layer began in late April and descended down to the deep soil with corresponding increases in liquid water content and a reduction in ice content. By late August, the temperature of upper layers was postive, while that of the lower layers remained negative. The seasonally active layer at appoximately 0–80 cm thawed completely in the beginning of September. High liquid water contents were concentrated at the bottom of the active layer because of the impermeability of the ice bed below.

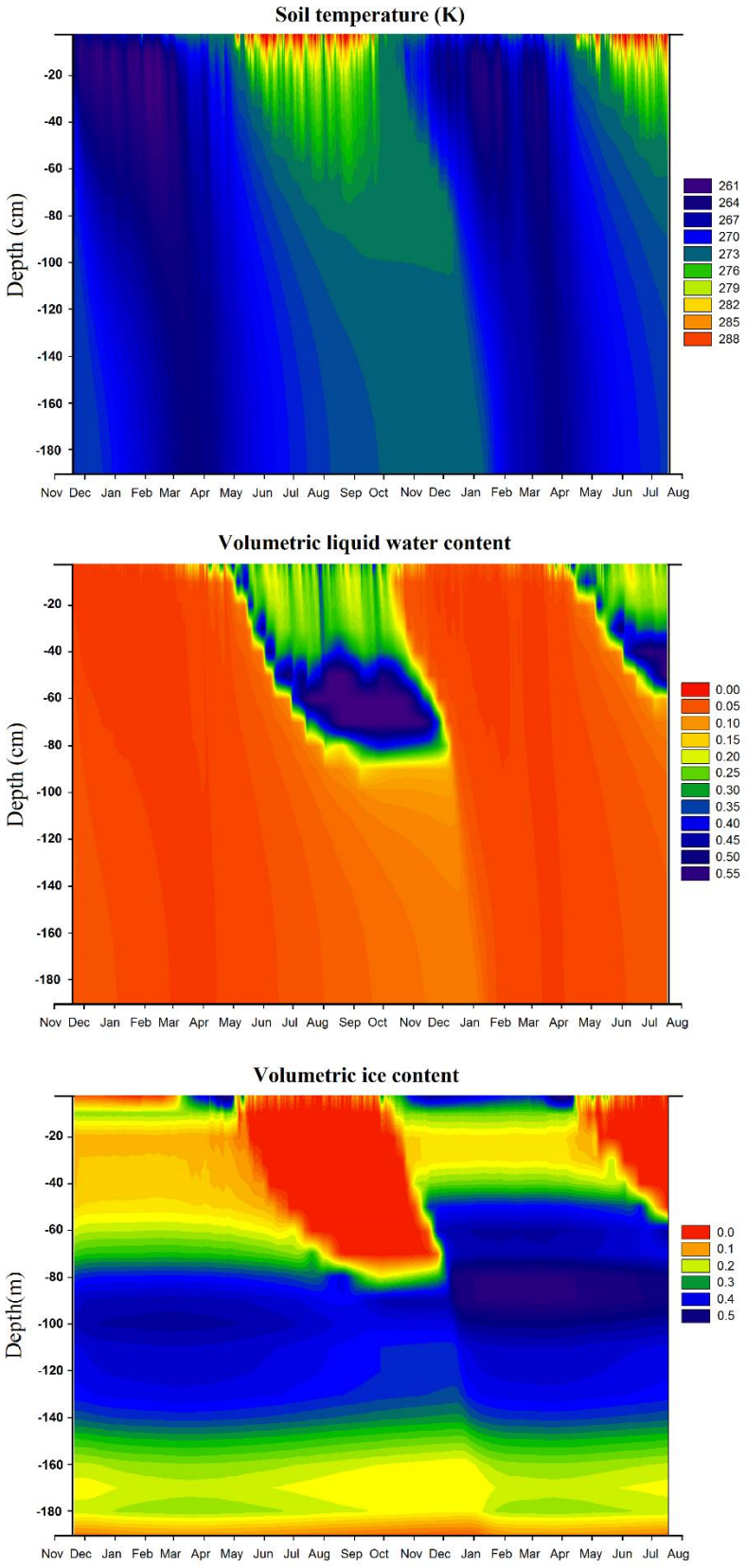

Figure 3.6. Evolution of the soil temperature, liquid water content and ice content profiles from November 2007 to July 2009 at the DY station.

Subsequently, the thawing front descended gradually and the soil began to refreeze downward from the surface again. From October, ice and negative temperatures started to appear as liquid water content dropped 0.1 or lower in the upper layers (0–70 cm). Meanwhile, the middle layers (70–120 cm) remained close to 0°C and the lower layers remained at negative temperatures. Then the soil entered the next freeze-thaw cycle in 2009. In general, soil from the surface to 80 cm depth was the active layer that seasonally thawed during the summer and the underlying soil remained as permafrost at the DY station. This pattern of the frozen soil evolution at the DY site is highly consistent with the features of permafrost reported by Yang et al. (1993).

The thaw front depth was represented by the 0°C isotherm in the simulated soil temperature profile (Figure 3.7). The thaw depth for comparison was determined by linearly interpolating from six depths of soil temperature observations. Thaw front depths were compared only from 21 November 2007 to 30 August 2008, because no observations were present under 120 cm (Figure 3.3) and during this period, the maximum thaw depth was at 120 cm below the lowest depth for zero ice content, because of the coexistence of ice and liquid water at 0°C. Figure 3.7 shows a good match between the simulated and observed thaw front in depth and duration. The early thawing in the surface layer is related to the inadequate snow insulation caused by weak snow simulation in the frozen soil model.

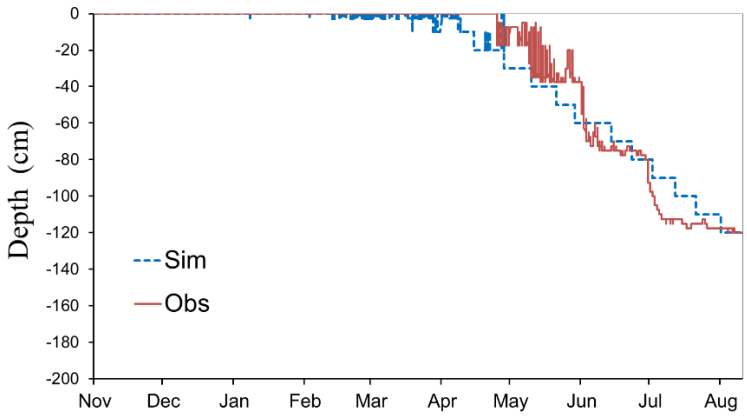

Figure 3.7. Thawing front depths derived from the 0°C isotherm and observation from 1 May to 30 August, 2008 at the DY station.

3.3.4 River Discharge

Hourly hydrographs simulated from Jan 17 2008 to July 16 2009 are displayed in Figure 3.8 against the discharge observation. Note that the discharge were not measured hourly, about 1-3 times per day at the timing of diurnal maximum or minimum. A comparison between the

frozen soil model and WEB-DHM with no frozen scheme is made and it can be seen that the frozen soil model and WEB-DHM have similar performance in summer (June-Sept.). However, there are obvious overestimation during the frozen periods (Oct.-next March) and underestimation during the thaw periods (April-May) by WEB-DHM. While the river flow simulated by the frozen soil model matches well with the true situation. These differences get prominent in the logarithmic hydrograph (Figure 3.9).

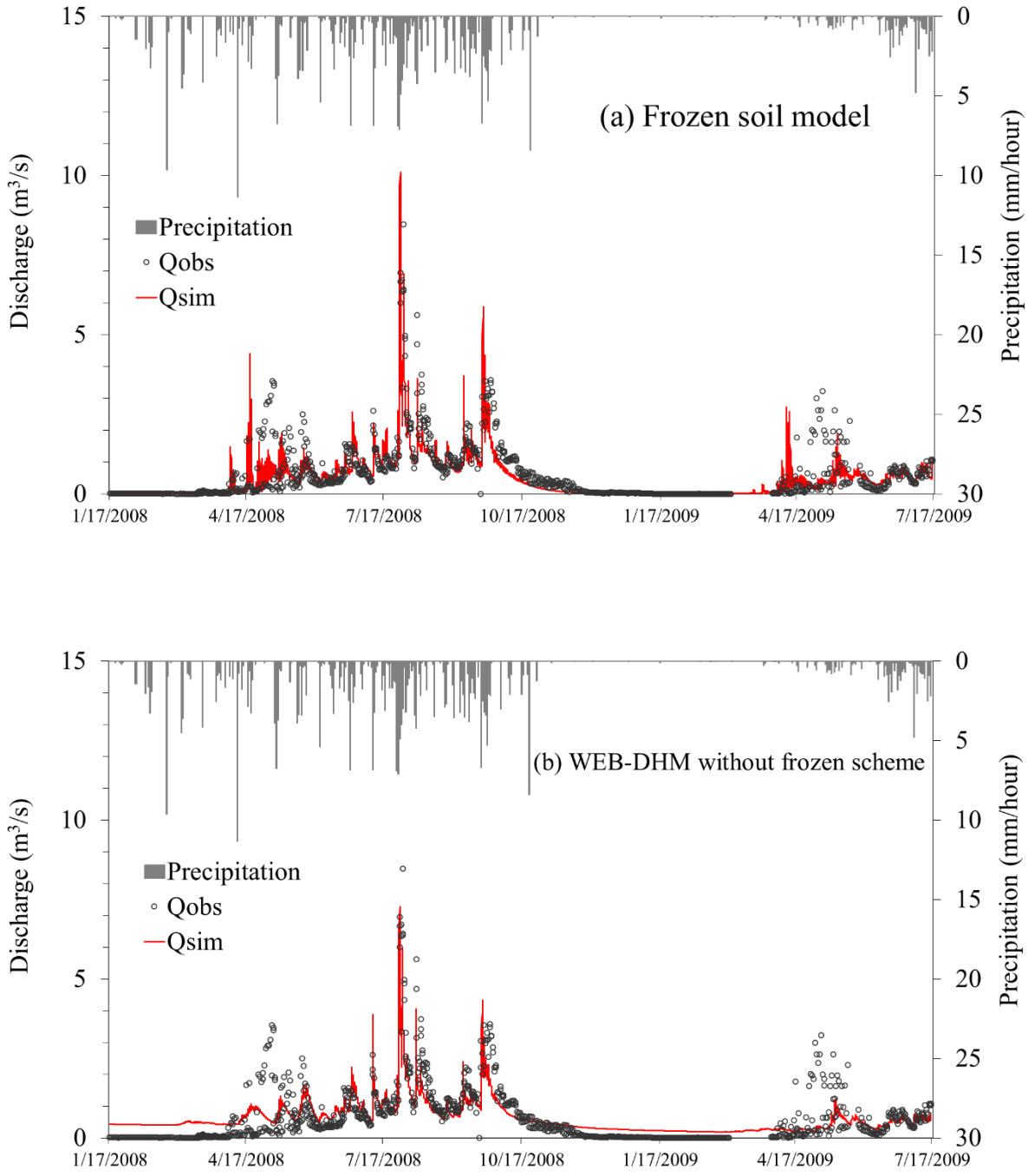

Figure 3.8. Hourly hydrographs simulated by frozen soil model (a) and WEB-DHM model without frozen scheme (b) from 17 January to 21 December, 2008 against the discharge observation at the BG station.

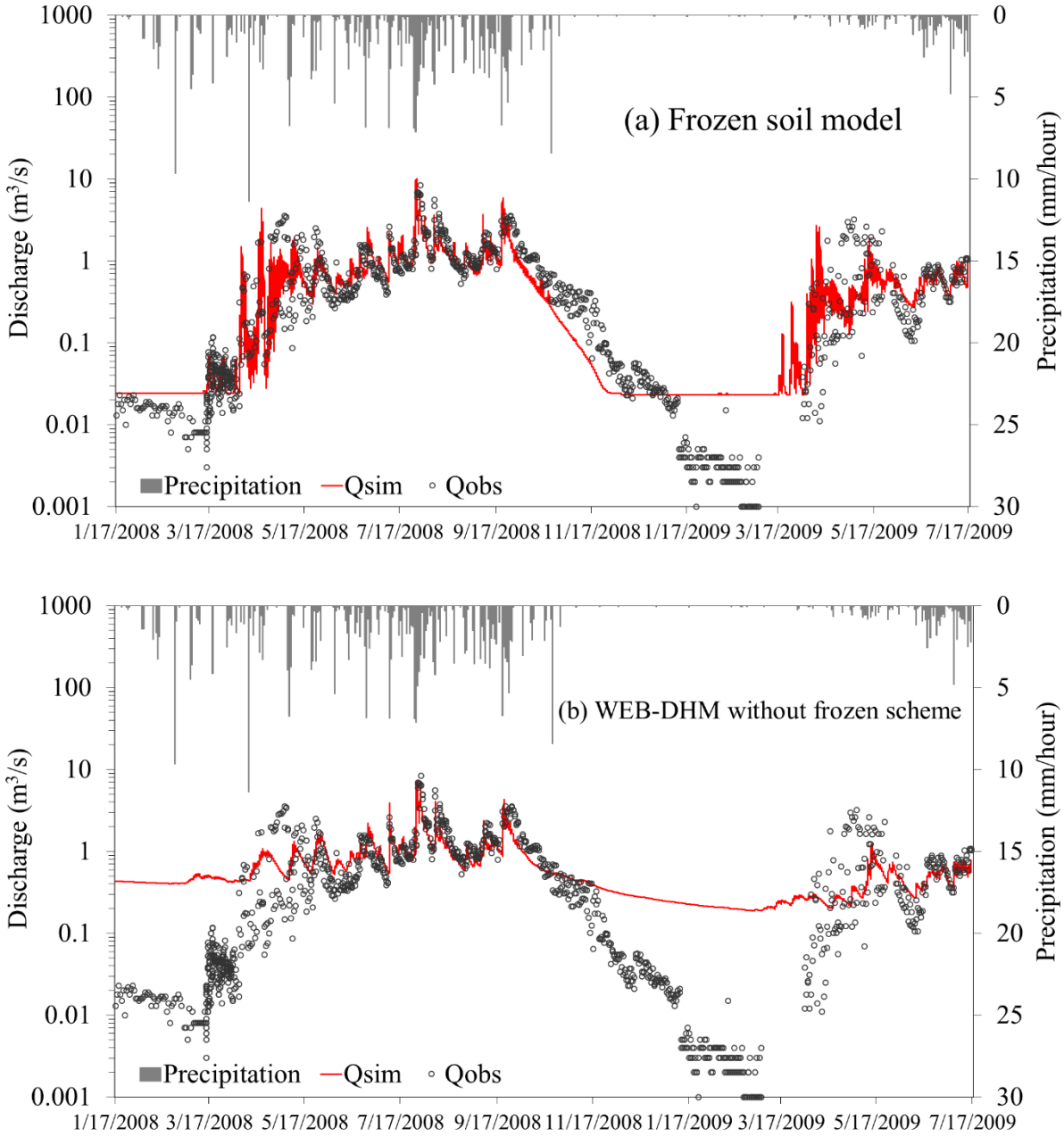

Figure 3.9. Logarithmic hourly hydrographs simulated by frozen soil model (a) and WEB-DHM model without frozen scheme (b) from 17 January to 21 December, 2008 against the discharge observation at the BG station.

From the logarithmic hourly hydrographs, it is clear that the streamflow in winter are significantly overestimated and the snowmelt runoff in spring are underestimated. Actually in this permafrost basin, snow is accumulated over ground and soil water, even river channel, gets frozen due to the extreme cold air temperature in winter. In the Binggou basin, annual hydrological processes stop for almost a half year because of the frozen effect [*Z Yang et al.*, 1993]. WEB-DHM with no frozen soil scheme fails to represent this hydrological characteristic of the permafrost basin. On the contrary, in spring (April-May) river flow increases with air temperature rising, because snowmelt infiltrates a little due to the

impermeability of underlying frozen ground, and snowmelt runoff flows over ground.

We use the Nash–Sutcliffe model efficiency coefficient (NSE) [*Nash and Sutcliffe*, 1970] to quantitatively assess two models' capability of predicting hourly river discharge in the frozen soil basin. The Nash–Sutcliffe coefficient is defined as follows:

$$NSE = 1 - \frac{\sum_{i=1}^{N}(Q_{sim} - Q_{obs})^2}{\sum_{i=1}^{N}(Q_{obs} - Q_{mobs})^2}. \quad (3.3)$$

Here Q_{sim}, Q_{obs} and Q_{mobs} are the simulated discharge, observed discharge and mean observed discharge, respectively.

As shown in table 3.2, frozen soil model (0.654) has generally better performance, compared with WEB-DHM (0.604) from 2008 to 2009 at the Binggou station. During warm periods (June-Sept.), the frozen soil model (0.654) predicted as well as WEB-DHM (0.651) did, because streamflow mainly depends on rainfall in summer and frozen soil in active layers disappeared. NSE of two models show a big difference in cold seasons (Oct.-next March). The NSE of the frozen soil model is as high as 0.719 and that of WEB-DHM is -0.243, which prove that the hydrological model is not able to produce water discharge without considering frozen effect in permafrost basin. In turn, it also brings out that the frozen soil model we developed has a good predictive power in characterizing the winter discharge. In thaw periods of spring (April-May), although both their performance are not so promising, frozen soil model still has better simulation which considered the impermeability of frozen ground. Snowmelt is the main water source during this period. Two possible reasons may account for the poor simulation in the thaw periods: bad snow accumulation/ablation modeling and inaccurate precipitation measurement of snow. The frozen soil model and WEB-DHM use the same snow scheme from Hydro-SiB2. Also, snow flake is difficult to be captured by the general rain gauge in windy conditions [*Woo and Steer*, 1979; *D Yang et al.*, 1988], which tends to underestimate snowfall.

Table 3.2 Nash–Sutcliffe coefficient of the frozen soil model and WEB-DHM with no frozen scheme at the BG station

Periods	2008 - 2009	Summer (June – Sept.)	Frozen Season (Oct. - next March)	Thaw Season (April - May)
Frozen soil model	0.654	0.654	0.719	0.067
WEB-DHM	0.604	0.651	-0.243	0.017

On the whole, the frozen soil model shows the good capability of simulating river

discharge in permafrost basin and capturing the characteristics of cold region hydrological processes.

3.4 Discussion

3.4.1 Diurnal Variation

The results showed that seasonal variation of the frozen soil temperature and moisture in magnitude and trend variation can be captured well by the frozen soil model. However, some frequent oscillations at surface layer can be seen in both soil temperature and moisture (Figure 3.3). We next consider whether these fluctuations are caused by the diurnal cycle of solar radiation or by instability of iteration. The performance of the new model in reproducing diurnal cycle is now discussed in detail. Five days of hourly-results from three typical seasons (a frozen season, a thawed season and a freezing/melting season) were extracted to verify the relationship between the fluctuations and the diurnal variation (Figure 3.10). From 26 to 30 December 2007, surface soil temperatures were consistently below freezing point and varied slightly corresponding to the solar radiation period. Because of its frozen state, the surface soil moisture content remained low (Figure 3.10(a)). When soil thawed completely in summer (5 to 9 July 2008), temperature fluctuations above 0°C became more significant and soil moisture increased, but did not vary according to the temperature fluctuations (Figure 3.10(b)). In the transition season, melting and freezing occurred with diurnal radiation change; surface soil thawed in the day time but froze again at night (Figure 3.10(c)). Soil temperature fluctuated with solar radiation, except during the period of phase change. Soil temperature remained at freezing point and soil moisture fluctuated during periods of alternating freezing and melting. The frozen soil model captured the freezing process at night very well, but the soil temperature increased too fast during the daytime. The overestimation of soil temperature may be attributed to the organic matters in topsoil, which alter soil's thermal and hydraulic properties and mainly leading to cool soil temperatures. The simulation accuracy should be further improved by introducing a soil organic matters into soil parameterizations. Although there are discrepancies between the simulations and the observations, we can still determine the diurnal freezing/thawing process from the timing and the curve shape.

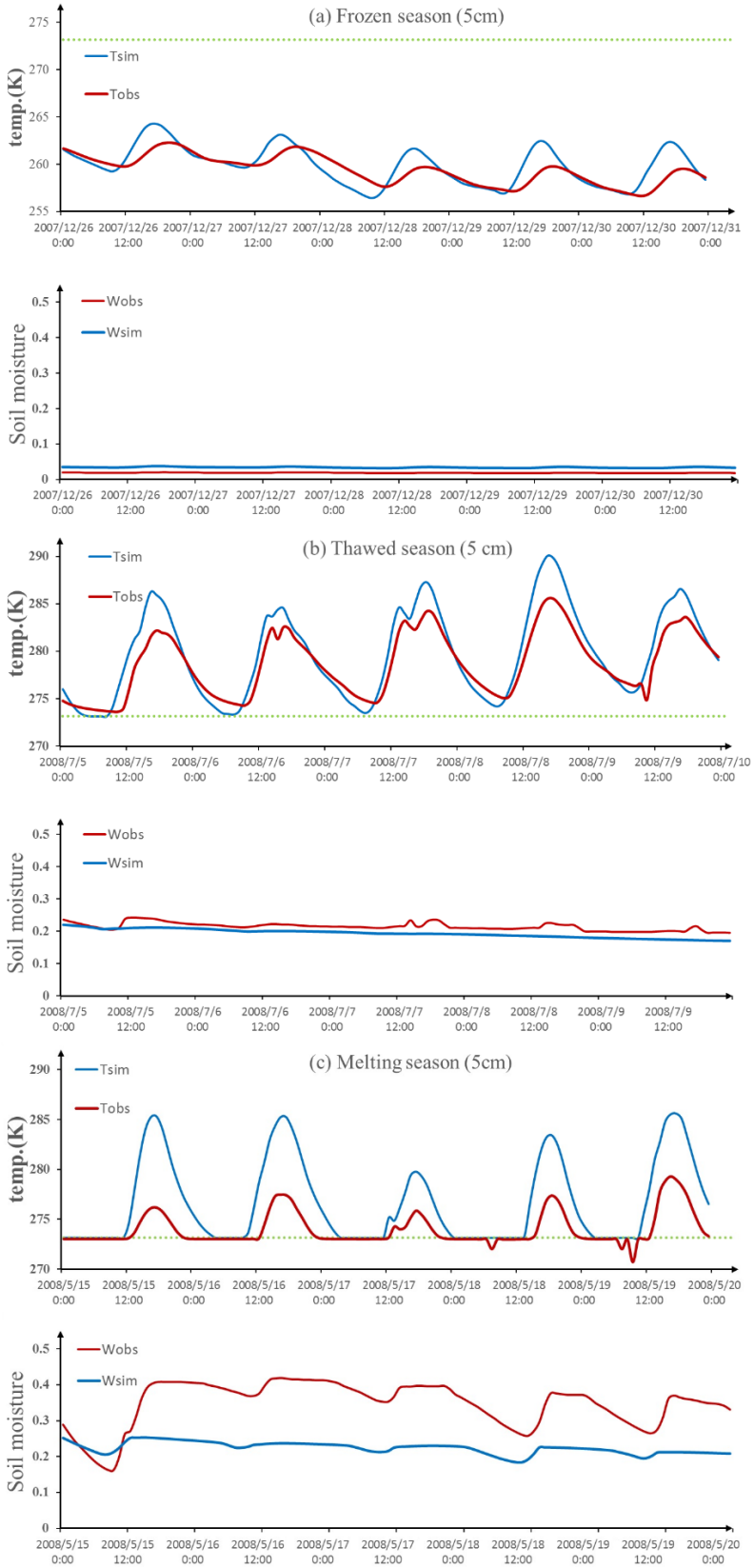

Figure 3.10. Five-day periods of soil temperature and soil moisture at surface layer (5 cm) in the frozen season (26 to 30 December 2007) (a), thawed season (5 to 9 July 2008) (b), and transition season (15 to 20 May 2008) (c). The green dotted line denotes 273.15 K.

It is clear that the new frozen model is able to realistically express diurnal variation of frozen soil temperature and water content at a typical time step (hourly) for different seasons. Notice that the fluctuations in surface temperature and moisture closely follow the diurnal cycle forced by solar radiation, suggesting that fluctuations are definitely not caused by instability of iteration. This in turn proves that the frozen model is stable for obtaining iteration solutions at the hourly time scale, and has the capability to model the diurnal cycle and the freezing/thawing cycle of frozen soil.

3.4.2 Sensitivity to soil depth

In the thermal diffusion part of this frozen algorithm, we assumed that the temperature gradient in the bottom of the soil column is equal to 0 and no heat flux is transferred across the lower boundary. This assumption is based on the understanding that the contribution of incoming energy can be neglected when the attenuated energy travels further down than a certain depth. However, we first need to investigate how deep the soil is enough to satisfy this assumption. To obtain an insight into this, we conducted a sensitivity analysis study on soil depth. Five simulations were carried out at different soil depths (1.5, 2, 4, 8, and 10 m) using the same setting for other parameters. The biases of soil temperature and moisture of the six layers were calculated against observations from the DY station (equation 3.2).

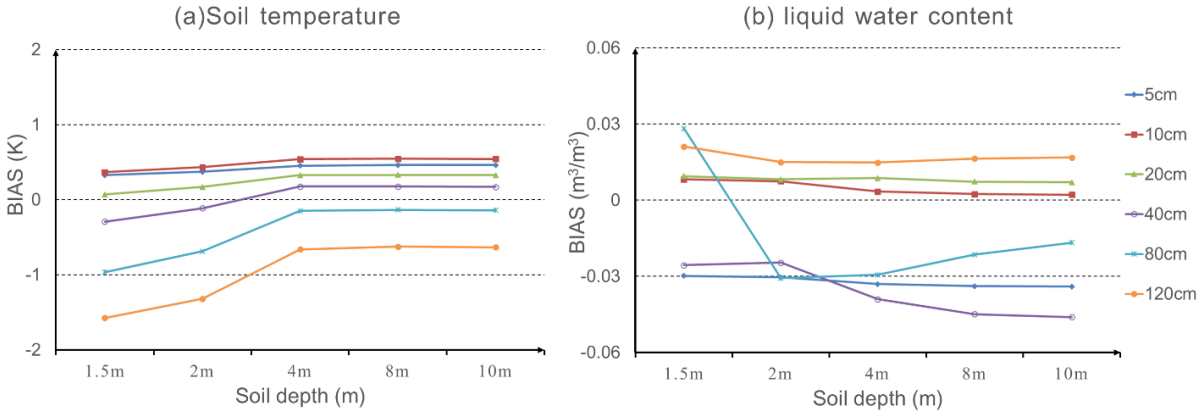

Figure 3.11. Statistical bias between simulated results from new model using different soil depths and the observation from the DY station: (a) bias of soil temperatures; (b) bias of soil liquid water content.

Figure 3.11 shows that the biases decrease as soil depth increases for most soil layers until 4 m is reached. When the soil depth is greater than 4 m, frozen soil modeling shows similar performance on accuracy and less dependency on soil depths. This modeling was validated by soil observations from 0 to 1.2 m, so it is reasonable to set the soil depth range over 4 m for this study in Binggou. This also represents a proof that over a certain depth the assumption is valid

within a given tolerable error range. For permafrost study, a proper soil depth can reduce computation cost without an accuracy cost [*Lawrence et al.*, 2008].

3.4.3 Sensitivity to soil layer thickness

Regardless of soil total depth, there may be uncertainties in soil discretization schemes. Appropriate soil discretization should be considered to balance both simulation accuracy and computational cost. To reveal the relationship between soil layer thicknesses and simulation accuracy, a sensitivity analysis was performed on soil layer thicknesses by dividing 2 m of soil into multiple layers using five soil layered structures (Table 3.3).

Table 3.3. Layer numbers and thicknesses of five soil layered structures.

Number of layers	Surface thickness(cm)	Sublayer thickness(cm)
100	1cm	2cm
40	2.5cm	5cm
20	5cm	10cm
10	10cm	20cm
6	20cm	40cm

As shown in Figure 3.12, the soil temperature simulation is not sensitive to the layer thickness and layer number and its accuracy is relatively stable; whereas, the mean bias of soil moisture clearly increases with increased layer thickness, especially for the deepest section of the active layer (40 or 80 cm). The best result was obtained in the 20-layer simulation. We found that the model tends to overestimate soil moisture for all layers when soil layers are thicker than 10 cm. When soil layers are thinner than 10 cm only soil moisture at 40 cm and 80 cm shows an increased underestimation and the soil moisture accuracy of other depths remains stable. From this sensitivity analysis, it is clear that the new frozen model can be run on a wide range of soil layer thickness from 1 to 40 cm within a certain error range. Furthermore, this analysis showed that too thick a soil layer may reduce computational cost but also introduces errors to the soil moisture estimation.

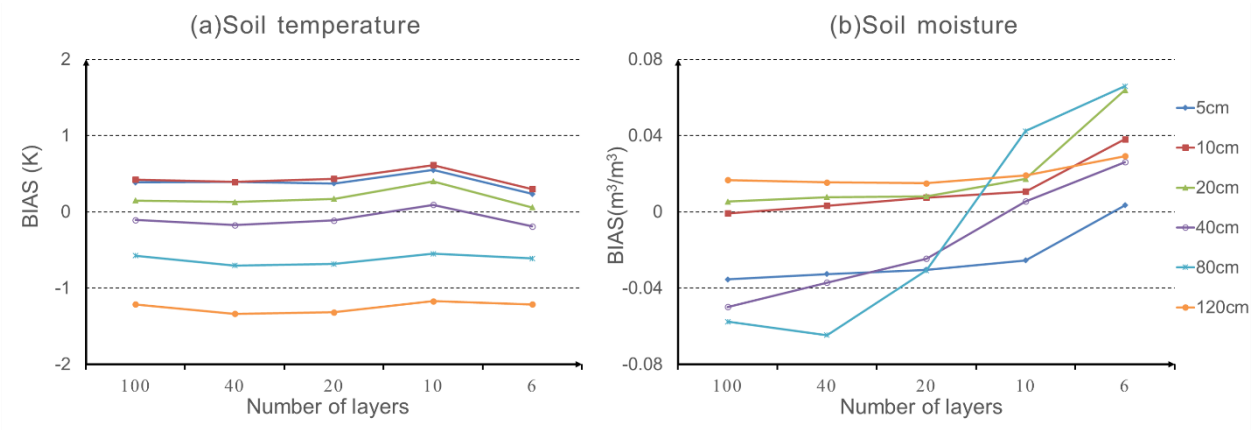

Figure 3.12. Statistical bias between simulated results from the new model with a different number of layers and the observation from DY station: (a) bias of soil temperatures; (b) bias of soil liquid water content.

3.4.4 Sensitivity to time step

To obtain an insight of the model stability and available step size for this frozen soil algorithm, we performed a sensitivity analysis of different time steps (5, 15, 30 min, and 1, 2 and 3 hours). Statistical errors were calculated between simulations and observations (Figure 3.13).

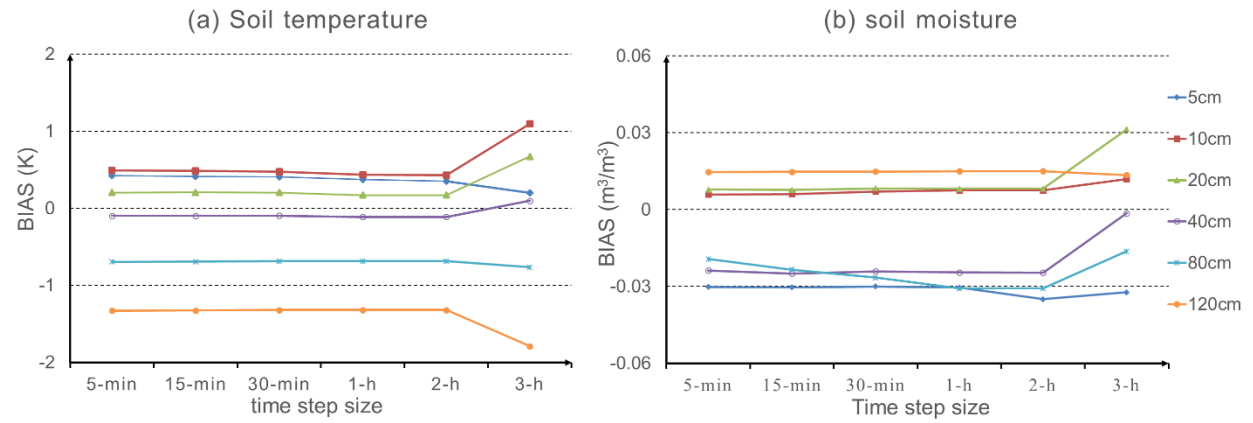

Figure 3.13. Statistical bias between simulated results from the new model using different time steps and the observation from the DY station: (a) bias of soil temperatures; (b) bias of soil liquid water content.

It is evident that the new frozen algorithm is able to obtain stable solutions at a wide range of time steps. Figure 3.13 shows that the simulation errors of different time steps from 5 min to 2 hours are relatively stable and change very little with time steps. When the time step increases to 3 hours, the model may still be run, but the mean biases of soil temperature and soil moisture increase relative to those of other time steps; for example, using 3-hourly reanalysis data may

lower the simulation accuracy. From this analysis, we conclude that this model can be applied to a wide range of time step sizes from 5 min to 2 hours with stable and similar accuracy.

Overall, the sensitivity analyses show that the new frozen soil model is capable of obtaining a stable solution of both soil moisture and soil temperature at a wide range of time steps and layer thicknesses within a given tolerable error range.

3.5 Summary

To evaluate the performance of the frozen soil model, we applied this model to a permafrost basin of the Qilian Mountains, Binggou, in a typical cold region of northwestern China. Firstly, we proposed a practical method for permafrost ice content profile initialization to overcome the difficulties caused by unavailability of ice content observation at different depths. Then, point simulations of soil temperature, ice, liquid water content, and thaw depth were compared with observations at the permafrost station in Binggou Watershed. The simulated results are in good agreement with the observations and the characteristics of permafrost, which demonstrates that the frozen soil model has a good capability for predicting the internal frozen soil process at the point scale. Finally, we validated the simulated hourly river discharge through frozen - thaw periods by using streamflow rate measured at Binggou basin outlet from Jan 17 2008 to July 16 2009. The results prove that the frozen soil model can predict hourly river discharge in permafrost basin with a reliable accuracy and capture the characteristics of cold region hydrological processes.

Sensitivity analyses also show that this frozen soil model can be applied to a certain wide range of time step and layer thickness, and achieve convergent solutions with stable accuracy. It should be pointed out that this frozen soil model can also be used for studying the heat and water transfer processes occurring in arid and semi-arid areas, even when no frozen soil is present. In unfrozen soil regions or summer season, the phase change scheme and the ice effect on water flow can be skipped according to the phase state judgment to remove freezing/thawing effect and save computation time. Furthermore, this model is also suitable for vegetated regions. The heat insulating effect and evapotranspiration of vegetation are also considered.

Although the frozen soil model is capable of capturing the basic pattern of liquid water content and temperature, some biases remain in the soil temperature, moisture and river discharge during the thawing period, owing to the poor simulation of snow by the simple snow

parameterization. Snow processes are critically important for both temperature and soil moisture modeling in cold regions because snowmelt in spring is the main water source for soil moisture and snow cover reflects most of solar energy back into the atmosphere, causing a delay of surface soil cooling in the early winter and warming in the early spring.

In summary, the three-step frozen soil algorithm we developed can solve highly non-linear energy and mass equations of frozen soil stably and reduce the computation time for greater efficiency. The validation result of the frozen soil model proves that the model is capable of continuously reproducing the diurnal and seasonal freeze-thaw cycle, heat and water transfer within frozen soil and predicting streamflow in permafrost basin, which can be widely applied in simulating hydrological processes of cold regions.

4. PASSIVE MICROWAVE REMOTE SENSING OF FROZEN SOIL

4.1 Introduction

Passive microwave remote sensing have outstanding advantages for monitoring the ground freezing and thawing processes, because of less atmosphere effects, ability of vegetation and soil penetration, strong sensitivity to soil water, high revisit frequency and all-weather working ability. Thus, the distinct microwave radiative characteristics of frozen soil produced by the significantly different dielectric constants between freeze and thaw states open the possibility of microwave radiometers for remotely monitoring freeze-thaw states of frozen soil from satellite platforms. Although the microwave remote sensing applications on frozen soil have been researched for around 30 years, the mechanism of radiative feature and transfer processes inside frozen soil have not been sufficiently investigated and there are only few quantitative studies on microwave radiative transfer simulation of frozen soil.

The study targets at developing a radiative transfer model for frozen soil to reveal the mechanism of radiative transfer within frozen soil, reproduce the processes of radiative transfer and predict the brightness temperature out of frozen ground quantitatively.

In this chapter, we firstly described the dielectric constant of frozen soil and improved the common used dielectric constant model by considering the ice effect. Then we analyzed mechanism of microwave radiative transfer process in frozen soil using AMSR-E satellite observation. Next, based on the theoretical analysis of radiative transfer process, the multilayer RTM for frozen soil was developed considering both surface scattering and volume scattering effects by coupling AIEM, DMRT and 4 stream fast model. Finally, the correctness and reliability of this frozen soil RTM is assessed by applying to a seasonal frozen soil region on Tibet Plateau and comparing with the AMSR-E brightness temperature.

4.2 Dielectric Constant of Frozen Soil

Dielectric constant is one of important parameters for microwave radiative transfer model and microwave remote sensing, which is closely related to the radiative feature of ground objects. The behaviors of the reflection, emissivity, and attenuation are directly determined by dielectric constant of materials.

Dielectric constant ε is a measure of the polarity of a medium, which is generally a complex function, composed of a real part, ε'; and an imaginary part ε'':

$$\varepsilon = \varepsilon' - j\varepsilon'' \tag{4.1}$$

where the real part ε' is referred to permittivity of material, which is related to the stored energy within the material when it is exposed to an electric field, while the imaginary part ε'' is referred to as the dielectric loss factor of material, which is related to the dissipation (or loss) of energy [Komarov et al., 2005]. There is a large dielectric contrast between frozen soil and thaw soil, which provides the basis for microwave remote sensing of frozen soil.

4.2.1 Dielectric constant of frozen soil constitutes

Frozen soil is a mixture of solid particles, liquid water, ice and air. Its dielectric constant mainly depends on the volume ratio and dielectric constant of each constitutes.

(1) Air : dielectric constant of air is independent of temperature and frequency in microwave region, ε_{air}=1+0j.

(2) Solid material: the dielectric constant of soil matrix is generally independent of temperature and frequency [*F Ulaby et al.*, 1986]. The real part is mainly depends on the mineral composition. As we can see in the Figure 4.1, the permittivity of 32 different solid rocks varies from 2.4 (pumice) to 9.6 (tholeiitic). While the imaginary part is usually < 0.05.

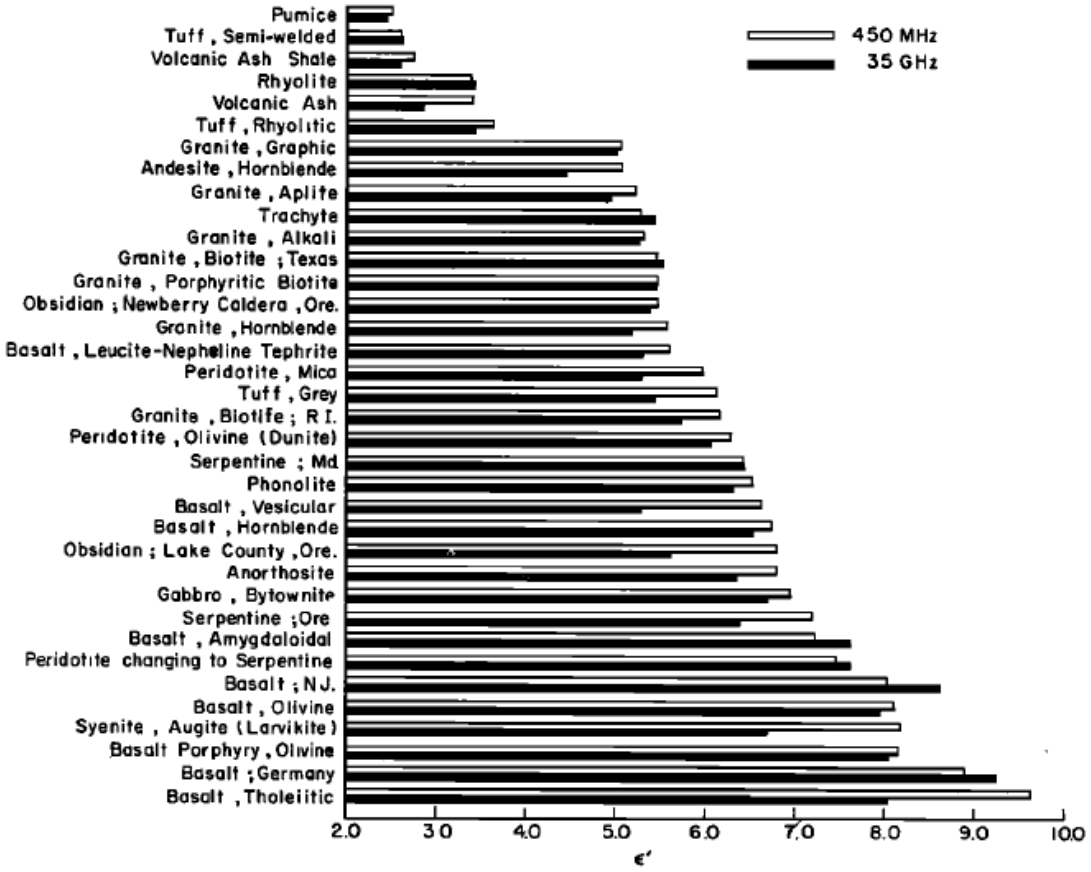

Figure 4.1 the permittivity of solid materials at frequencies of 35GHz and 0.45GHz [*Campbell and Ulrichs*, 1969]

If dry soil is simply considered as the solid inclusion (ε_{ss}') merging in the air host (ε_{air}'), its permittivity ε_{soil}' can be expressed by a linear model:

$$\varepsilon_{soil}' = [\varepsilon_{air}'^{1/2} + v_{ss}(\varepsilon_{ss}'^{1/2} - \varepsilon_{air}'^{1/2})]^2 \tag{4.2}$$

where v_{ss} is the volume fraction of soil matrix, $v_{ss} = \rho_b/\rho_{ss}$, ρ_b and ρ_{ss} is bulk density of soil and solid density, respectively. Based on experiment data for several soil types, $\varepsilon_{ss}' = 4.67$ and $\rho_{ss} = 2.65 g/cm^3$ [Hallikainen et al., 1985].

(3) Liquid water: Soil liquid water can be divided into 2 types: bound water and free water.

Free water is movable among soil pores under gravity and its dielectric constant ε_{fw} can be given by the well-known Debye equation:

$$\varepsilon_{fw} = \varepsilon_{fw\infty} + \frac{\varepsilon_{fw0} - \varepsilon_{fw\infty}}{1 + j2\pi f \tau_{fw}} \tag{4.3}$$

where $\varepsilon_{fw\infty}$ is high frequency limit of ε_{fw}, $\varepsilon_{fw\infty} = 4.9$; ε_{fw0} is static dielectric constant of pure water; τ_w is relaxation time of pure water and *f* is frequency of microwave. Note that ε_{fw0} and τ_{fw} are both functions of temperature, as following empirical regression expressions[*Klein and Swift*, 1977; *Stogryn*, 1971]:

$$2\pi\tau_{fw}(T) = 1.1109\times10^{-10} - 3.824\times10^{-12}T + 6.938\times10^{-14}T^2 - 5.096\times10^{-16}T^3 \quad (4.4)$$

$$\varepsilon_{wo}(T) = 88.045 - 0.4147T + 6.925\times10^{-4}T^2 + 1.075\times10^{-5}T^3 \quad (4.5)$$

Figure 4.2 depicts how the dielectric content of free water varies with frequency at 0°C and 20°C. In general, the dielectric constant of water is relative higher than other ground materials, this is, the distinct dielectric constant of water enable microwave signal to detect soil water content. The real part of water ε'_w decreases with frequency and 20°C water has relative higher permittivity than that at 0°C; while 0°C water has highest loss factor at 9GHz and 20°C at 17GHz. 9GHz for 0°C and 17GHz for 20°C are the relaxation frequency of water at which water has its maximum ε''_w. Before the relaxation frequency, ε''_w increases with frequency; while after that, it decreases with frequency.

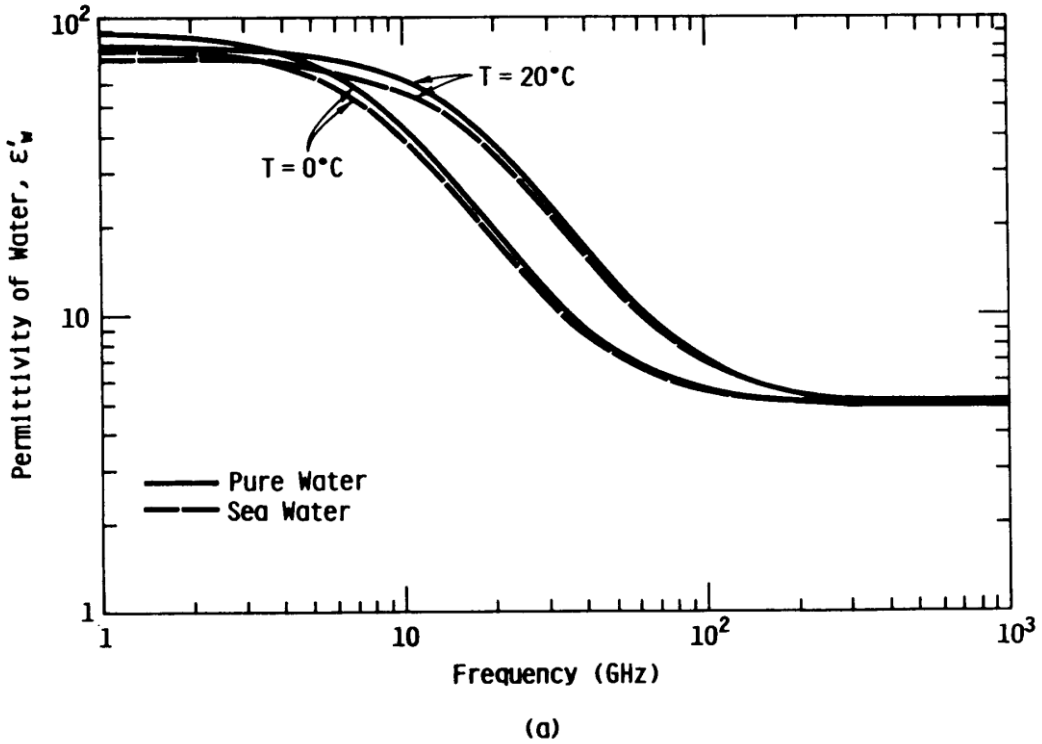

(a)

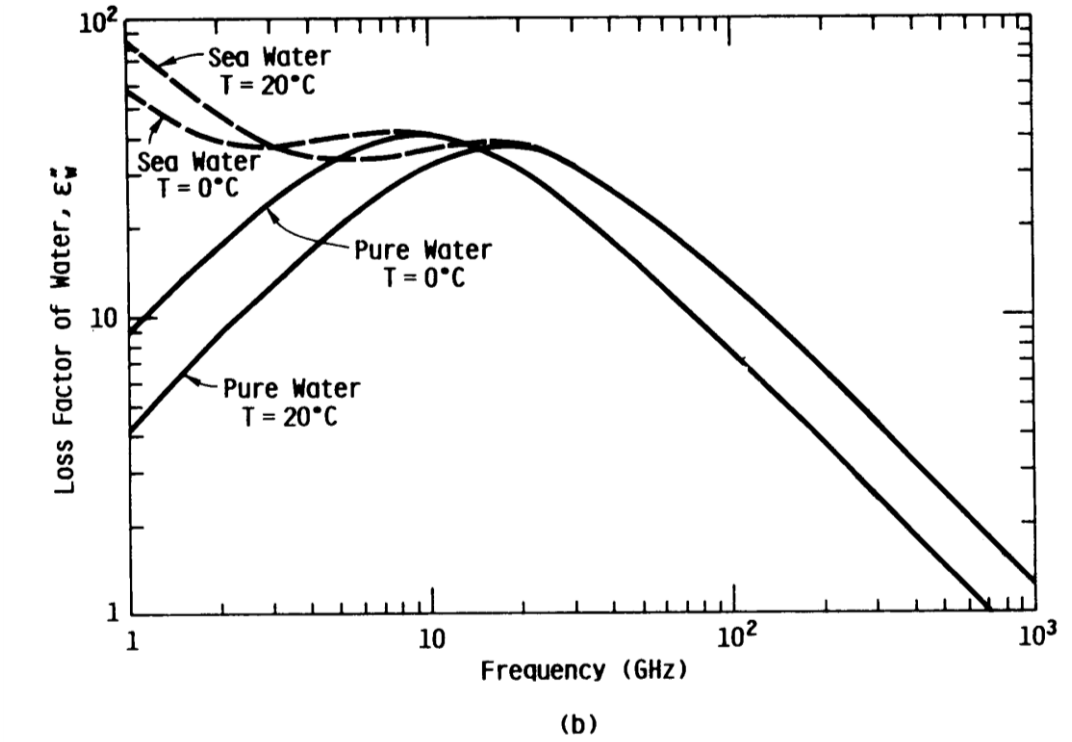

Figure 4.2. Permittivity (a) and loss factor (b) of liquid water at 0°C and 20°C [*F Ulaby et al.*, 1986].

Bound water is an extremely thin layer of water surrounding mineral surfaces held by surface adhesive force. According to experiments [*Grim*, 1968], the dielectric properties of bound water are considered very different from that of free water. Compared to free water, bound water is much more difficult to be polarized and its dielectric constant are relatively smaller[*J R Wang and Schmugge*, 1980]. Its relaxation frequency fbw is between free water (9-17 GHz) and ice (kilohertz) and tends to shift toward that of free water ffw with increasing thickness of water film surrounding soil particle surface, until it is as thick as 10 molecular $f_{bw}=f_{fw}$ [*Hoekstra and Delaney*, 1974; *Pennock and Schwan,* 1969].

(4) Ice: unlike liquid water, ice has a constant permittivity independent of both temperature (< 0°C) and frequency within microwave scope (>10MHz), $\varepsilon_{ice}' = 3.15$. However, the loss factor is in very small magnitude (10^{-4} - 10^{-2}) and varies with frequency and temperature. According to the measurement (Figure 4.3), ε_{ice}'' has the lowest value around 1 GHz at -1°C and decreases with temperature decreasing.

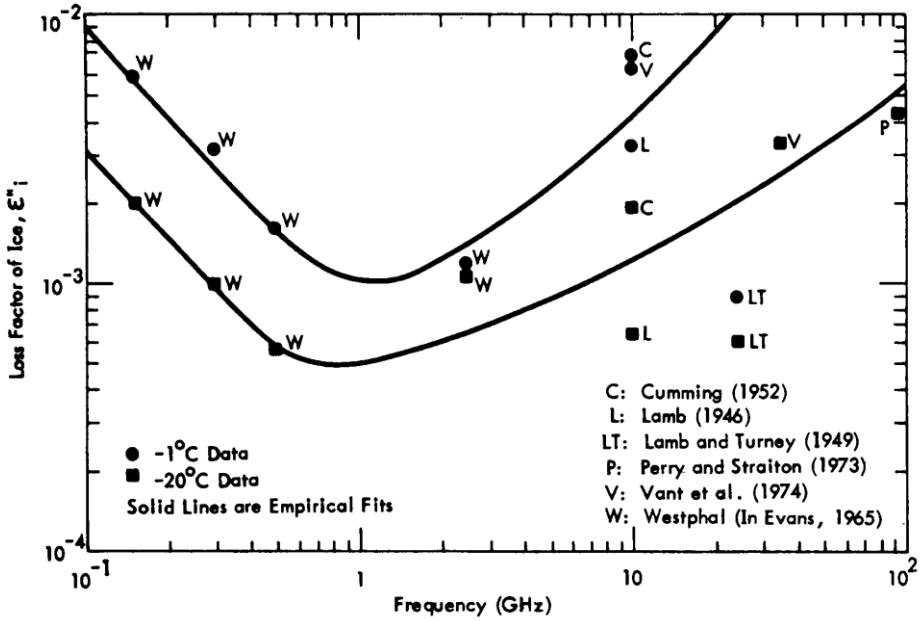

Figure 4.3. Loss factor of ice at -1°C and -20°C [*F Ulaby et al.*, 1986].

4.2.2 Dielectric model of soils

The dielectric constant of the soil is a function of frequency, soil texture, soil temperature, bulk density, volumetric water content and volume fraction of bound water and free water. Several dielectric constant models have been made, including physical models and semi-empirical models. Physical models are not widely applied because most of input parameters are difficult to obtain such as thickness of the water film, number density of quartz particle and ice; phase function of single scattered particle [*Boyarskii et al.*, 2002; *Tikhonov*, 1994]. Here we introduce 2 widely-use semi-empirical models, Dobson model and Wang-Schmugge model and a modified Wang- Schmugge model suitable for semi-arid region:

(1) Dobson model

Dobson et al. [1985] considered the dielectric constant of bound water is not well understood and the volume fraction of bound water is difficult to estimate out of whole water volume content. So they proposed an empirical parameter β to treat the effect of bound water on the soil water dielectric constant implicitly. This dielectric mixing model is widely applicable to a broad range from 1.4 to 18 GHz and a wide range of soil moisture (0.01~saturation).

$$\varepsilon_{soil}^{\alpha} = V_{ss}\varepsilon_{ss}^{\alpha} + V_{air}\varepsilon_{air}^{\alpha} + V_{fw}\varepsilon_{fw}^{\alpha} + V_{bw}\varepsilon_{bw}^{\alpha}$$

$$\cong \rho_b / \rho_{ss}(\varepsilon_{ss}^{\alpha} - 1) + 1 + m_v^{\beta}(\varepsilon_w^{\alpha} - 1) \tag{4.6}$$

where constant shape factor α=0.65, m_v is whole water content, ρ_b and ρ_{ss} are bulk density and specific density of soil matrix, respectively. β can be obtained from an empirical regression expression: β=1.09-0.11S+0.18C, S is sand fraction and C is clay fraction of soil.

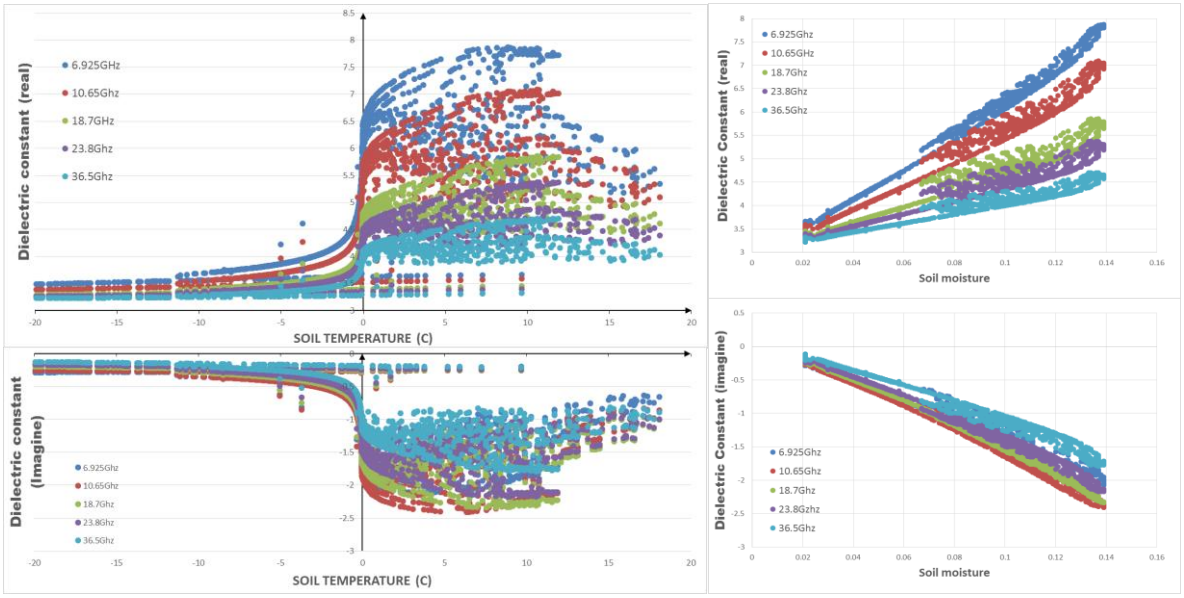

Figure 4.4 dielectric constant of soil at 5 frequencies (6.925-36.5GHz) as a function of soil temperature and soil moisture, calculated by Dobson model.

(2) Wang-Schmugge model[*J R Wang and Schmugge*, 1980]

Wang and Schmugge found that in two distinct regions, soil dielectric constant increases slowly with m_v before a transition moisture; and increases rapidly with m_v after a transition moisture. The transition point is closely related to soil texture and increases with clay content. Moreover, the dielectric properties of bound water behaves in much the similar way that it does when it is in the form of ice, so they use both ε_{ice} and ε_{fw} to express bound water dielectric constant. They proposed an empirical mixing model over two cases, wet soil and dry soil:

1) dry soil: water content is less than or equal to the maximum bound water fraction ($m_v < m_t$).

$$\varepsilon_{soil} = (1-\phi)\varepsilon_{ss} + (\phi - m_v)\varepsilon_{air} + m_v\varepsilon_{bw} \tag{4.7}$$

$$\varepsilon_{bw} = \varepsilon_{ice}(1 - \frac{m_v}{m_t}\gamma) + \varepsilon_{fw}\frac{m_v}{m_t}\gamma \tag{4.8}$$

2) wet soil: water content is in excess of the bound water fraction ($m_v > m_t$).

$$\varepsilon_{soil} = (1-\phi)\varepsilon_{ss} + (\phi - m_v)\varepsilon_{air} + (m_v - m_t)\varepsilon_{fw} + m_t\varepsilon_{bw} \tag{4.9}$$

$$\varepsilon_{bw} = \varepsilon_{ice}(1-\gamma) + \varepsilon_{fw}\gamma \tag{4.10}$$

where m_t is the transition point, which can be expressed by a linear regression equation $m_t = 0.49W_p + 0.165$. ϕ is the soil porosity, bound water dielectric constant ε_{bw} is calculated from ε_{ice} and ε_{fw}, and an empirical parameter γ is used as the weight for ε_{ice} and ε_{fw}, $\gamma = 0.57Wp + 0.481$. W_p is the wilting point of soil, $Wp = 0.06774 - 0.00064S + 0.00478C$.

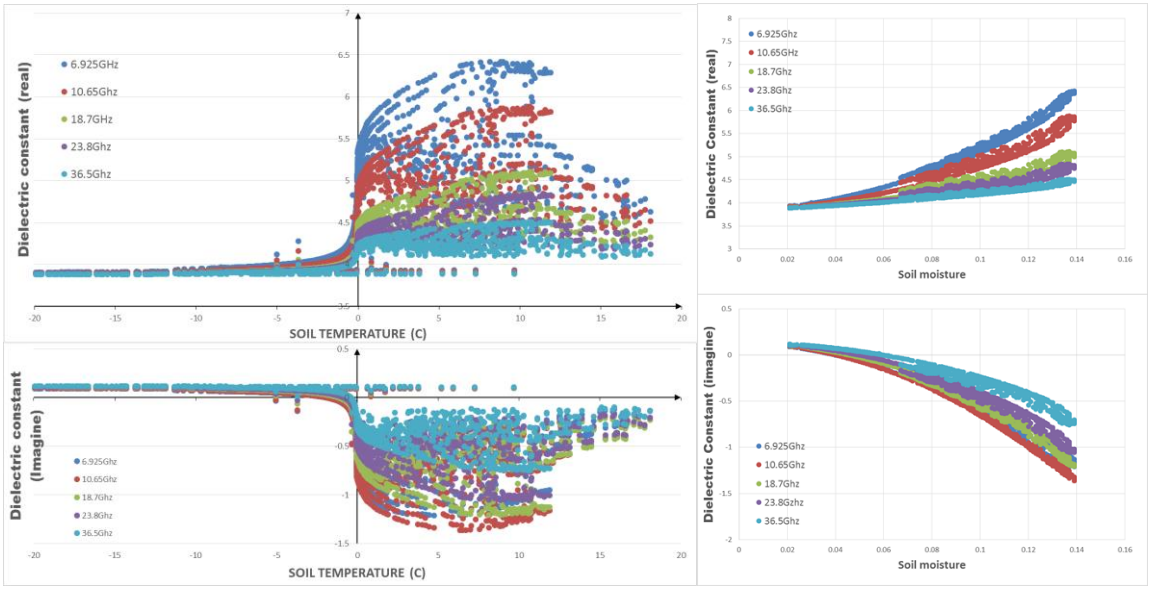

Figure 4.5 dielectric constant of soil at 5 frequencies (6.925-36.5GHz) as a function of soil temperature and soil moisture, calculated by Wang-Schmugge model.

(3)Modified Wang-Schmugge model by Neluwala

Neluwala [2015] optimized the Wang-Schmugge model by changing the parameters γ and m_t and introduce a new factor for correcting ε_{fw} using ground based soil observation. The modified model was verified by ground based microwave radiometer observation at Tanashi, in Tokyo. A promising result have been achieved in the application in the summer of a semi-arid region Gaize, in Tibet.

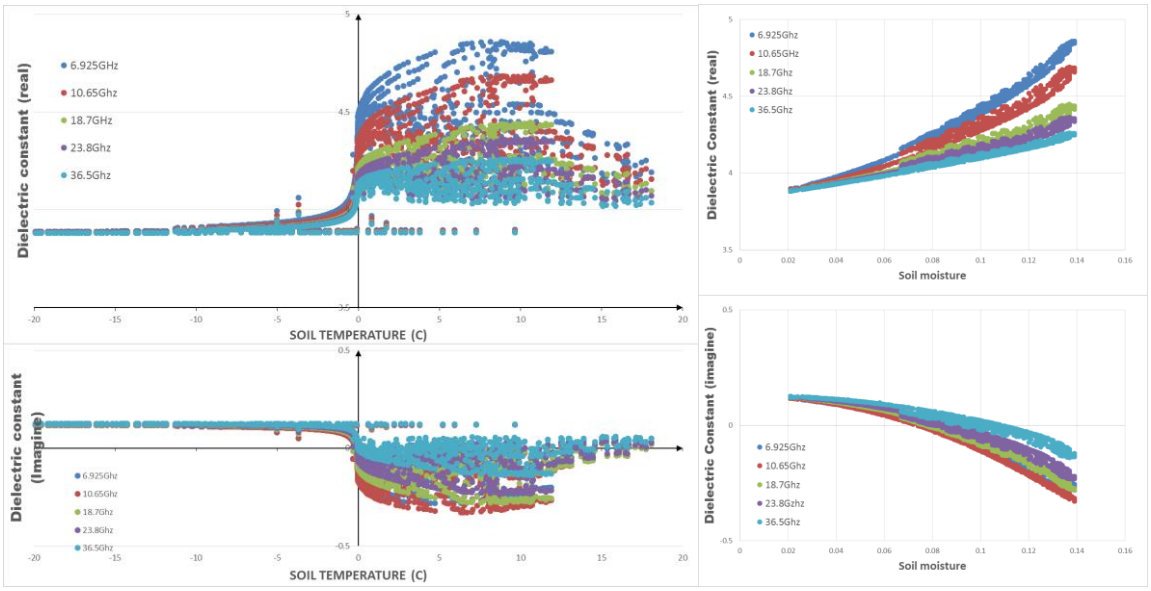

Figure 4.6 dielectric constant of soil at 5 frequencies (6.925-36.5GHz) as a function of soil temperature and soil moisture, calculated by Neluwala model.

4.2.3 Dielectric model of frozen soil and its improvement

The successful application of Neluwala model[*Neluwala*, 2015] in summer of semi-arid region has proved that this optimized model has a good capability for predicting dielectric constant in low soil moisture areas. So we choose this optimized model for the research in frozen soil region, where is usually located in the arid or semi-arid region. In frozen soil at or below 0°C, most of water is stored in the form of ice and left water remains as liquid bound water, adhering to soil particles. A mixing dielectric constant model of frozen soil should consist of 5 components: solid particles, ice, free water, bound water and air. However, the ice constituent has not been included yet in this modified model.

The dielectric constant of ice is independent of temperature and frequency and much smaller than that of liquid (ε_{fw} ~80), which can be treated as constant ($\varepsilon_{ice} = 3.15 + 0j$). During freeze-thaw cycle, the amount of ice rises (falls) while liquid water content falls (rises). Due to the great dielectric difference between ice and liquid water, the dielectric constant of frozen soil fluctuates drastically corresponding to freezing and thawing. For frozen soil dielectric constant modeling, the ice term is introduced into the Neluwala optimized model[*Neluwala*, 2015]:

1) dry soil (fully frozen): liquid water content is less than or equal to the maximum bound water fraction ($m_v < m_t$).

$$\varepsilon_{soil} = (1-\phi)\varepsilon_{ss} + (\phi - \theta_l - \theta_i)\varepsilon_{air} + \theta_l \varepsilon_{bw} + \theta_i \varepsilon_{ice} \tag{4.11}$$

$$\varepsilon_{bw} = \varepsilon_{ice}(1 - \frac{\theta_l}{m_t}\gamma) + \varepsilon_{fw}\frac{\theta_l}{m_t}\gamma \tag{4.12}$$

2) wet soil (thawing): liquid water content is in excess of the bound water fraction ($m_v > m_t$).

$$\varepsilon_{soil} = (1-\phi)\varepsilon_{ss} + (\phi - \theta_l - \theta_i)\varepsilon_{air} + (\theta_l - m_t)\varepsilon_{fw} + m_t \varepsilon_{bw} + \theta_i \varepsilon_{ice} \tag{4.13}$$

$$\varepsilon_{bw} = \varepsilon_{ice}(1-\gamma) + \varepsilon_{fw}\gamma \tag{4.14}$$

where θ_i is ice content, ε_{ice} is dielectric of ice(ε_{ice} =3.15+0j); ε_{air} is dielectric of air(ε_{air} =1+0j); ε_{ss} is dielectric of air(ε_{ss} =5.5-0.2j), ϕ is the soil porosity; ε_{fw} is dielectric of free water, which is calculated by Debye equation (see section 4.2.1); transition point m_t is set as 0.2. Note that Wang-Schmugge model has a shortage that when soil moisture is extremely small, it tends to give positive loss factor, which is physically wrong. Because the negative imaginary part represents the time lag of molecular polarization under electromagnetic wave. Here, a simple correction is adopted that setting the positive loss factor equal to *0*.

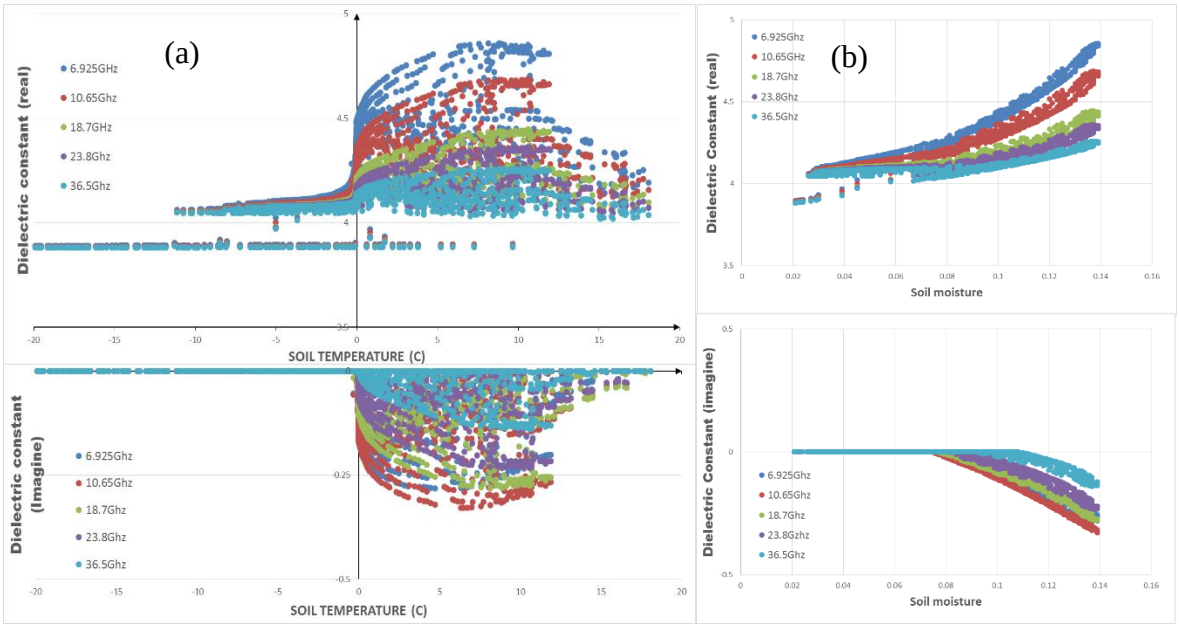

Figure 4.7 dielectric constant of soil at 5 frequencies (6.925-36.5GHz: dark blue, red, light green, purple, light blue) as a function of soil temperature (a) and soil moisture (b), calculated by the new modified model.

We applied this model to Gaize, a seasonal frozen soil ground, and calculated dielectric constant of soil at 5 frequencies (6.925 – 36.5GHz). The soil observation and modeling data

are used in this model including soil temperature, moisture, ice content and soil texture information (detail in section 4.5.1). The dielectric constant result is shown in Figure 4.7.

The real part of dielectric constant increases with both temperature (Figure 4.7(a))and soil moisture (Figure 4.7(b)). During thawing, soil temperature increases and ice melts to liquid water, dielectric constant rises; whersas contrary to the soil freezing. It aslo can be seen that lower frequency has higher permitivity, because water has high permitivity at lower frequency (see in Figure 4.2 (a)). Noteworthy, the permitivities arround 4 are not continous when soil mositure is low. That is because the dielectric contrast between ice and liquid water. In wet situation, soil water could be froze into ice. In some extreme dry soil (Gaize m_v <0.06), the little liquid water is closely bounded to the particle surface and not able to freeze. These soil with neither ice nor free water have distinct soil dielectric constant from normal soil.

On the whole, the imaginary part of dielectric constant decreases with both temperature (Figure 4.7(a))and soil moisture (Figure 4.7(b)). 10.65 GHz has the highest loss facor, because water at relaxation frequency arround 9GHz has the maximum imaginary dielectric contant (see in Figure 4.2(b)). When soil freezes, most of water exsits in the form of ice, so the loss factor is set to 0. Overall, the dielectric constant of frozen soil is dominated by the variation of liquid water during freeze - thaw cycle.

4.3 Radiative transfer theory in frozen soil

4.3.1 Radiative characteristics of frozen soil

To capture the radiative characteristic of frozen soil, it is necessary to observe and analysis the brightness temperature from satellite based microwave radiometer. AMSR-E brightness temperature data of 14 months from 2003 to 2004 at a seasonal frozen soil station, Gaize, are used and detail about the data can be seen in table 4.1.

The AMSR-E brightness temperature time series of 5 frequencies are plotted in Figure 4.8. On the whole, brightness temperature varies seasonally with annual ground temperature cycle (black dash line in Figure 4.8). From the characteristics of each seasonal flucuation, it is obvious that the time series can be seperated into 2 periods: one is rainy and warm season from June to August, another one is dry and cold season from September to next May.

Table 4.1. Description of AMSR-E brightness data from 2003 to 2004 at the Gaize station

AMSR-E Tb data	**JAXA L1**
Location	Gaize, Tibet (Lat. N32.30° , Lon. E84.05°)
Period	2003-10-2 ~ 2004-12-31
Time	Descending, 4:00 local time, daily
Frequency	6.925, 10.65, 18.7, 23.8, 36.5GHz
Polarization	vertical, horizontal polarizations

In dry and cold season, the brightness temperature is relative low, compare to warm season. And there is a negative spectral gradient among 5 frequencies, that is, brightness temperature in low frequency is relatively high than that in high frequency (Tb6> Tb10> Tb18> Tb23> Tb36) (Figure 4.9), which is usually taken for the indicator of frozen soil and widely adopted in most of current frozen soil mapping algorithms [*Duguay et al.*, 2005; *T Zhang and Armstrong*, 2001; *Zuerndorfer and England*, 1992]. From Figure 4.9, it can be seen that this negative spectral gradient trend is much more apparent in vertical polarization (a) than in horizontal polarization (b).

In rainy and warm season, the brightness temperature is higher than that in winter season. Moreover, brightness temperature fluculates very much with soil moisture. Especially, after rainfall ground surface gets wet and low frequency brightness temperature drops sharply. Thus, the spectral gradient becomes positve in warm season (Tb 6< Tb10< Tb18< Tb23). 8 years AMSR-E data from 2003 to 2011 are available and they all show similar characteristics as we decribed above (see in appendix 2).

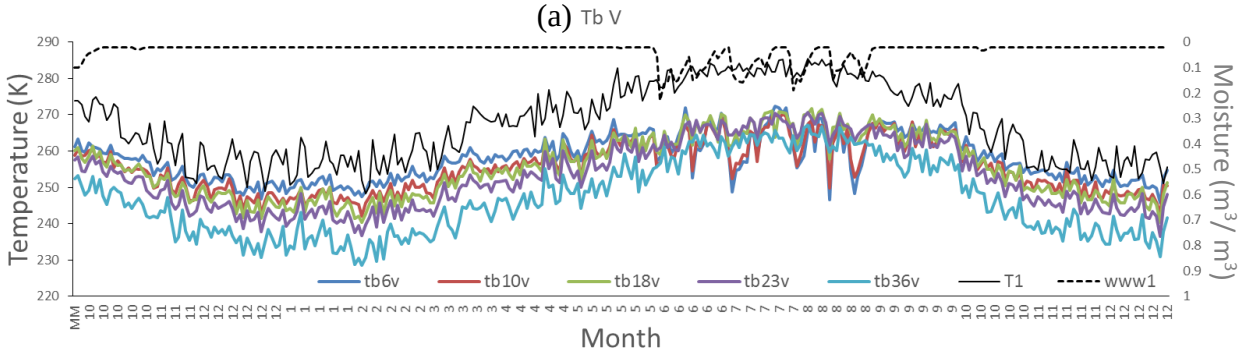

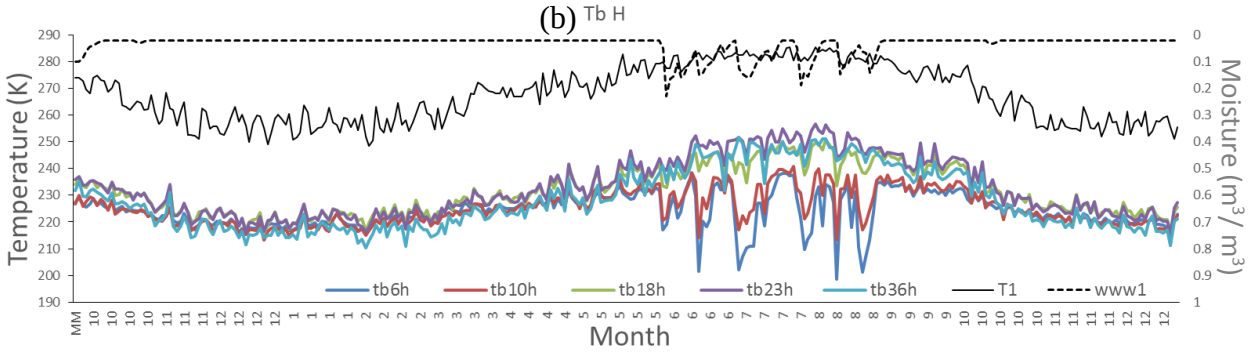

Figure 4.8 AMSR-E brightness temperature time series of vertical polarization (a) and horizontal polarization (b) at 5 frequencies (6.925-36.5GHz: dark blue, red, light green, purple, light blue), surface physical temperature (T1: black line) and surface soil moisture (www1: black dash line) at Gaize, Tibet.

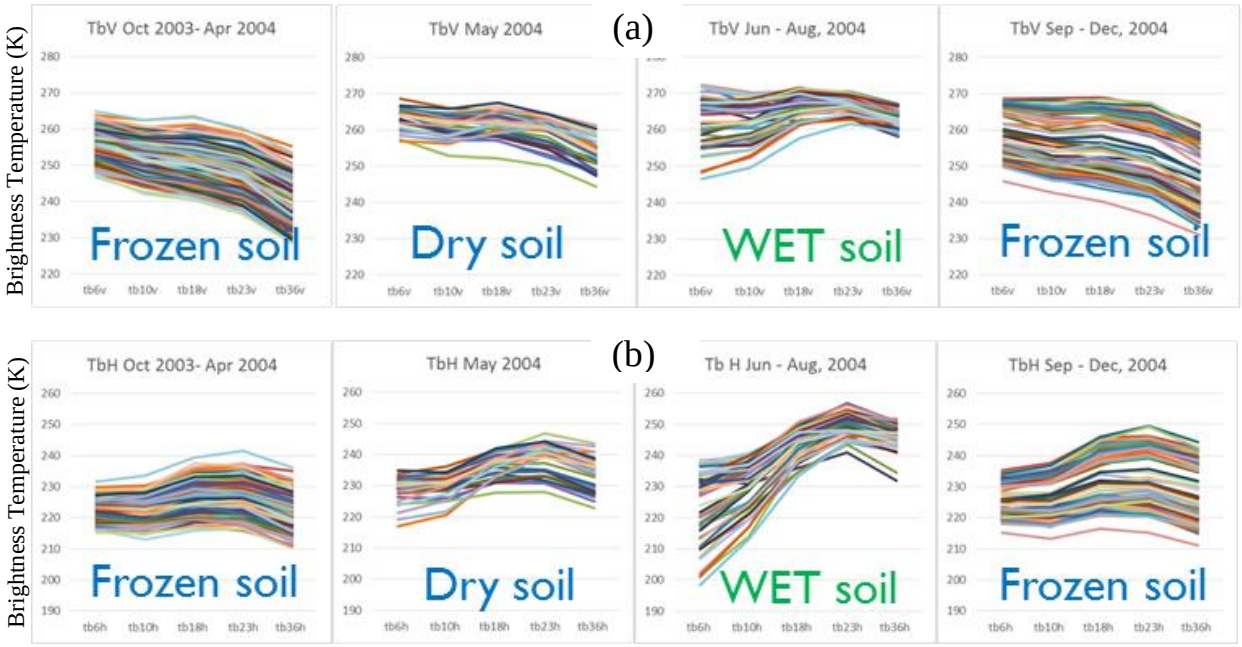

Figure 4.9 Microwave spectrum (frequency range from 6.925 to 36.5GHz) of frozen soil in vertical polarization (a) and horizontal polarization (b). The spectrum is divided into 4 parts according to time (Oct. 2003-April 2004), (May 2004), (June – Aug., 2004) and (Sept.-Dec., 2004).

The brightness temperature characteristics of frozen dry soil and warm wet soil are completely different and their spectrum features are so distinct. These radiative characteristice of freeze-thaw cycle should be attributed to the distinguishing radiative processes within frozen soil. However, until now there's no comprehensive description of radiative transfer processes in frozen soil and adequate explanation for the radiative characteristics of frozen soil.

4.3.2 Mechanism of radiative transfer in frozen soil

The radiation transfer processes starts from soil emission source, passing through medium between the source and sensor, ends at a sensor. The radiative transfer processes of frozen soil can be classified into 3 parts: 1)emitted radiation transfer from deep ground to soil top within soil medium ,2) radiation pass the interface from soil medium to air medium and 3) electromagnetic radiation transfer through atmosphere, and finally reach the sensor.

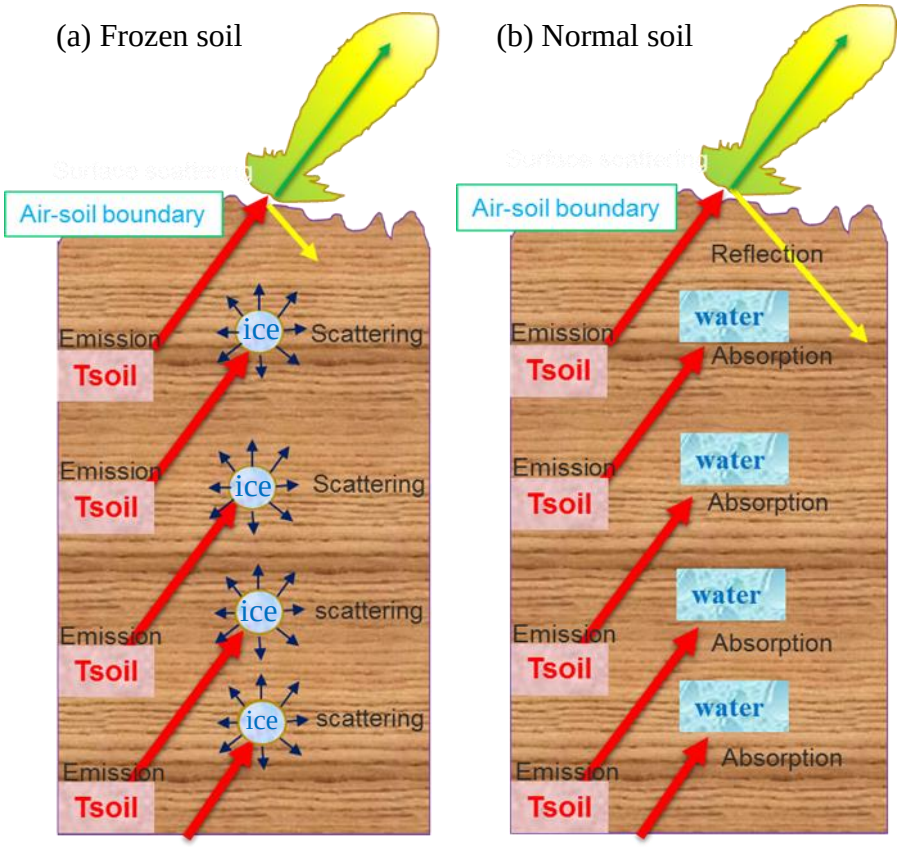

Figure 4.10 Schematic of radiative transfer processes of frozen soil (a) and normal wet soil (b)

(1) Emission

The radiation transfer processes start from soil emission (Figure 4.10). And the emissions mainly depend on the physical temperature of the soil T_{soil}, which can be described by the Rayleigh-Jeans approximation in microwave region:

$$B_f = \frac{2kTf^2}{c^2} = \frac{2kT}{\lambda^2}. \tag{4.15}$$

where B_f is radiated brightness at frequency f, T is physical temperature. k is Boltzman's constant, c and λ are light speed and wavelength, respectively. B_f is proportional to T, this is the reason that brightness temperature time series waves seasonally with ground temperature.

(2) Volume scattering and absorption

From the previous section, it is known that during thaw and frozen season, the radiative characteristics of frozen ground are quite different. For frozen soil in cold season, freezing reduces liquid water, which results in the decreasing imagery part of soil dielectric constant, ε_{soil}''. The absorption coefficient K_a varies approximately with ε_{soil}'':

$$K_a = 2\alpha \tag{4.16}$$

where absorption constant $\alpha = k_0 \left| \mathrm{Im}\left(\sqrt{\varepsilon_{soil}}\right) \right|$ (4.17)

with $k_0 = 2\pi/\lambda_0$ is the wave number in free space, λ_0 is the wavelength in free space. If ε_{soil}'' is as low as 10^{-3}, the absorption coefficient K_a can be about 0.3Np m^{-1}. Such a small value is likely to be smaller than scattering coefficient K_s, which means that the absorption effect is much smaller than scattering effect in frozen soil. The effective emitting depth δ_p also is inversely proportional to K_a:

$$\delta_p \cong 1/K_a, \tag{4.18}$$

so that the frozen soil is more transparent for microwaves than the normal moist soil is. Thus, the radiation contribution from deep soil has to be considered. Along the propagation path to the surface, scattering by soil and ice particles plays a dominating role rather than absorption in a total extinction (Figure 4.10(a)). Oppositely, normal soil has more water inside which absorbed emission from deep soil and the penetration depth δ_p is so shallow that deep soil emission and volume scattering can be neglected.

Volume scattering is that scattering takes place within the volume of medium which cause a redistribution of the energy from the transmitted wave into other directions and results in a loss in the transmitted wave [*F T Ulaby et al.*, 1982]. The intensity of volume scattering is proportional to both geometric size of particle size *r* relative to the incident wavelength λ and density of the embeded inhomogeneities. For high frequency, the particles are relative large and they scatter much more seriously than they do for low frequency. So scattering attenuation is more severe at higher frequency and leads to the negative spectral gradient. Indeed, Tb decreases with increasing frequency exhibited by the average spectra in Figure 4.11(a).

(3) Surface scattering

After the electromagnetic wave passes through the volume scattering and scattering, it

impinges on the air-soil interface. Part of the incident energy is scattered backward and the rest cross the boundary into the air (see in upper part of Figure 4.10). The surface scattering intensity is proportional to the relative dielectric constant of soil-air surface ε_r, and the angular scattering pattern is determined by the surface roughness. The magnitudes of the polarized Fresnel reflectivity for air-soil boundary can be described as the function of $\varepsilon_r = \varepsilon_{soil}/\varepsilon_{air}$:

$$R_h = \left| \frac{\cos\theta - \sqrt{\varepsilon_r - \sin^2\theta}}{\cos\theta + \sqrt{\varepsilon_r - \sin^2\theta}} \right|^2 \tag{4.19}$$

$$R_v = \left| \frac{\varepsilon_r \cos\theta - \sqrt{\varepsilon_r - \sin^2\theta}}{\varepsilon_r \cos\theta + \sqrt{\varepsilon_r - \sin^2\theta}} \right|^2 \tag{4.20}$$

The soil surface dielectric constant ε_{soil} is strongly dependent on the soil moisture. Dry frozen soil is quite close to air in term of dielectric constant. The less surface discontinuity of dielectric constant between air and soil, the less scattering and higher transmissivity (=1-$R_{h/v}$) of the air - soil interface. Surface scattering of frozen soil is not as strong as normal wet soil in air-soil surface. The reflectivity of surface increases with increasing soil moisture, due to its high permittivity ε_{soil}'. Furthermore, at low frequency the higher permittivity of water results in a higher soil surface permittivity (detail in section 4.2.3), which in turn leads to high reflectivity in lower frequency, conversely, low reflectivity in higher frequency. While transmissivity is opposite to reflectivity. This behavior of surface reflectivity is illustrated in Figure 4.11(b), which shows low Tb in 6GHz and high Tb in high frequency 36GHz for wet soil.

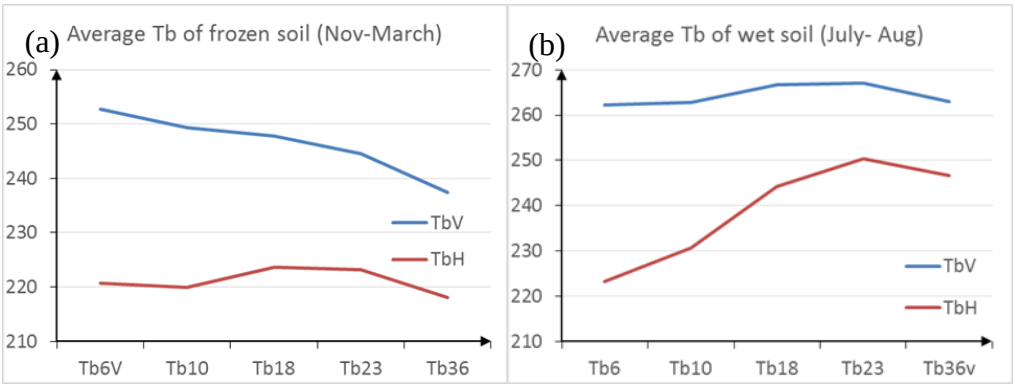

Figure 4.11 Average spectral brightness temperatures at horizontal and vertical polarizations by AMSR-E. (a) frozen soil from November to next March, (b) wet soil from July to August.

In sum, for frozen soil, volume scattering is more significant than absorption loss in the total extinction, while surface scattering is very weak. However, in normal wet soil

absorption dominates attenuation effects, so the deep soil contribution can be neglected, whereas surface scattering plays as a key process during radiation transfer. The difference of radiative processes between frozen soil and normal soil are listed in the table 4.2.

Table 4.2. Comparison of frozen soil and normal soil in radiative transfer processes

	Frozen soil	Normal soil (wet)
Dielectric constant	Low, slightly larger than air	High, high permittivity at low f
Emission	Weak, the lower T, the lower Tb	Strong, The higher T, the higher Tb
Absorption	Weak	Strong, $K_a >> K_s$ The more water, the larger K_a
Volume scattering	Strong, $K_s >> K_a$ The higher f, the strong scattering	Weak
Surface scattering	Weak	Strong, the lower f , the higher $R_{v/h}$

(4) Atmosphere effect

Atmosphere is transparent for most microwave bands used for land surface remote sensing in common used sensors, such as AMSR, AMSR-E and AMSR-2. Quantitatively, atmosphere effects are quite small for frequencies lower than 18 GHz. Therefore, we neglected the atmosphere effect and treat it as transparent in our study.

4.4 Development of multiple-layer RTM for frozen soil

4.4.1 Model structure

The study targets at developing a radiative transfer model for frozen soil to reveal the mechanism of radiative transfer within frozen soil, reproduce the processes of radiative transfer and predict the brightness temperature out of frozen ground quantitatively. According to the radiative transfer theory in frozen soil, emission from deep soil need to be considered and volume scattering dominates in the extinction processes within frozen soil. Surface scattering of frozen ground is not as strong as normal wet soil, however it still should be taken into account, especially in summer when the active layers of frozen soil thaw. So

we adopted a multiple plane-parallel layer structure with spherical soil particles for describing the radiative transfer processes inside deep soil medium (Figure 4.12). It is assumed that all microphysical properties (e.g., temperature, liquid/ice content, particle density, particle size) are uniform within each soil layer and reflection only occurs in air-soil interface without reflection between soil layers.

We modified a coupled soil RTM [*Lu et al.*, 2006] developed by Hui Lu to simulate both surface scattering and volume scattering effects in radiative transfer of frozen soil. The frozen soil RTM structure is shown in Figure 4.12. An atmosphere RTM, 4 stream fast model, was simplified to reproduce the up-welling radiation from the soil to atmosphere. Not like sparse particles in atmosphere, soil is a dense medium and a Dense Medium Radiative Transfer theory based Model (DMRT) are modified to describe volume scattering and absorption effect. And the Advance Integral Equation Model (AIEM) is employed to represent surface scattering process in the air- soil interface as well.

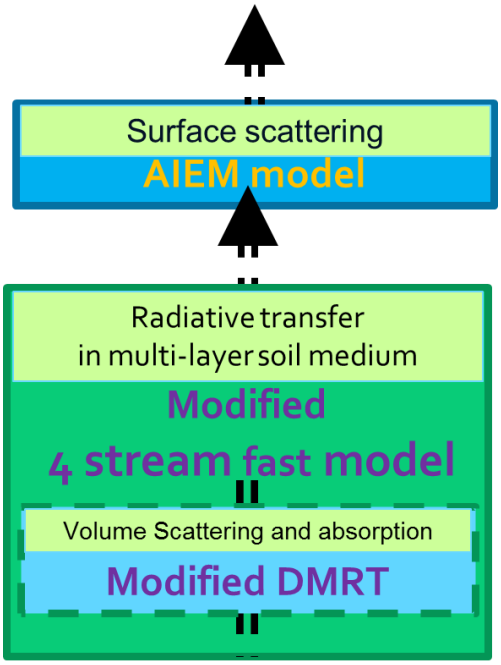

Figure 4.12 Schematic of multi-layer frozen soil RTM structure

Compared to other common-used ground surface emission models, which usually neglect emission from deep soil for simplification [*K-S Chen et al.*, 2003; *Y-A Liou and England*, 1996; *Weng et al.*, 2005], this RTM has a more realistic, complete and physical description of the radiation transfer process inside soil. Upward Radiation processes start from bottom boundary, which is set at several penetration depths δ_p, and end at the upper boundary, air-ground interface. All the soil layers contribute to the upwelling emission and the intensity of

emission depends on the soil temperature of each soil layer. On the upward propagation path, soil particles including soil material, liquid water and ice serve as scatterers and attenuate the electromagnetic wave by scattering. The transmitted energy are also attenuated by the absorption of soil medium. The attenuation effect is determined by the soil dielectric constant, particle size relative to frequency and the density of soil particles. Once the upwelling radiation impinges on the air- soil boundary, the surface scattering only allows a portion of radiation to cross the boundary and reach to a sensor. The transmissivity and surface reflectivity are mainly governed by the dielectric properties and roughness condition of soil surface. The detail RTM algorithm is described in the following section.

4.4.2 Frozen Soil RTM Algorithm

4 stream fast model [*Liu*, 1998] is originally developed for microwave radiative transfer in atmosphere. It is assumed a plan-parallel and azimuthally-symmetric atmosphere with spherical particles. Radiance calculation starts from the top of atmosphere downward until the downward radiation at the ground surface is derived. Then partial of radiation is reflected back to atmosphere by the ground and some ground emission also join the up-welling energy flux. Next, similarly upward radiation can be continuously solved from the ground surface to top of the atmosphere (Figure 4.13(b)). It starts from the top of atmosphere because the cosmic microwave background radiation is known as constant (3k). However, it is not necessary for soil radiation transfer to start from the soil surface since the upper boundary radiation is unknown. So we simplified the radiation transfer processes in 4 stream fast model by removing the down-welling radiation processes. As Figure 4.13(a) shows, radiation starts from the bottom boundary layer and transmits upward until the top of soil.

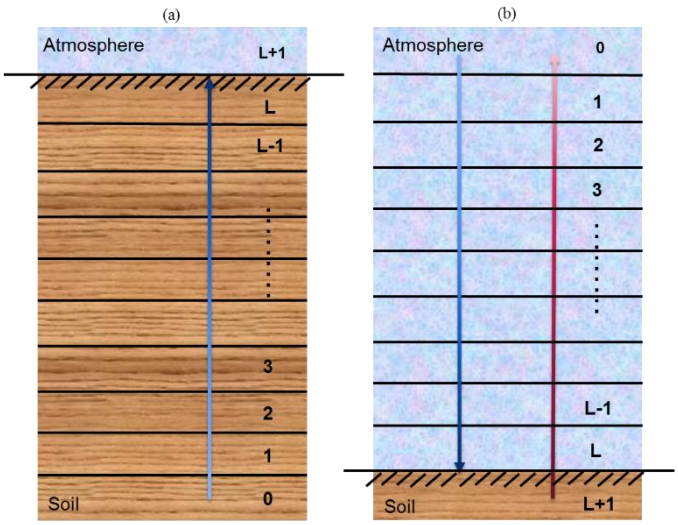

Figure 4.13 Comparison of modified 4 stream fast model in frozen RTM (a) and Original 4 stream fast model in atmosphere RTM (b)

The upward radiances I at optical depth τ (τ=0 at the bottom of the soil layer), in direction μ (the cosine of zenith) can be expressed as [*Liu*, 1998]:

$$I(\tau,+\mu) = I(0,+\mu)e^{-\tau/\mu} + \sum_{j=-n}^{n} L_j W_j(\mu)(e^{-k_j\tau} - e^{-\tau/\mu}) + Z_0(1-e^{-\tau/\mu}) - B_1[\tau - \mu(1-e^{-\tau/\mu})] \quad (4.21)$$

Where $I(0,+\mu)$ is the upward radiance at the bottom of soil layer. This is 4 stream model, so n=2. L_j can be solved by the standard procedure as described by Liou [1974]. k_j, *and* $W_j(\mu)$ eigenvalue and eigenvector. Within each layer, it is assumed that soil temperature has a linear relationship with optical depth, which means that emission B at τ is a linear function of τ $B_1=(B(\tau)-B_0)/\tau$, B_0 is the emission from bottom of the layer; Z_0 refers to a scattering and emission term, see detail in [*Liu*, 1998]. Except solving radiance by formal solution, it determines the scattering source term by a 4 stream discrete ordinate solution using Henyey-Greenstein scattering phase function. The cross-polarization scattering in the scattering source term is neglected, so the radiation transfer is calculated in terms of energy with no difference between H and V polarization.

The scattering occurs in the air can be assumed as independent scattering, because particles in air distribute sparsely and the scattering coefficient k_s can be simply expressed as the sum of scattering cross sections of all the particles in an air layer. Differently from air, soil is a dense medium in which the scattering is correlated. Independent scattering assumption may cause the overestimation of k_s for soil [*Ishimaru and Kuga*, 1982; *Kuga and Ishimaru*, 1984]. Therefore, the correlated scattering of dense packed particles need to be considered by the Dense Medium Radiative Theory under the Quasi-Crystalline Approximation with Coherent Potential (QCA-CP). Instead of using Mie or Raleigh expression of independent scattering for atmosphere, the extinction coefficient k_e and single scattering albedo ω of soil layers are calculated by the DMRT accounting for the pair distribution function of the particle positions and coherent mutual interactions[*Tsang et al.*, 1992].

Note that DMRT equations based on QCA-CP are originally developed for snow radiation transfer. The density of snow is 100~350kg/m^3, that is, volume fraction of ice in snow is 0.1~0.38. However, the density of soil is much denser that snow, the volume fraction of soil solid is usually larger than 0.4. The application of DMRT on the snow or foam over ocean have been proved that the DMRT can provide reasonable results for low density medium

[*Guo et al.*, 2001; *Liang et al.*, 2008; *Tsang et al.*, 2000]. While until now the applicability of QCA-CP for large volume fraction (>0.4) has not been explored. After comparing the NMM3D/DMRT, QCA/DMRT, independent Mie scattering model and Liang et al.[2006], Tsang et al.[2008] and Picard et al. [2013] found that different models give divergent results for fractional volume higher than 0.3. Picard et al. [2013] also suggested that it is better to limit the density lower than 350kg/m^3 rather than to use the real high density of snow in the DMRT model. The extinction coefficient k_e of DMRT can be overestimated if volume fraction is larger than 0.4 by the QCA-CP. So Here we introduced a correction factor to lower k_e in QCA-CP, as shown in table 4.3:

Table 4.3. Ke adaptation coefficient for soil at each frequency in QCA-CP

f(GHz)	6.925	10.65	18.7	23.8	36.5
K_e/coef	K_e /6	K_e /15	K_e /50	K_e /50	K_e /50

The new relationship between k_e and volume fraction, and particle size is shown in Figure 4.14. On the whole, k_e of large particles decreases with volume fraction increasing; whereas, large particles have higher k_e than small particles do.

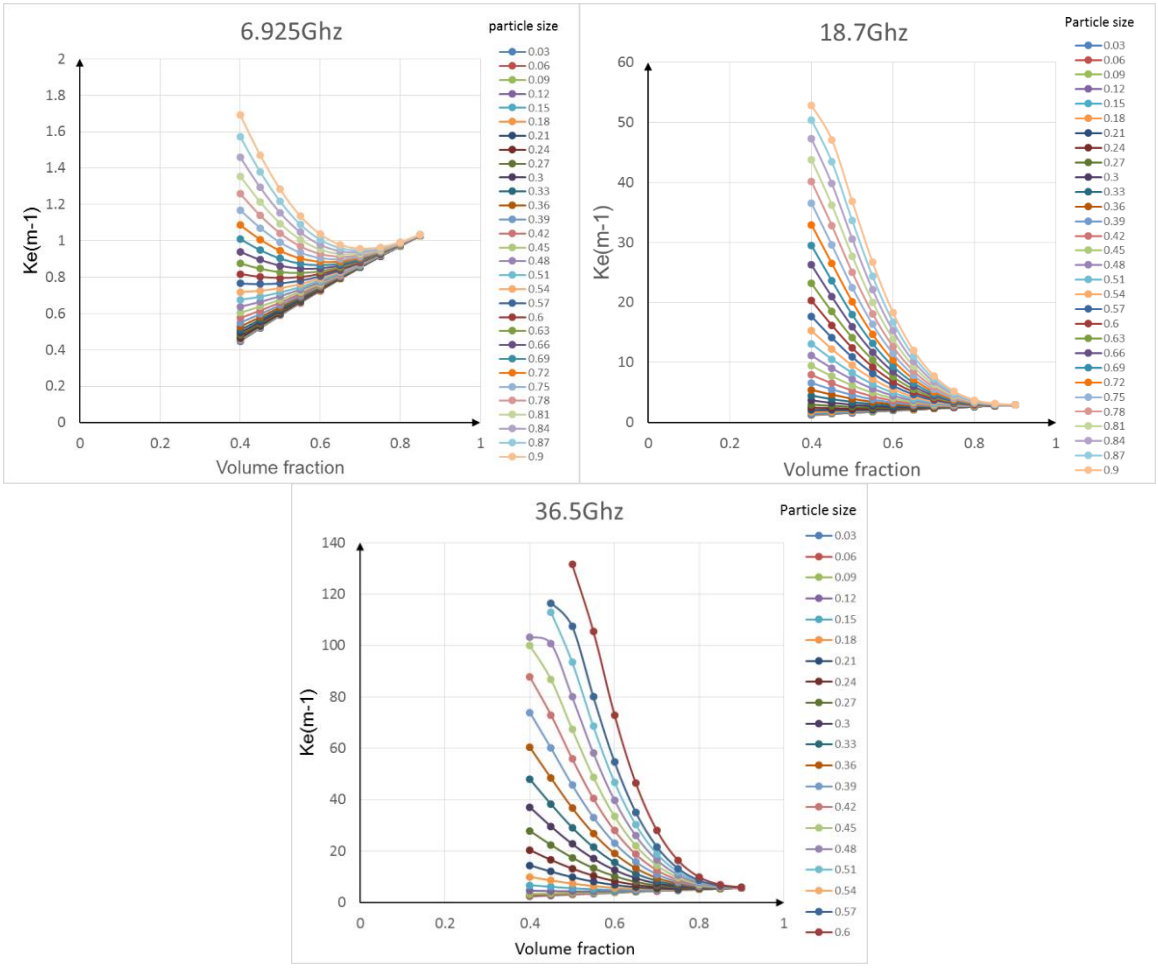

Figure 4.14 Relationship between extinction coefficient k_e, volume fraction and particle size at 6.925, 18.5 and 36.5 GHz in modified QCA-CP.

Once the upward radiance is derived at the top of soil in the new 4 stream fast model, the surface scattering between 2 media will be handled by the Advanced Integral Equation Model (AIEM)[*K-S Chen et al.*, 2003]. Reflectivity $R_{v/h}$ of surface scattering is calculated by the following equation (4.22) accounting for roughness effect and diffuse reflection:

$$R_{v/h} = R_s \cdot \exp[-(2k\sigma\cos\theta)^2] + \frac{1}{4\pi\cos\theta}\int_0^{2\pi}\int_0^{\pi/2}[\sigma_{vv/hh}(\theta,\theta_j,\phi_j) + \sigma_{vh}(\theta,\theta_j,\phi_j)]\sin\theta_j d\theta_j d\phi_j \tag{4.22}$$

where R_s is specular reflectivity calculated from Fresnel equations (4.19-4.20), k is wave number, σ is the roughness parameter RMS height, $\sigma_{hh/vv}$ and σ_{vh} are like-polarized and co-polarized bistatic scattering coefficients, respectively; θ are zenith angle of sensor(AMSR-E: 55°), θ_j and ϕ_j are zenith and azimuth of scattering angle, respectively. The first term on the left side refers to the coherent component, while the second term on the left side refers to diffuse component (the reflection components are depicted in Figure 4.15).

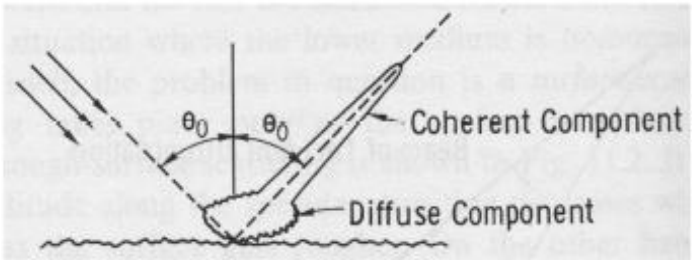

Figure 4.15 Schematic of surface reflection including coherent and diffuse component [*F T Ulaby et al.*, 1982].

Therefore the soil surface transmissivity $\Gamma_{v/h}$ is $1 - R_{v/h}$, the horizontal and vertical polarized radiance out of soil surface can be expressed by brightness temperature Tb, which can be calculated from radiance using Plank's law:

$$T_b = T_b(\tau^*)\Gamma = T_b(\tau^*)(1 - R_{v/h}) \tag{4.22}$$

where Tb is the brightness temperature out of the soil, $Tb(\tau^*)$ is the brightness temperature at the top of soil($\tau=\tau^*$).

4.5 Validation of the multiple-layer RTM for frozen soil

4.5.1 Site introduction

A seasonal frozen soil site in Western Tibet Plateau, Gaize, is chosen for validation of this RTM. Gaize station, located at 84°03′ E, 32°18′ N, is one of important reference site in CEOP Asian Monsoon project (Figure 4.16). Gaize is a cold semi-arid or arid region with an altitude of 4,416 m. Average annual air temperature is -0.2 °C. Average annual precipitation rate is as low as 189.60 mm and rainfall largely concentrates in summer season. As the photo 4.6 shown, the dominant land cover at the observation site is bare land with sparse weed like plant. Vegetation is sparse and limited to rainy season (June - August), which are only a few tens of mm height at the measurement location. The soil is silt loam with a bulk density of $1.49 \times 10^{3} kgm^{-3}$ and porosity of 0.37. The ground status is very homogeneous in a large scale which is very suitable for the application using 25km resolution satellite based AMSR-E data.

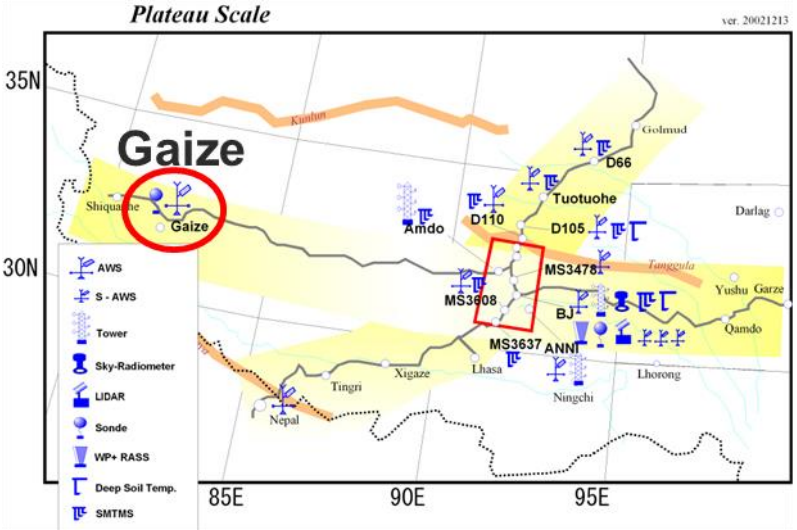

Figure 4.16 Map of the Gaize station in Tibet, China[*Ceop_AP*].

Figure 4.17 Ground status of the Gaize station in Tibet, China [*玉川勝徳 et al.*, 2009].

Hourly meteorological data, including precipitation, air temperature, relative humidity, wind speed, and the downward long- and short-wave radiation, from 1October 2003 to 31 December 2004 were collected from an automatic weather station at Gaize. The soil temperature is measured at six depths: 0, 3, 10, 20, 40 and 80cm, while soil water content at only three depths: 3, 20, 40 cm every 1 hour.

AMSR-E JAXA 1L brightness data of 14 months from 2003 to 2004 at Gaize station is used to validate the performance of the frozen soil radiative transfer model, which is same to the dataset we show in section 4.3.1. Detail information about the dataset we use in this research can be seen in table 4.1.

4.5.2 Frozen soil state variables simulation and parameter calibration

Before running the RTM for frozen soil, the frozen soil state variables, such as soil temperature, moisture and ice content at different depths, have to be prepared as the model input. However, usually soil ice content observation is not available and not all the observation have comprehensive and continuous soil observations in deep soil. Our frozen soil model introduced in chapter 2 and 3 can provide a nice solution for this obstacle.

Firstly, the frozen soil model was applied at Gaize station from Oct. 1st 2003 to December 31st 2004, forced by the hourly meteorological data collected from an automatic weather station. Parameter calibration was applied on the summer (1 July–31 August) of 2004. The thicknesses of soil layers were uniformly set to 10 cm, except 5cm for surface layer. The soil column was divided into 21 layers and the lower boundary condition was placed at 2.05 m depth.

As for soil properties, soil porosity, residual soil moisture, bulk density were given as 0.37, 0.021 and 1490kg/ m^3, respectively. Soil type, land use, vegetation parameter are set according to the soil field observation log. The Van Genuchten parameters α and n, which control soil hydraulic conductivity, were calibrated based on a comparison between the simulated and observed soil moisture during the summer season. The other hydraulic properties were obtained from the original FAO values for [*FAO*, 2003].

The initial soil temperature and liquid water content of each layer were given by interpolating the observed soil temperature and liquid water content at 3 depths using the inverse distance weighting method. Since we started the simulation from summer, the initial ice content can be simply set as 0 for all the layers.

The model was run at hourly time steps from Oct. 1st 2003 to December 31st 2004 at the Gaize station to obtain the soil state variables for RTM. The simulated soil temperature time series at 6 depths (0, 5, 10, 20, 40, 80 cm) are shown in Figure 4.18, compared with the observational soil temperature. The soil moisture time series against observation at 3 depths (3, 20, 40cm) are shown in Figure 4.19. It is clear that the simulated both soil temperature and soil moisture have a good agreement with soil observation in magnitude and trend variation, which again proves that the frozen soil model has a good capability for predicting realistic estimates of both soil moisture and temperature profiles in seasonal frozen soil region with a reliable accuracy.

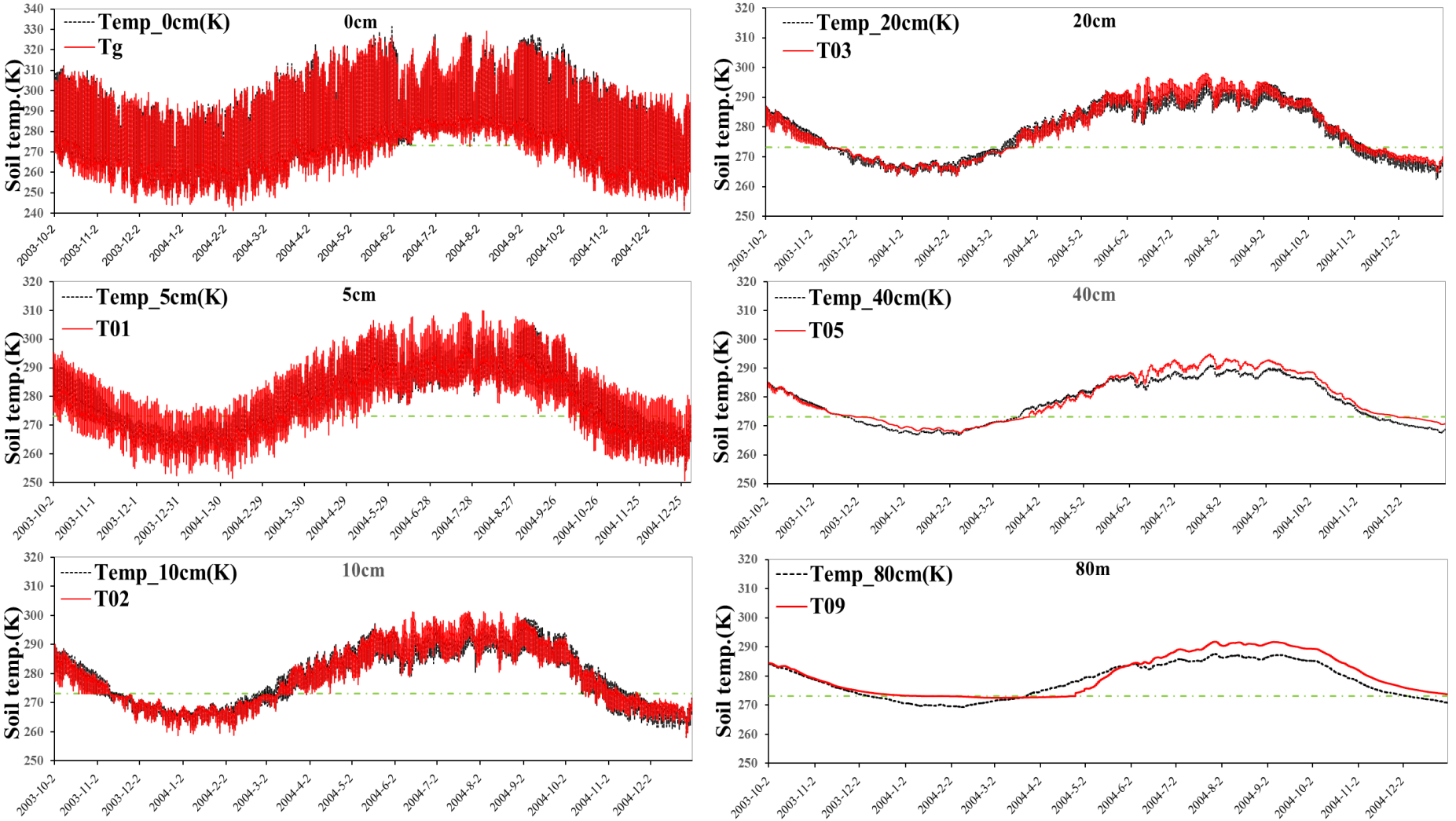

Figure 4.18 Simulated soil temperature at six soil depths at the Gaize station (2003–2004). Red solid line denotes results from soil temperature simulated by the frozen soil model (see in chapter 2 and 3). Black dash line denotes observation data. The green dotted line denotes 273.15 K.

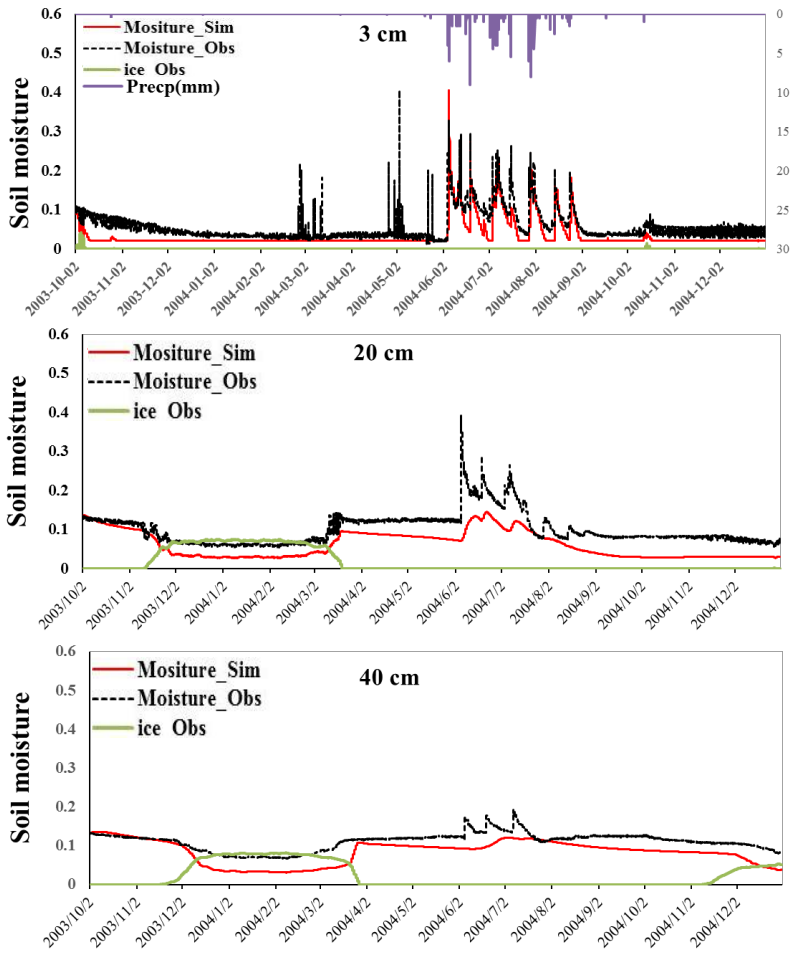

Figure 4.19 Simulated soil moisture at three soil depths at the Gaize station (2003–2004). Red solid line denotes results from soil moisture simulated by the frozen soil model (see in chapter 2 and 3). Black dash line denotes observation data. The green solid line denotes simulated ice content.

Figure 4.20 and Figure 4.21show that the freeze and thaw processes in winter and spring from Oct to next April. Ground gets freeze from November, then frozen for around 3 months until frozen soil thaws from the middle of March. In Figure 4.20, it can be seen that ground surface temperature fluctuates drastically with solar energy and lowest temperature can reach to 240K (-33°C). The time lag and amplitude damping of temperature become pronounced with increasing depth. Lowest soil temperature at 20, 40, 80 cm are not lower than 260K. During the frozen period, soil moisture is lower than 8% (lowest 2.1%); while when it thawed, soil moisture is larger than 12%. From Figure 4.21, we can see that soil moisture increased with soil depth in winter. The surface soil is too dry to generate ice and ice formed in deeper soil (more than 10 cm).

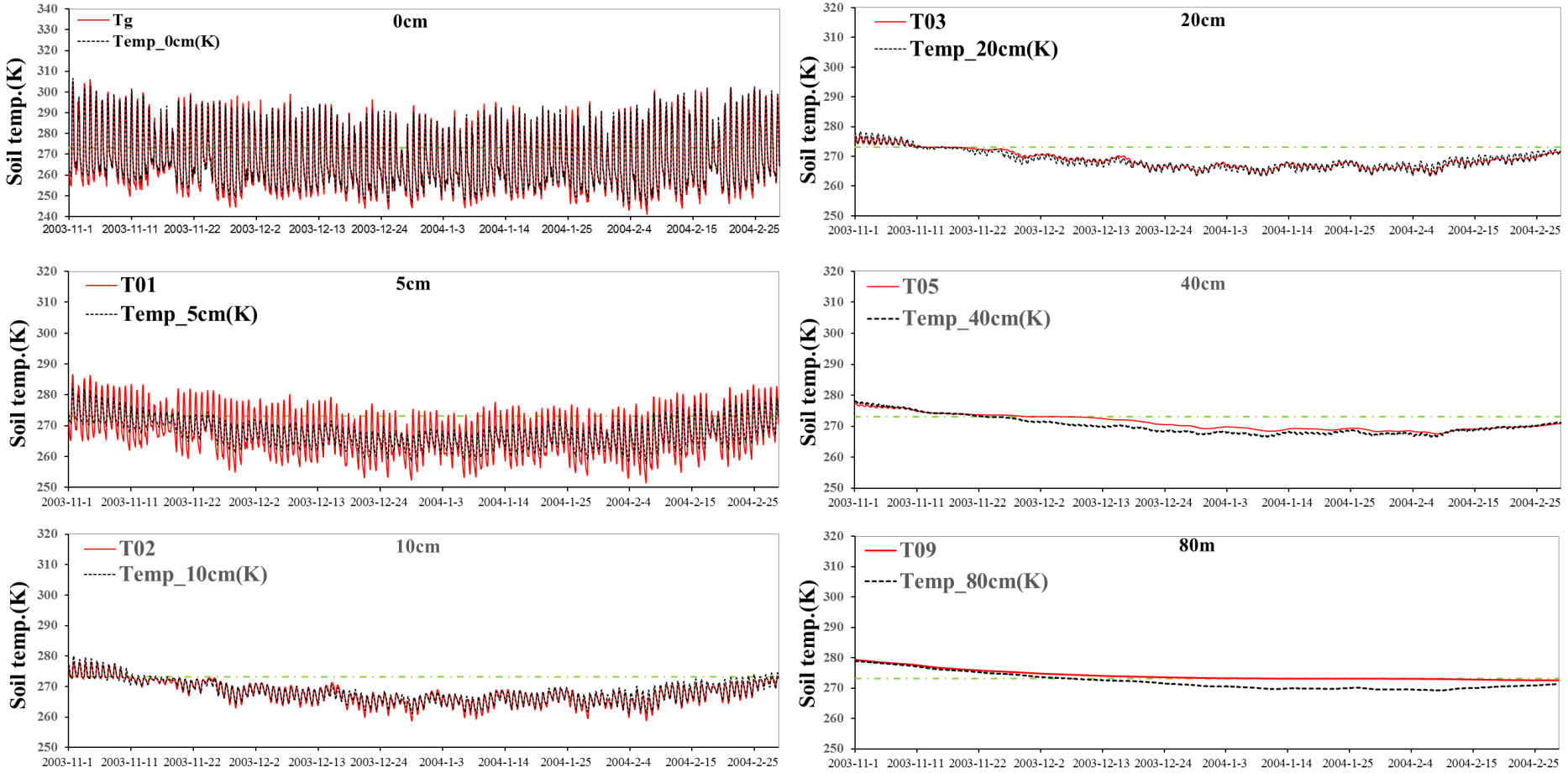

Figure 4.20 Simulated soil temperature at six soil depths at the Gaize station in winter of 2003–2004. Red solid line denotes results from soil temperature simulated by the frozen soil model (see in chapter 2 and 3). Black dash line denotes observation data. The green dotted line denotes 273.15 K.

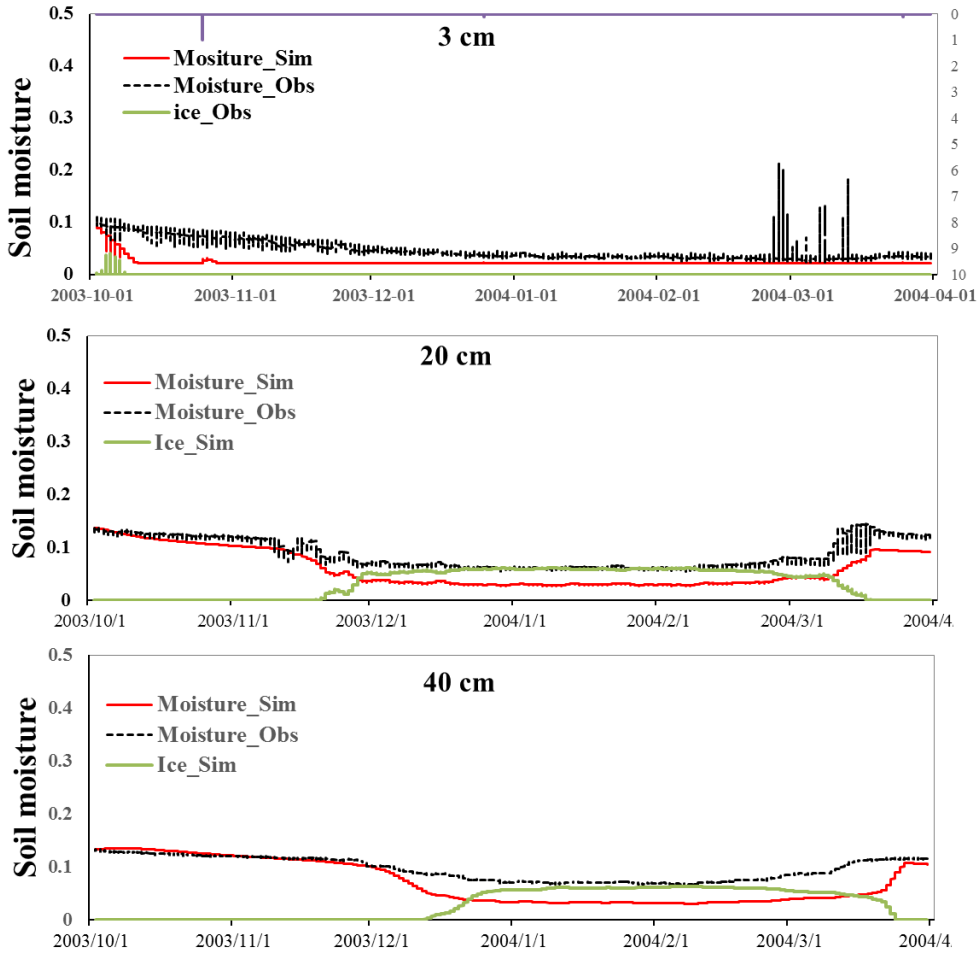

Figure 4.21 Simulated soil moisture and ice content at three soil depths at the Gaize station in winter of 2003–2004. Red solid line denotes results from soil moisture simulated by the frozen soil model (see in chapter 2 and 3). Black dash line denotes observation data. The green solid line denotes simulated ice content.

After completing frozen soil states simulation, it is possible to set up the frozen soil RTM at Gaize station. The 85 cm depth soil column is discretized into 9 layers. Except 5cm surface layer, sublayers are uniformly set as 10cm. In case of AMSR-E, view angle of AMSR-E sensor is 55°. The soil porosity and volume fraction are set as 0.37 and 0.63, according to the field observation. Due to little vegetation growth in summer, the vegetation effect can be neglected and the leave area index is set to 0. Then the calibration is applied in summer to obtain suitable roughness parameters: RMS height and correlation length. In summer, the deep soil emission are masked out and surface emission dominates the observed signal. Next, by matching the AMSR-E data of wet days, sand and clay content can be calibrated. The optimized parameters can be seen in table 4.4. Finally, calibrate particle size in dry and cold days. The strength of volume scattering is proportional to geometric size of particle size *r* relative to frequency and volume scattering effect are particularly apparent in winter. The best calibration of particle size are shown in table 4.5.

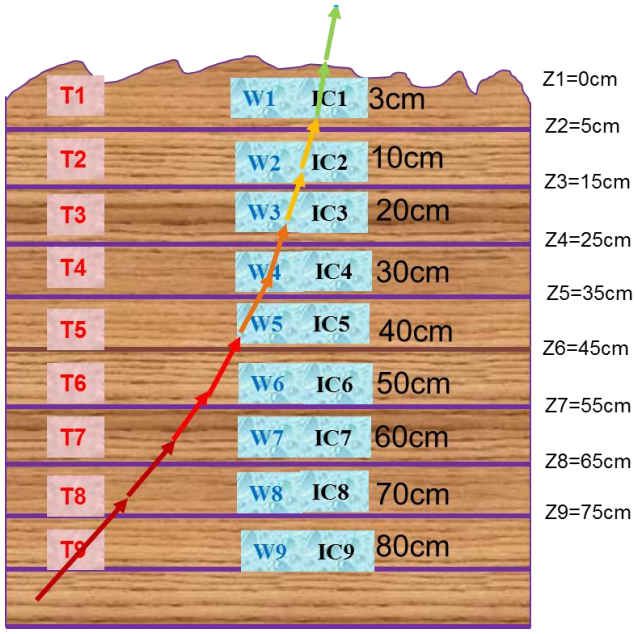

Figure 4.22 Structure of the numerical discretization for frozen soil modeling at Gaize.

Table 4.4. Optimized parameter for frozen soil RTM modeling at Gaize

RMS height (cm)	correlation length (cm)	Sand content (%)	Clay content (%)
0.51	1.60	42.4%	14.18

Table 4.5. Particle size setting for each frequency

f(GHz)	6.925	10.65	18.7	23.8	36.5
Rd (cm)	0.9	0.8	0.7	0.65	0.42

4.5.3 Result and analysis

We run the frozen soil RTM at daily time steps with the soil states variables simulated by the frozen soil model from 1 October 2003 to 1 June 2004 to evaluate the model's performance. The simulated brightness temperature results of vertical and horizontal polarization were compared with the AMSR-E brightness temperature at the Gaize station, shown in Figure 4.23 and Figure 4.24, respectively.

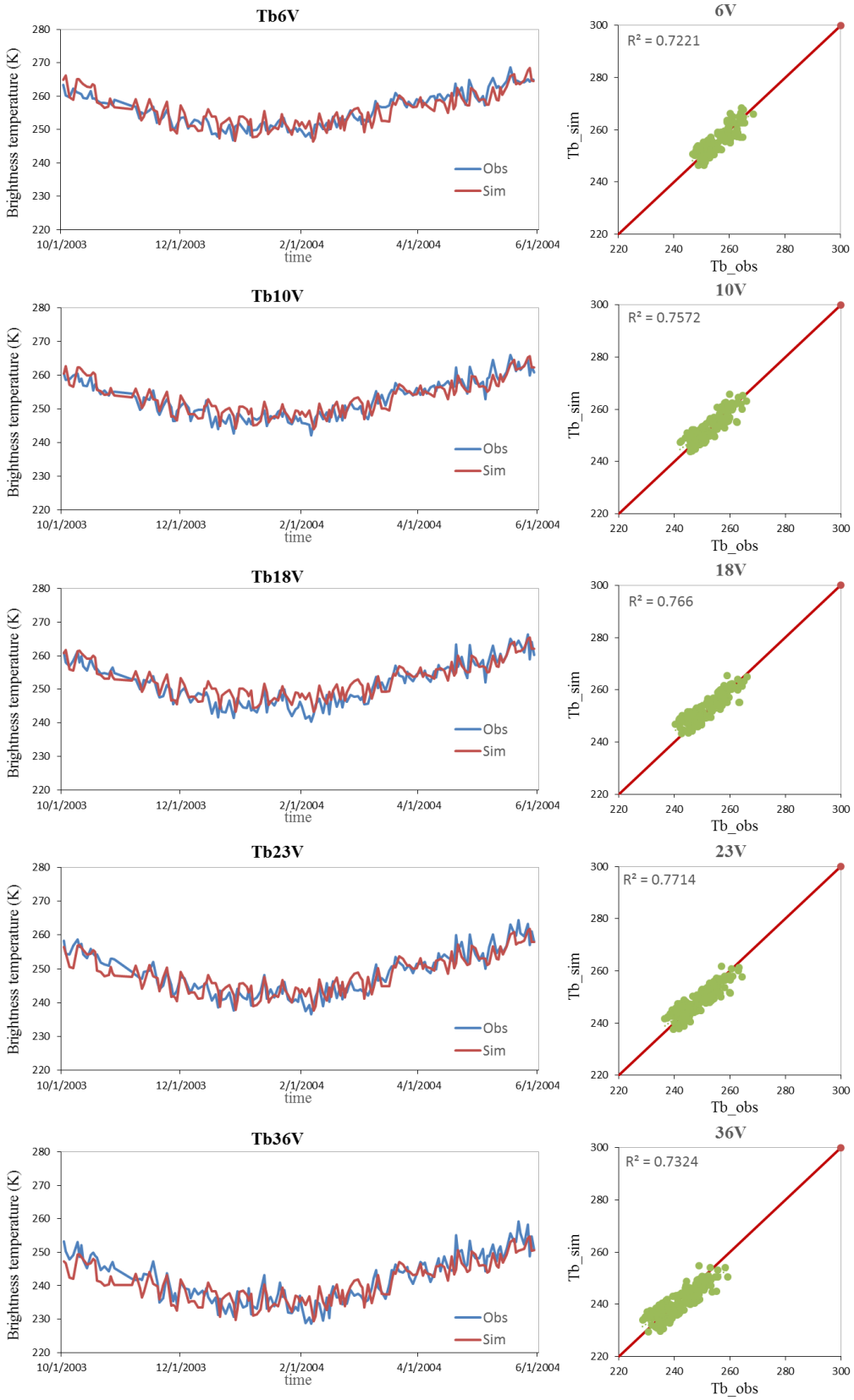

Figure 4.23 Simulated vertical polarized brightness temperature of 5 frequencies (6.925 - 36.5 GHz) against the AMSR-E observation from October 1st 2003 to June 1st 2004 at Gaize station. Red line (Sim) denotes Tb simulated by the RTM for frozen soil; blue line (Obs) denotes AMSR-E Tb data

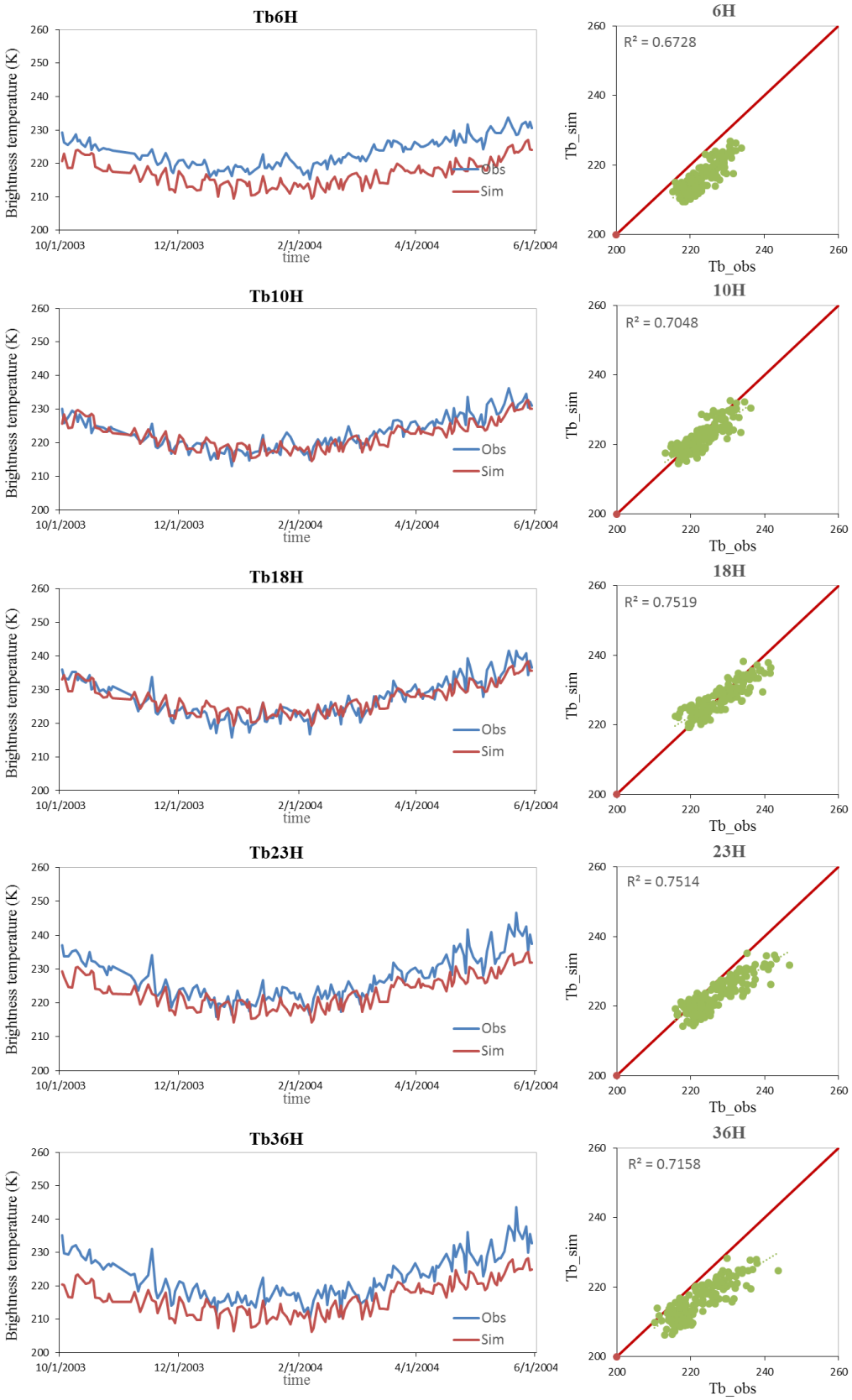

Figure 4.24 Simulated horizontal polarized brightness temperature of 5 frequencies (6.925 - 36.5 GHz) against the AMSR-E observation from October 1st 2003 to June 1st 2004 at Gaize station. Red line (Sim) denotes Tb simulated by the RTM for frozen soil; blue line (Obs) denotes AMSR-E Tb data

From the brightness temperature time series and scatter plot, it is clear that that the simulated brightness temperature at 5 frequencies are all in good agreement with AMSR-E Tb. The RMSE and correlation coefficient of 5 frequencies at horizontal and vertical polarization are shown in table 4.6. It is demonstrated that this multi-layer frozen soil RTM can predict Tb of frozen soil from 6 GHz to 36 GHz with good accuracy and the phenomenon of negative spectral gradient are also successfully reproduced, which has not been achieved in previous studies. In turn, it is also proved that the frozen soil radiative transfer mechanism we proposed does correspond to the reality and can explain the phenomenon of microwave radiation transfer in frozen soil. Moreover, the modeling algorithm coupled volume scattering and surface scattering processes can reproduce the radiation transfer processes within frozen soil and reflect the radiative characteristics of freeze- thaw cycle.

Table 4.6. RMSE and R^2 of the frozen soil RTM at 6 frequencies from October 1st 2003 to June 1st 2004

RMSE	6GHZ	10GHZ	18GHZ	23GHZ	36GHZ
VERTICAL	2.7424	2.7222	3.1435	3.0634	3.7257
HORIZONTAL	7.0196	2.8165	3.0047	5.2516	7.2084
R^2	6GHz	10GHz	18GHz	23GHz	36GHz
VERTICAL	0.7221	0.7572	0.7660	0.7714	0.7324
HORIZONTAL	0.6728	0.7048	0.7519	0.7514	0.7158

4.6 Summary

Spectral gradient of frozen soil is negative, that is, brightness temperature (Tb) of low frequency (6GHz) is relative higher than Tb in high frequency (36GHz). This characteristic is regarded as an indicator of frozen soil and widely adopted in most of current frozen soil mapping algorithms. Although this phenomenon was qualitatively explained as the volume scatter darkening within frozen soil like that recognized for microwave emission as is snow, the complete physical mechanism for frozen soil radiative transfer processes is still not clear and quantitative simulation is still defective. By contrast, for soils that contain liquid water, the spectral gradient is positive because the Debye process has a greater darken effect at low frequency than high frequency and the Tb is relative high than that of frozen soil due to its high physical temperature.

We tried to clarify the mechanism of frozen soil radiation transfer processes by developing

a frozen soil radiative transfer model. The radiative transfer processes of frozen soil are described as 2 separate processes: 1). soil emission transfers within frozen soil: In cold season, water absorption is so weak that the penetration depth becomes deep. Emission from deep soil and the volume scattering effect of soil particles is considered in this RTM. However when frozen soil thaws in warmer season, the penetration depth is so shallow because of water absorption that the radiation from deep soil can be neglected. 2). Soil radiation passes through soil-air boundary: the difference of dielectric constant between frozen soil and air is small, because of low water content, which means the transmissivity of air-soil boundary is high and surface scattering of frozen soil is very weak. While the dielectric constant of wet soil and air is large, which in turn causes strong surface scattering in air-soil boundary.

This frozen soil RTM employed a multiple parallel-layer soil structure, similar as frozen soil physical model. Soil properties are assumed homogeneous within each layer and soil particles are assumed as sphere. An atmosphere RTM 4 stream fast model was modified for representing the soil emission transfer from bottom to top soil layer. A dense media radiative transfer model QCA-CP was adopted to calculate the extinction coefficient and single scattering albedo of each soil layer. Surface scattering is also considered by implementing Advanced Integral Equation Model (AIEM). In addition, roughness and shadow effects are also taken into account.

By inputting simulated frozen soil profile information into this frozen soil RTM, the Tb of different frequencies can be simulated. And an validation is conducted by comparing the simulated Tb with the AMSR-E Tb. Results show that this RTM can predict Tb of frozen soil from 6 GHz to 36 GHz with good accuracy and the phenomenon of negative spectral gradient are also successfully reproduced, which has not been achieved in previous studies. According to simulation and AMSR-E observation, it is proved that volume scattering dominates the radiative transfer process in frozen season and the negative spectral gradient is attributed to the strong scattering in higher frequency. In turn, it is also proved that the frozen soil radiative transfer mechanism we proposed does correspond to the reality and can explain the phenomenon of microwave radiation transfer in frozen. Moreover, the modeling algorithm coupled volume scattering and surface scattering processes can reproduce the radiation transfer processes within frozen soil and reflect the radiative characteristics of freeze- thaw cycle. Therefore, it is demonstrated that the frozen soil RTM offers a realistic and quantitative understanding for frozen soil radiative transfer mechanism and has a good capability of simulating the radiative transfer processes in frozen soil at frequencies from 6GHz to 36 GHz.

5. INITIALIZATION OF FROZEN SOIL PROFILE FOR FROZEN SOIL MODELING

5.1 Introduction

Even if the model was perfect, we cannot forecast very well without good initial condition. This is especially true for frozen soil modeling. Initial soil states including soil moisture, temperature and ice content are critical parameters for simulation frozen soil processes. For example, initial soil states not only affects initial thermal and hydraulic properties, but also determines how much water will be stored in winter and how much energy will be needed for melting in the next warm season. Different initial conditions can therefore lead to considerable differences in soil moisture results and the freezing/thawing simulation. To correctly simulate the heat-water transfer and freeze- thaw processes in frozen soil modeling, there is an urgent need to obtain accurate initial frozen soil states.

Frozen soil are mainly distributed in polar and mountainous region far away from inhabited areas with harsh climate. Comprehensive soil observations are only available for several well-equipped weather or hydrological stations and underground information are difficult to obtain in scarcely gauged areas. Obtaining realistic initial soil profiles is a major challenge for permafrost modeling. Generally, most of frozen soil modeling applications obtained soil state variables by long term spinup simulation with repeat year forcing till the hydrological equilibrium. However, rainfall spatial data, such as reanalysis data and satellite product, have strong biases and coarse time resolution. The uncertainty of rainfall may bring large bias to soil moisture.

Microwave signal is very sensitive to both soil temperature and liquid water. As we all know, freeze and thaw processes of frozen soil are characterized by the drop and raise of soil temperature and water content. Another advantage of passive microwave remote sensing is that in very dry situation, microwave penetration depth becomes deeper, which means that the deep frozen soil signal is detectable (detail in section 5.2.1). In addition, satellite based passive microwave remote sensing has high revisit frequency and all-weather working ability.

Considering these advantages, assimilating the microwave satellite data into frozen soil modeling could be a potential solution for frozen soil initialization problem and can improve the skill of frozen soil models to simulate frozen soil states variables.

Data assimilation is the processes by incorporating observations of actual system into the model state of numerical model of that system, which has been widely applied in land surface modeling. Data assimilation technique had already been used for frozen soil modeling to optimize soil properties parameters from in-situ temperature measurement [*Nicolsky et al.*, 2009]. However, it is hard to find studies using data assimilation to recover the initial soil conditions and improve forecast of frozen soil modeling based on passive microwave satellite data.

In this chapter 5, we put forward a new soil profile initialization method that estimate soil moisture profile by coupling dry soil penetration of passive microwave sensor and physical mechanism of frozen soil modeling. Firstly, the penetration depth of microwave at different frequencies are estimated for wet soil and dry soil. Then sensitivity studies on soil temperature and soil moisture initialization are conducted separately. In the next sections, we proposed our assimilation method. Finally, a point scale experiment is conducted to test this method in the seasonal frozen site, Gaize by assimilating AMSR-E brightness temperature data.

5.2 Soil Profile Initialization method

5.2.1 Penetration depth

To quantitively evaluate how deep the microwave signal from frozen soil is detectable, we compute the penetration depth of each frequency at a wide range of soil moisture (0%-20%).

Assuming a wave incident upon a soil surface (z=0) from air in the direction: transmitted power P_0 just beneath the surface ($z=0^+$) is attenuated during the propagation in soil medium and the remainder is transmitted into the deep soil, K_e represents extinction coefficient. The power at depth z can be expressed as[*F T Ulaby et al.*, 1982]:

$$P(z) = P(0+)\exp(-\int_0^z k_e(z')dz') \tag{5.1}$$

The penetration depth δ_p is defined as the depth z at which the transmitted power

attenuated to the 1/e of original incident power at surface (z=0+)[*Njoku et al.*, 1980].

$$\frac{P(\delta_p)}{P(0+)} = \frac{1}{e}$$

(5.2) that is, $\int_0^{\delta_p} k_e(z')dz' = 1$ (5.3)

by assuming soil is a scatter-free medium,

$$K_e \approx K_a = 2\alpha, \quad (5.4)$$

where K_a is the absorption coefficient and α is the absorption constant, $\alpha = k_0 \left|\mathrm{Im}\left(\sqrt{\varepsilon_{soil}}\right)\right|$. If assume α does not vary with depth, equation (5.3) could be simplified: $2\alpha^*\delta_p=1$. Finally, the effective emitting depth δ_p can be given as:

$$\delta_p = \frac{1}{2\alpha} = \frac{1}{2k_0\left|\mathrm{Im}\left(\sqrt{\varepsilon_{soil}}\right)\right|} \quad . \quad (5.5)$$

with $k_0 = 2\pi/\lambda_0$ is the wave number in free space, λ_0 is the wavelength in free space, ε_{soil} is soil dielectric constant, the modified Wang-Schmugge model by Neluwala is adopted here to considering ice and unfrozen water in frozen soil (detail in section 4.2.3).

According to the equation (5.5), penetration depth varies with soil moisture, ice content, and soil temperature and soil texture. To calculate the typical penetration depth for frozen soil, soil temperature is set as 273.15K at which ice and liquid water can co-exist; ice content is fixed as 0.05; sand and clay contents are 42.4% and 14.18%, separately. The range of liquid water content is from 1%-20%, which is relative lower than the normal soil.

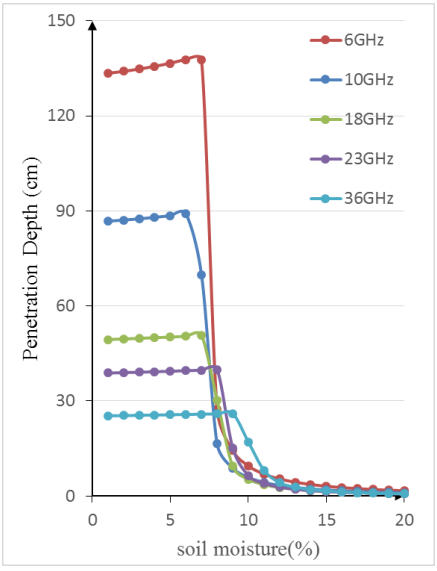

Figure 5.1 Penetration depth of frozen soil as a function of moisture content for 6.925, 10.65, 18.7, 36.5 GHz

Table 5.1 Penetration depth (cm) of frozen soil for 5 frequencies for typical soil moistures

Moisture (%)	6GHz	10GHz	18GHz	23GHz	36GHz
1	133.44	86.76	49.40	38.81	25.31
5	134.04	88.48	50.18	39.38	25.64
10	9.50	5.87	5.31	6.49	17.07
15	3.07	1.89	1.41	1.39	1.58
20	1.67	1.02	0.72	0.68	0.68

From Figure 5.1 and table 5.1, we can see that the frozen soil is more transparent for microwaves bands than the normal moist soil is. It is clear that the lower frequency and the lower liquid water content, the deeper penetration depth of frozen soil. For lower frequency, 6.925 GHz, the penetration depth is deeper than 1m, in the extreme dry case. For higher frequency, the maximum penetration depth is lower than 26cm. If the soil moisture is higher than 10%, the penetration depth is lower than 10 cm, except 36 GHz.

5.2.2 Sensitivity study to soil temperature and moisture initialization

To evaluate the effect of different initial conditions on soil temperature and moisture simulations, we conducted 2 sensitivity studies for soil temperature and soil moisture initialization, separately. The sensitivity analysis study was carried out at the Gaize site using the same forcing data and parameters as section 4.5.2 and all the experiments started from Oct 2nd 2003 with different initial conditions, when no ice appeared in this season.

(1) Sensitivity study to soil temperature initialization

The sensitivity analysis study on soil temperature is performed using 2 different soil profiles as initial soil temperature conditions. One is cold soil profile using air temperature (278.35 K) for all the layers, which is 6~8K colder than actual soil temperatures. Another one is warm soil profile using 292.35K for all the layers, which is 6~8K warmer than the actual soil temperature. The soil temperature simulation results with cold and warn initial conditions are shown in Figure 5.2 and 5.3, separately.

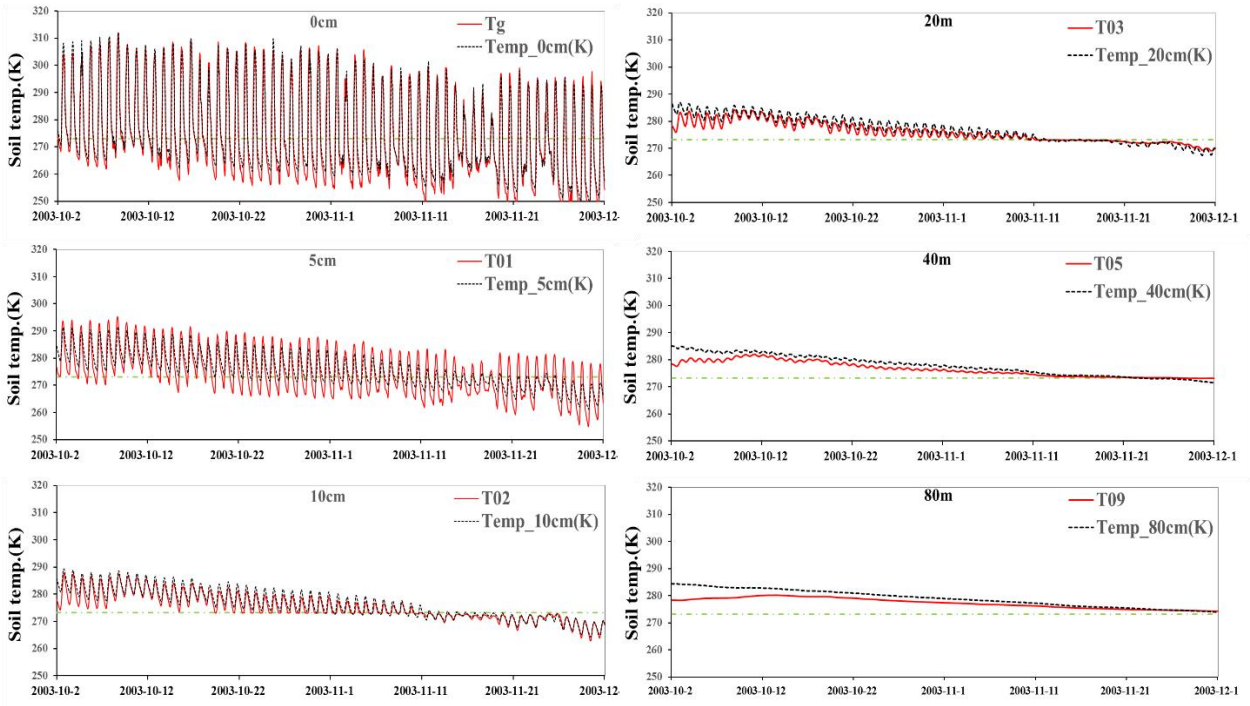

Figure 5.2 Soil temperature simulation at 6 depths with cold initial soil profile (air temperature: 278.35K).

We can see that no matter cold or warm soil profiles, soil temperatures at depths from 0 cm to 80 cm all run on the right track after a period range from several hours to 40 days. The time period depends on the depth. In Figure 5.2, ground surface temperature is adjusted to the right track within few hours. While for soil at 5cm and 10 cm, it takes less than 1 day to reach the actual situation. However, for 20 and 40cm, they take 7 days and 10 days separately. Soil at 80 cm takes the longest time around 40days. Because it takes time for energy to travel down to the deep soil, there is a delay in the time with the increasing of soil depth. So it takes longer time for deeper soil to reach the soil observation.

Compared to the cold profile (278.35K), it takes shorter time to obtain the good simulation for the warm soil profile (292.35K) (Figure 5.3). Soil at 0cm, 5cm, 10cm and 20 cm can be simulated very well within 2days. It takes 20days for 40cm depth temperature to match the observation. Soil temperature at 80cm takes around 40days to approach good simulations. According to the results of sensitivity studies, soil temperature can be simulated very well within 2-5 weeks for different initial soil temperature profiles. It is because that soil temperature simulation is forced by the solar radiation daily. Therefore, we can simply use air temperature with offsets as the initial condition and the good simulation of frozen soil can be obtained with several weeks.

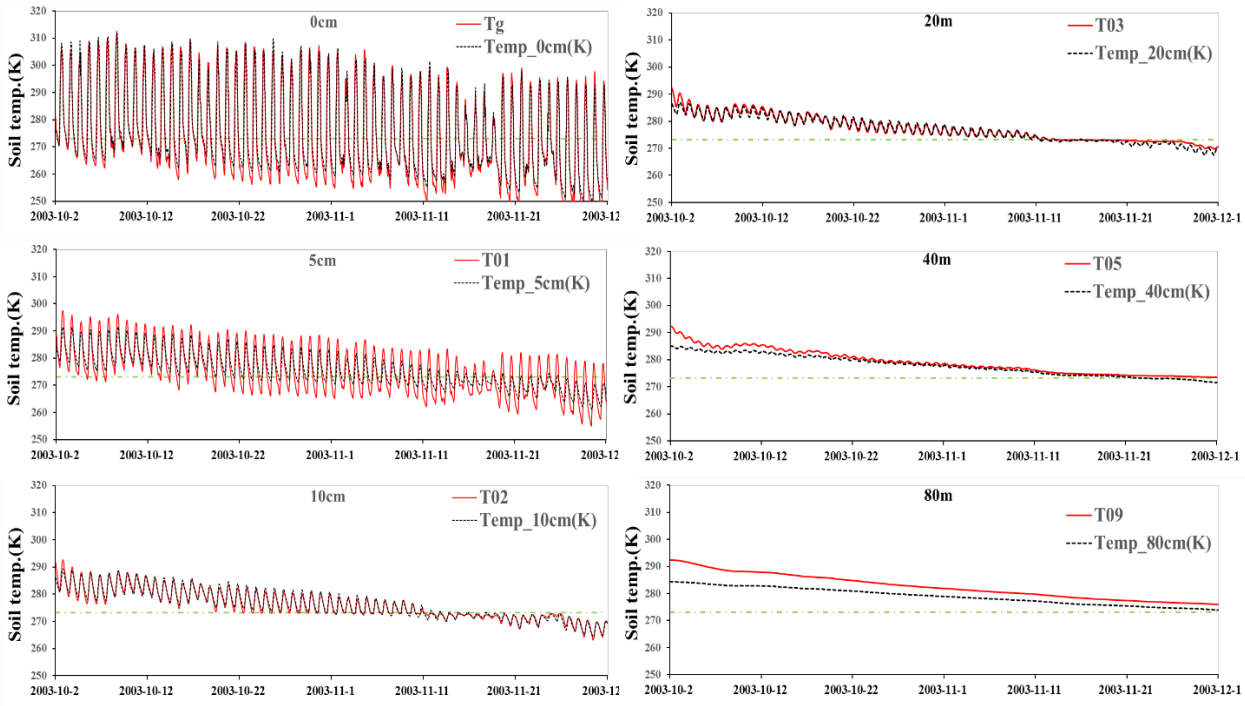

Figure 5.3 Soil temperature simulation at 6 depths with warm soil profile (292.35K) as initial conditions.

(2) Sensitivity study to soil moisture initialization

The sensitivity analysis study on soil moisture is performed using 2 different soil profiles as initial soil moisture conditions: One dry soil profile, which only has 50% content of actual soil moistures; another wet soil profile, which is 1.5 times wetter than the actual soil moisture. Figure 5.4 and 5.5 show the soil moisture simulation results against the observation with dry and wet initial conditions, separately.

From the Figure 5.4, we can see that the once the initial soil moisture is underestimated, the soil moisture simulation will continue to be underestimated for 6 months from Oct. to next April without improvement. It is because that there is little rain in the autumn and winter. The period of the water cycle is usually 1 year, longer than the diurnal cycle of solar radiation.

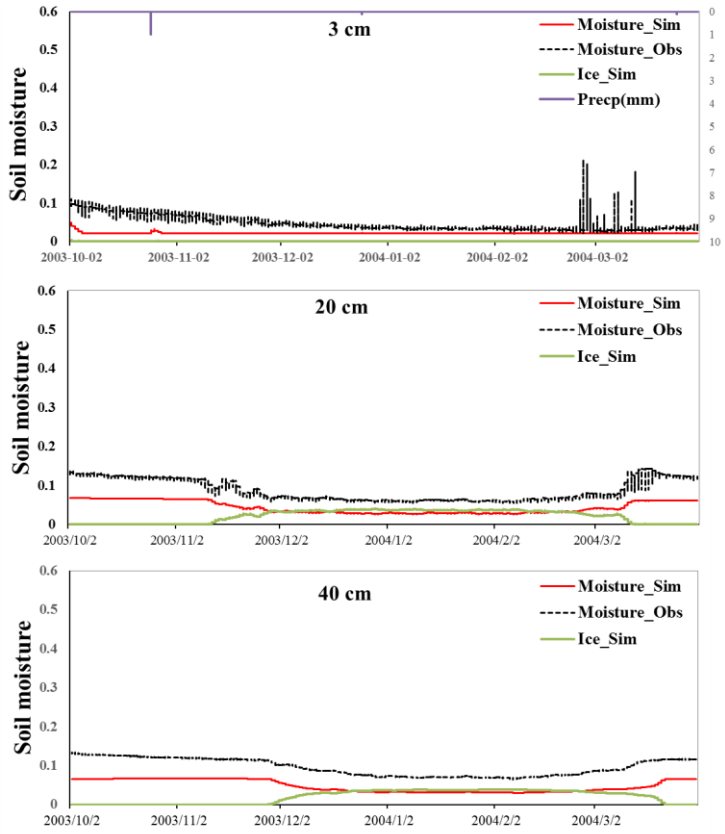

Figure 5.4 Soil moisture simulation at 6 depths with dry soil profile as initial conditions.

On the other hand, simulation with wet initial condition (Figure 5.5) is much better than that with dry one. Soil moisture was simulated well after one month and it was a little bit overestimated. Because soil moisture is mainly controlled by the gravity drainage and freezing/ thawing process, so the extra liquid is either drained out to the deep soil or frozen as ice. It may bring large biases to the estimation of deep soil moisture content (>40cm).

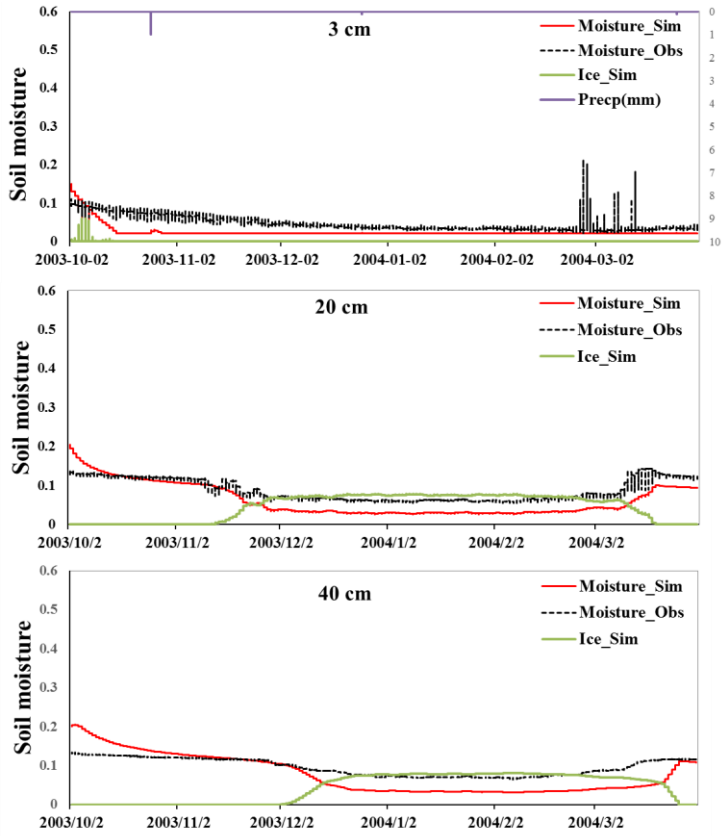

Figure 5.5 Soil moisture simulation at 6 depths with wet soil profile as initial conditions.

Therefore, it can be clearly seen that initial soil moisture profile considerably affect the soil moisture simulation for long time, especially for low water content initialization, which cannot be improved though long time model running.

According to the sensitivity analysis on different initialization conditions, it is proved that the improper value set of initial soil moisture can bring more serious effect on the accuracy of frozen soil simulation than that of initial soil temperature. It is suggested that using air temperature or temperature plus offsets as the initial soil temperature profile is good enough for obtaining accurate soil temperature simulation in the short time. However, the soil moisture cannot be simulated well without suitable initial conditions in frozen soil regions.

5.2.3 Initialization method design

Satellite based passive microwave sensors are sensitive to both soil temperature and moisture. In addition, satellite based passive microwave sensors can frequently and continuously monitor large scale area in all-weather condition. According to the sensitivity

study above (section 5.2.1), it is proved that deep frozen soil information are detectable for microwave signal, especially at low frequency, which is operated by the current common used sensors, such as AMSR-E and SSM/I. By assimilating the passive microwave brightness temperature (AMSR-E Tb) into the frozen soil modeling, we proposed a method for estimating the optimum initial soil moisture profile method to improve frozen soil simulation in place with insufficient observation.

First of all, as the sensitivity studies show in section 5.2.2 that soil temperature can be forced by the solar radiation daily and it can be simulated very well using different initial conditions within short time period. However, the soil moisture is much more difficult to be driven to the actual soil moisture by the forcing. Therefore, this study focused on initializing the soil moisture profile. Secondly, there's hardly any ice in active layer of frozen soil before ice period. Given that the initial ice content can be assigned as 0 in autumn, the initialization of frozen soil profile can be simplified. Thirdly, Tb at different frequencies represent the total emission of different soil thickness. At high frequency, the relative contribution from shallow soil may take up a great portion, while at low frequency, the weight of deep soil emission contribution could be considerable. Taking advantage of Tb at each frequency may provide multi-level information for frozen soil simulation. Last but not least, freeze and thaw cycles always come along with the fluctuation of soil moisture and temperature, which give the chance to microwave signal to reflect and record the distinct states.

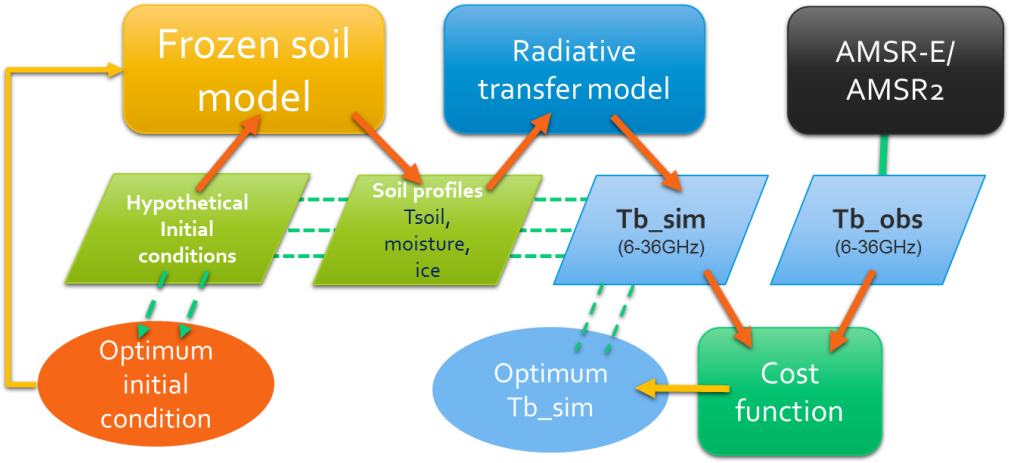

Figure 5.6 flow chart of initialization method by assimilating the AMSR-E brightness temperature

Given the above analysis, a method that assimilating multi-frequency Tb time series over a span of freeze and thaw seasons, not instantaneous Tb observation, is designed for initializing soil moisture profile before freezing. The flow chart of the initialization method is shown in Figure 5.6. Generally ground surface information is obtainable from land surface

data assimilation system or ground surface observation. So we can generate hypothetical soil profiles according to ground surface moisture as initial conditions. Then the frozen soil states can be simulated by the frozen soil model using the hypothetical soil profiles, separately. Next, taken the output frozen soil state profiles as input data, frozen soil RTM can simulate brightness temperature. By comparing the simulated Tb time series with AMSR-E Tb, we could find the best match simulated Tb time series, At last, the hypothetical initial condition of this best match Tb series is selected as the optimum initial soil profile.

By giving the optimum initial soil profile to frozen soil model as the initial condition, the frozen soil prediction accuracy should be improved in the application of poorly gauged regions and the performance of frozen soil model can be maximized for large scale application.

5.3 Application Soil Profile Initialization method

This assimilating method is applied and validated in the seasonal frozen soil site, Gaize (detail about Gaize in section 4.5.1). Soil generally freezes in the cold season from the middle of November to the end of March and all the soil layers thaw completely in the warm seasons (freeze-thaw cycle of Gaize can be seen in section 4.5.2). So October 2nd before freeze, is chosen for test.

Firstly, 10 hypothetical soil profiles were generated according to surface soil moisture simply using exponential relationship. We limited the bottom soil moisture between saturated moisture and residue water content. The surface and bottom soil moisture of October 2nd are given in table 5.2. It is assumed an exponential relationship between the soil moisture and soil depth:

$$\theta_l(z) = \theta_{l\_srf} + (\theta_{l\_btm} - \theta_{l\_srf})[1 - \exp(-5z)] \quad (5.6)$$

where $\theta_l(z)$ is the soil moisture at different depth, θ_{l_srf} and θ_{l_btm} are surface soil moisture and bottom soil moisture, respectively. z is the soil depth. The center of the bottom soil layer is 80 cm. The numerical discretization of soil layer structure is same as Figure 4.22. Figure 5.7 shows 10 hypothetical soil profiles for each day.

Table 5.2. Surface and bottom moisture of hypothetical soil profiles on October 2nd.

Time	Surface Moisture	Bottom moisture range	Relation
2003, Oct 2nd	0.0987	0.02-0.37(saturation)	Exponential

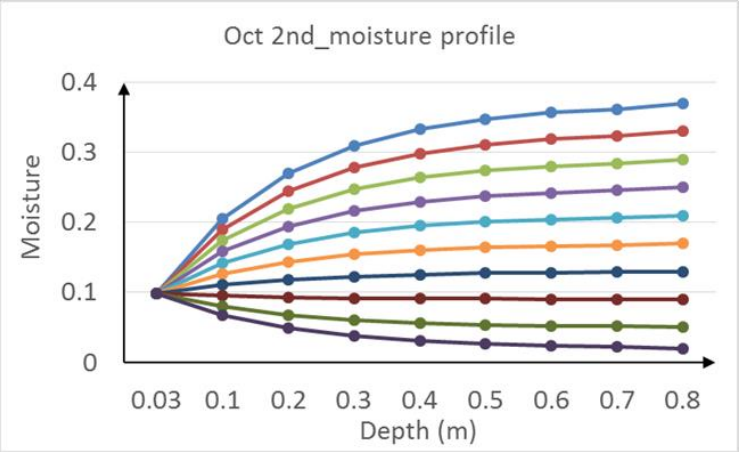

Figure 5.7 10 hypothetical soil profiles for initialization on October 2nd.

After getting the hypothetical soil profiles, the frozen soil model starts its run with different hypothetical soil profile. Then forcing data of the frozen soil states for the RTM simulation can be obtained from frozen soil modeling. The output of frozen soil moisture at 20cm and 40 cm with different initial condition can be seen in Figure 5.8 that soil moisture and ice content show large difference in freeze and thaw season from October to May.

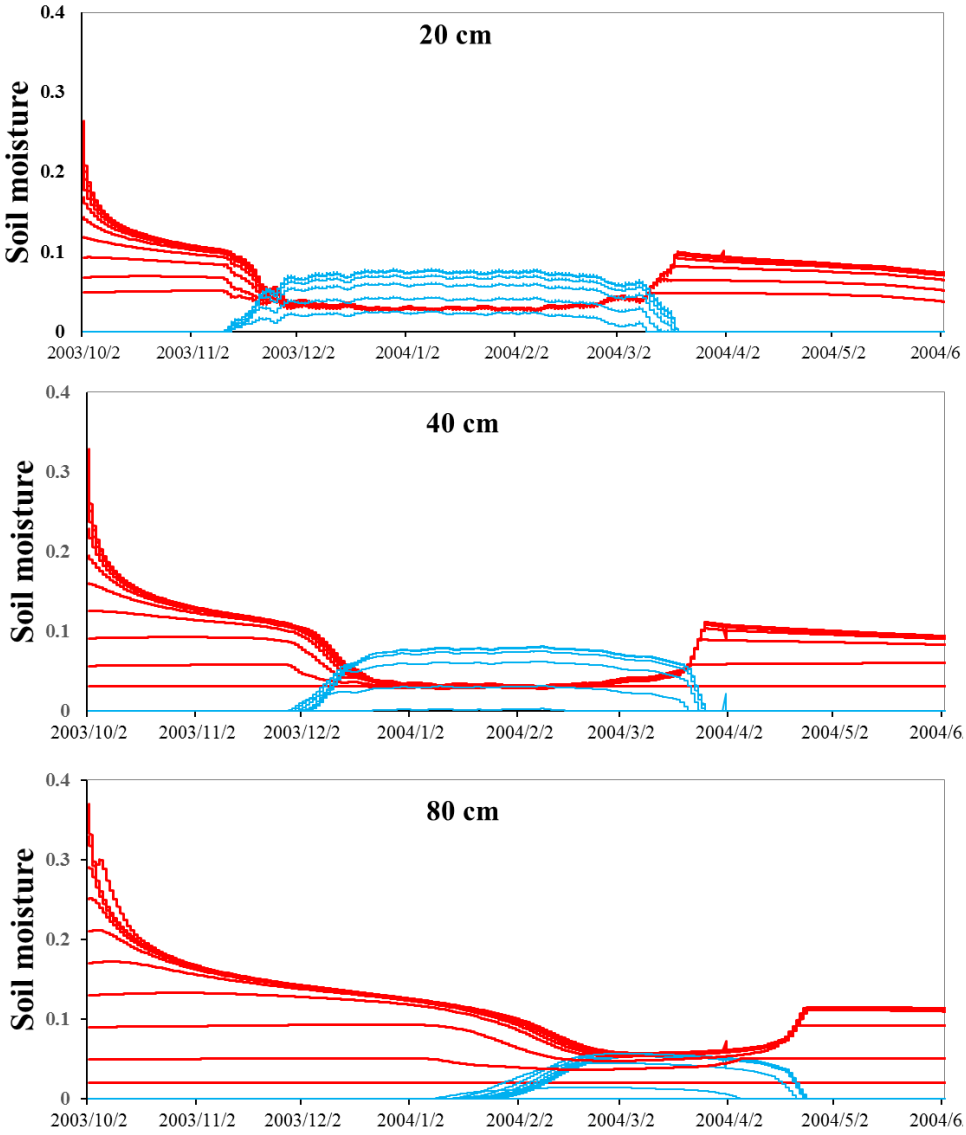

Figure 5.8 the simulated soil moisture time series at 20cm, 40cm and 80cm with 10 different initial conditions

Next, pass the simulated frozen soil state variable to the frozen soil RTM as forcing data, the Tb time series of 5 frequencies (6.925, 10.65, 18.7, 23.8 and 36.5 GHz) can be calculated over frozen and thaw seasons of 2003-2004. By comparing the simulated Tb time series with those of AMSR-E (Figure 5.9) and computing the root mean square error (RMSE), the best match simulated Tb time series can be found by identifying the Tb time series with lowest RMSE.

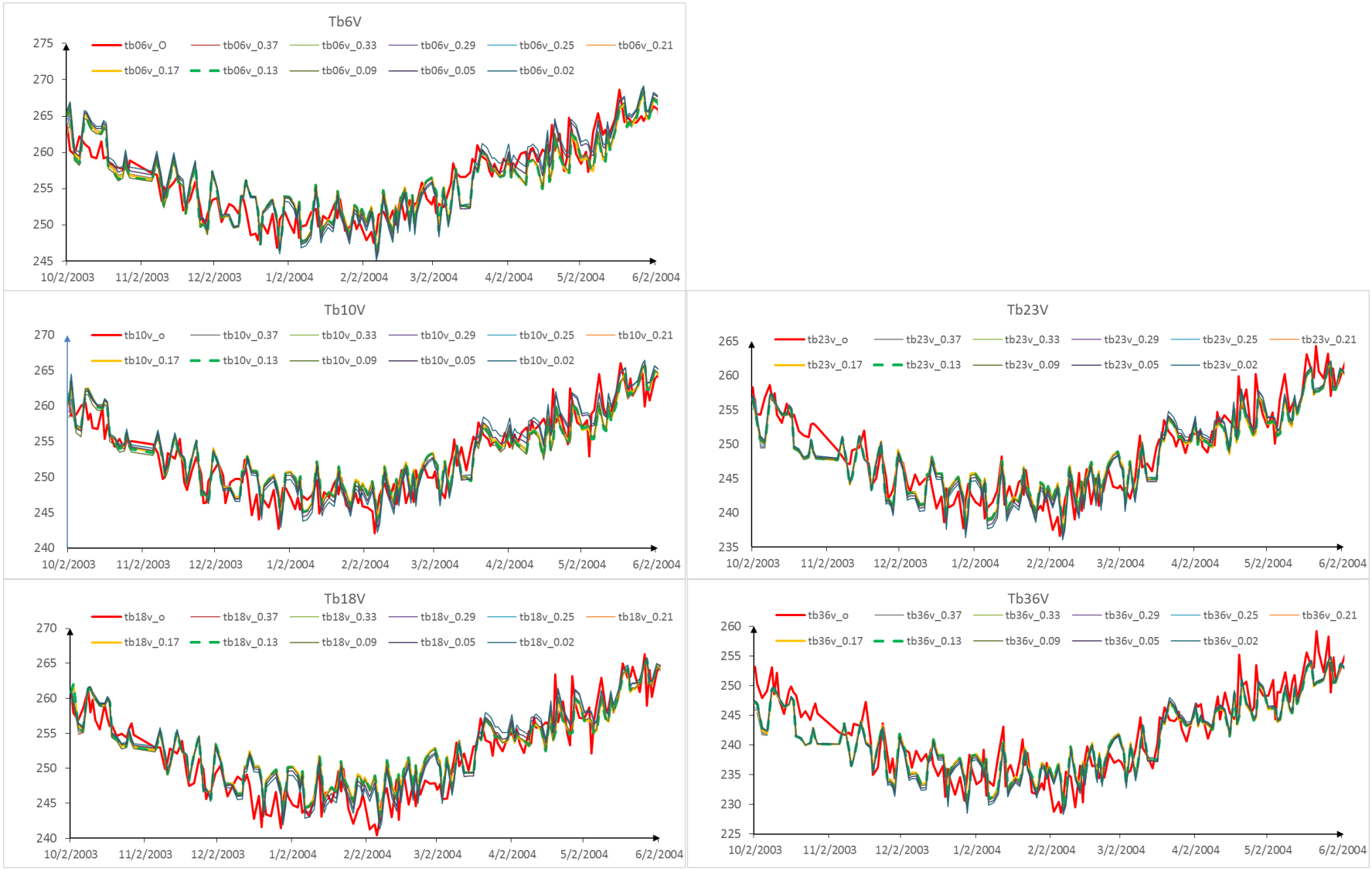

Figure 5.9 Comparison of 10 simulated brightness temperature and AMSR-E brightness temperature (red line) at 6.925, 18.7 and 36.5 GHz. With initial conditions of Oct. 2nd.

Considering that the penetration depth of 6GHz is deep enough to detect deep soil information. Tb at 5 frequencies from 6GHz to 36 GHz may provide multi-level frozen soil information, we defined 2 RMSE expressions for all 5 frequencies (5.8) and 6GHz (5.7), separately. The RMSE of different initial conditions are shown in table 5.3.

$$RMSE_{\_6GHz} = \sqrt{\frac{\sum_{i=1}^{N}(Tb_{sim}(6GHz) - Tb_{obs}(6GHz))^2}{N}} \tag{5.7}$$

$$RMSE_{\_6-36GHz} = \sqrt{\sum_{f=6GHz}^{36GHz}\frac{\sum_{i=1}^{N}(Tb_{sim}(f) - Tb_{obs}(f))^2}{N}} \tag{5.8}$$

Table 5.3. RMSE statistics of different initial conditions marked by the bottom soil moisture

Bottom moisture	0.37	0.33	0.29	0.25	0.21	0.17	0.13	0.09	0.05	0.02
6-36GHz	4.671	4.360	4.358	4.356	4.351	4.347	**4.337**	4.351	4.392	4.417
6GHz	4.485	4.485	4.487	4.484	4.479	**4.477**	4.489	4.531	4.722	4.556

The minimum values of RMSE are shown in bold in table 5.3. Hence, the soil moisture profile with bottom moisture 0.17 and 0.13 are selected as the optimum initial soil profile for frozen soil modeling.

We validate the result through the comparison with the observed soil profile on Oct 2nd, shown in Figure 5.10. The soil profile selected by 6GHz Tb (green line) and that optimized by 5 frequencies Tbs (orange line) are both in closest proximity to the observed soil profile among 10 hypothetical profiles. Because of deeper penetration capacity of 6GHz, deep part of green soil profile selected by 6GHz is in good agreement with observation. Whereas, other high frequencies are more sensitive to the shallow soil moisture, the shallow part of orange soil profile selected by 5 frequencies has good consistency with the observation. All in all, it is proved that the method can effectively obtain suitable initial soil profile for frozen soil modeling and may enhance the performance of frozen soil model in the poorly gauged cold regions.

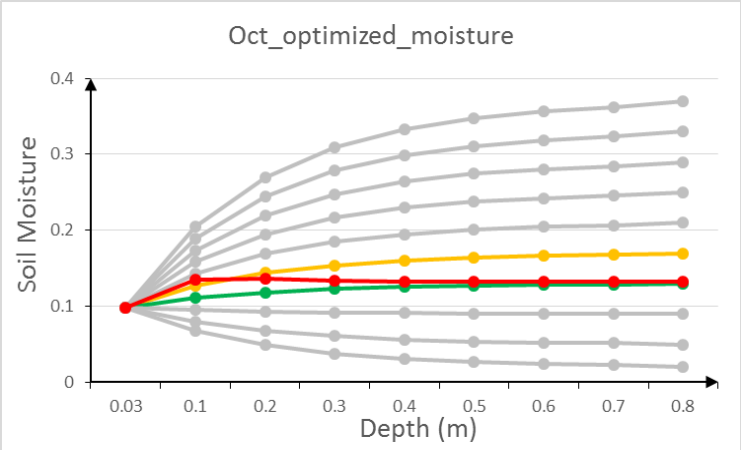

Figure 5.10 Optimized soil moisture profile on October 2nd and Nov 6th, 2003. Red line denotes the observed soil profile; green line refer to the soil profile selected by 6GHz Tb; orange line refers to the soil profile optimized by 5 frequencies Tbs.

5.4 Discussion

This assimilation method which combines both the physical model and satellite microwave remote sensing makes it possible to initialize and update frozen soil moisture profile in the region without soil observation. However, it is notable that there are limitations for this method:

(1) Applicable area: this method only is only applicable for frozen soil which is dry in winter and has soil moisture fluctuation with freeze / thaw process. It is not applicable to wet unfrozen soil.

(2) Applicable season: Autumn before ice period. In autumn, soil moisture become stable and relative lower than summer due to less rainfall. Moreover, there's no need to initialize ice and it can be simply set as 0. Because of gravity drainage and surface evaporation, it usually has low surface soil moisture and relative high content in depth with less variation. The soil moisture profile in autumn is usually not so heterogeneous. Summer and spring are not applicable, because soil moisture is too high that it may block out the deep soil signal. Soil is dry in winter, however ice appears inside of soil, which is difficult to estimate. What's more, snow may cover the ground in winter which also can mask out the deep soil signal.

(3) Detectable depth: the detectable depth of frozen soil depends on the soil moisture and microwave frequency. According to the penetration depth calculation in section 5.2.1, the detectable soil thicknesses range from 0.68 m to 1.3m. These depths mainly cover the shallow active layer of frozen soil, which directly has interaction with atmosphere and more important for land surface processes. While the deep part of permafrost is undetectable. The possible way to estimate the deep soil information is spin-up with repeat forcing for decades or hundreds of year or using long wave microwave channel, such as L band 1.4 GHz.

(4) Applicable frequency: Passive microwave 6-36 GHz brightness temperature dataset. As we suggested above, it is worth exploration to utilize the long wave L band radiometer from the Soil Moisture and Ocean Salinity (SMOS) mission and the Soil Moisture Active Passive (SMAP) mission to detect deeper frozen soil information.

Definitely, this frozen soil profile initialization method cannot initialize the soil profile in any seasons, any places and any depth. At limited time and within limited depth, the initialized soil profile can fit the main variation trend and magnitudes of true soil states approximately using exponential soil profile assumption and is not able to perfectly capture all the tiny variation with depth. Nevertheless, it is still a big improvement that this method makes it possible to obtain inside soil information in the area without soil observation by taking advantage of both microwave satellite observation and the frozen soil model. Furthermore, permafrost simulation results in poor gauged area can be greatly improved due to the availability of initial conditions.

5.5 Summary

Although we have not enough ground based soil observation stations uniformly distributed in broad area, satellite based passive microwave sensors can frequently and continuously monitor large scale area in all-weather condition. By utilizing both physical reality of modeling

and penetration capacity of passive microwave remote sensing, we developed a method for estimating the optimum initial soil profile.

Frozen soil is dry enough for microwave radiation to penetrate and make it possible to detect deep soil information. What's more, microwave radiation signal of different frequencies can reflect the freeze-thaw state of frozen soil at different depth. The initialization of soil moisture are more important for the frozen soil simulation than that of soil temperature. Therefore, this study focused on initializing the soil moisture profile. First hypothetical soil profiles are generated as initial condition for frozen soil modeling. Then the forcing data for the RTM simulation can be obtained from frozen soil modeling. Next, by comparing the simulated Tb time series with AMSR-E Tb through the frozen and thaw season, we could find the best match simulated Tb time series. At last, the hypothetical initial condition of this best fit Tb simulation is the optimum initial condition.

This frozen soil profile initialization method is applied on October 2nd in Gaize station. To recover the initial soil profile, 10 hypothetical soil profiles were made according to surface soil moisture. Results show that optimum initial soil profiles with lowest RMSE value are in close proximity to the observed soil moisture profile among 10 hypothetical profiles, which means that the method can effectively obtain suitable initial soil profile for frozen soil modeling.

Finally, we discussed the applicability and limitation of this method. The initialization method is only applicable to frozen soil in autumn within 1.3m depth by 6-36 GHz microwave observation. We also proposed that L band passive microwave data can be utilized for deeper soil information detection in the future study.

6. CONCLUSIONS

6.1 Conclusions

A multi-layer, enthalpy-based frozen soil model was developed to represent the phase change and heat–water flow in frozen soil based on the modified one-dimensional land surface scheme. We proposed a critical temperature criterion to judge the phase state, and introduced enthalpy and total water mass into the Clausius–Clapeyron equation to simulate the freezing/thawing process. This frozen soil scheme offers a simple method for solving highly non-linear equations stably and reduces the computation time for greater efficiency. The simulated results are in good agreement with the observations and the characteristics of permafrost, which demonstrates that the frozen soil model has a good capability for predicting the internal frozen soil process at the point scale. Sensitivity analyses also show that this frozen soil model can be applied to a certain wide range of time step and layer thickness, and achieve convergent solutions with stable accuracy. The model is capable of continuously reproducing the diurnal and seasonal freeze-thaw cycle, heat and water transfer within soil and simulating frozen soil hydrological processes.

It should be pointed out that this frozen soil model can also be used for studying the heat and water transfer processes occurring in arid and semi-arid areas, even when no frozen soil is present. In unfrozen soil regions or summer season, the phase change scheme and the ice effect on water flow can be skipped according to the phase state judgment to remove freezing/thawing effect and save computation time. Our development is based on a land surface model with enhanced hydrology, so the frozen soil model is portable and adaptable for coupling with various physical schemes, such as those for snow, glacier and river dynamics [*Shrestha et al.*, 2012]. These potential coupling applications also include atmospheric general circulation models [*Sellers et al.,* 1996] and radiative transfer models for remote sensing. The frozen soil modeling make it possible to simulate the radiative transfer process inside of frozen soil by using the simulated soil states as input.

A multi-layer frozen soil RTM was developed by consideration of both surface scattering and volume scattering to describe the radiation transfer processes in frozen soil and simulate radiation intensity out of frozen soil. This RTM predicted Tb time series of 5 frequencies (6GHz - 36GHz) through freezing, frozen, and thawing seasons with reliable accuracy and successfully reproduced the negative spectral gradient of frozen soil for the first time. According to simulation and AMSR-E observation, it is proved that volume scattering dominates the radiative transfer process in frozen season and the negative spectral gradient is attributed to the strong scattering in higher frequency. The good agreement between simulated Tb and AMSR-E Tb prove that our understanding of frozen soil offer a new quantitative explanation for the mechanism of frozen soil radiative transfer processes. And the frozen soil states simulated in our physical model can be a proper input for RTM. Overall, the RTM of frozen soil is capable

of capturing the radiative characteristics of freeze-thaw state and continuously predicting the radiative intensity variation in response to whole freeze-thaw process of soil.

Although we have not enough ground based soil observation stations uniformly distributed in broad area, satellite based passive microwave sensors can frequently and continuously monitor large scale area in all-weather condition. By utilizing both physical reality of modeling and penetration capacity of passive microwave remote sensing, we developed a method for estimating the optimum initial soil profile method according to the radiative characteristics variation with freeze- thaw state transformation. Through the tests on Oct 2nd in Gaize, the optimum initial soil profile which is most close to soil profile observation was selected from 10 hypothetical profile. Therefore, this method was found to be a practical and reliable method for solving the water profile initialization problem for frozen soil modeling in the absence of soil observation.

In conclusion, this research bridged the gap between frozen soil physical modeling and frozen soil radiative transfer investigation. It provides a deeper and quantitative understanding on the physics of freeze-thaw process, heat and water transfer inside of soil and hydrological processes of frozen soil region. And the mechanism of radiative transfer processes are clarified for the first time by a numerical simulation considering both surface scattering and volume scattering. These contributions can empower the frozen soil modeling application in permafrost prediction and hydrology research under climate change in cold regions at the basin or regional scale.

6.2 Suggestions for future study

This study developed a frozen soil assimilation system based on a frozen soil physical model and a radiative transfer model to simulate the heat - water transfer and freezing/ thawing process inside of frozen soil. However, the frozen soil process is so complex that its modeling is not able to involve all the impact factors. If the following aspects can be improved, it would greatly improve the models developed in this research.

(1) Snow scheme: Currently, a simple snow scheme originally from SiB2 is used in the permafrost model, which cannot describe snow compaction, surface albedo variation with aging and accumulation/ablation accurately. However, snow duration, timing and thickness can greatly influence the water and heat exchange between ground and atmosphere, especially an early snow can result in shallower frost depth and early snow thawing in the model may bring large errors into the soil moisture simulation. The albedo of snow is also a key parameter for permafrost which controls the amount of energy into ground. If a comprehensive physical based snow scheme such as snow scheme in WEB-DHMS [*Shrestha et al.*, 2012] can be connected to improve the snow physics of this model, the simulation accuracy of this permafrost model will be greatly improved.

(2) Integrated cold region hydrology model (snow+ glacier + permafrost): To understand the hydrological cycle and the water distribution in cold regions, it is necessary to develop an integrated hydrological model to describe soil freezing/thawing, snow accumulation/ablation, glacier advance/retreat, and their interactions with each other comprehensively. Incomplete knowledge or improper representation of one of these factors may result in the unrealistic

projection of other processes and thus a failure to accurately predict the hydrological and atmospheric processes in cold regions. Our frozen soil model development is based on a common land surface model with enhanced hydrology, so the frozen soil model is portable and adaptable for coupling with various physical schemes, such as those for snow, glacier and river dynamics. The integrated cold region hydrological model may empower its application in permafrost prediction and hydrology research under climate change in cold regions.

(3) Dynamic vegetation scheme: The dominant ecosystems in permafrost regions are boreal forests to the south and tundra to the north [*Schaefer et al.*, 2012]. In mountainous permafrost regions, forests distributes at lower elevations and tundra at higher elevations. Soil moisture and soil temperature have a great impact on vegetation growth. In turn, vegetation takes up water out of soil by transpiration and vegetation cover can block solar radiation partly and have good ground-insulting abilities to prevent the permafrost from thawing [*Briggs et al.*, 2014]. Similarly, the surface organic matters on the ground surface are also good insulator. Within this permafrost model, a simple vegetation scheme - big leaf model [*Deardorff*, 1978] is used. Coupling the permafrost model with a dynamic vegetation scheme may allow us to explore how the vegetation system in permafrost regions response to the climate change. Some researchers found that change of permafrost in Tibet tends to decrease species diversity and the primary productivity of vegetation [*YANG et al.*, 2010]. Vegetation covers may change in response to permafrost thaw because of warming temperature and more precipitation in the short term, and their species composition and distribution may be disturbed in the long term due to the water storage decreasing. Vegetation plays an important role in the carbon cycle and food chain in the cold regions where the ecosystem is especially sensitive and vulnerable.

(4) Radiative transfer within snow: Snow always covers the frozen ground in winter, which can scatter the soil emission during its transfer path to the microwave radiometer. Especially for high frequency, the scattering effect by snow particles becomes much stronger. Snow and frozen soil have similar dielectric properties and similar volume scattering effect [*Jin et al.*, 2009]. Consequently, the bared frozen soil may be misinterpreted as snow covered area, and even there's snow over frozen ground the snow depth also can be overestimated [*Che et al.*, 2008; *Grody and Basist*, 1996; *Tsutsui and Koike*, 2012; *Tsutsui et al.*, 2007]. Therefore, in order to apply the microwave remote sensing in the snow covered frozen ground area, snow layer should be introduced into our frozen soil RTM. The temperature, density, liquid water and ice content of snow varies with time, horizontal distribution and vertical depth, which should be considered in the coupled RTM. Two difficulties have to be overcome: one is that the snow particle changes with compaction and refreezing processes, another one is that wet snow can absorb most of the upwelling soil emission, which may mask out the underlying soil information. With this coupled snow-frozen soil RTM, the snow cover and the frozen ground can be distinguished well from each other, and the snow quantity retrieved from satellite data as well as radiation out of ground can be evaluated more accurately.

(5) Long wave (L band) RTM: In this study, we use microwave channels from 6.925GHz to 36.5 GHz, of which penetration depth is still limited (maximum 1.3m for 5% soil volumetric moisture). L band with low frequency 1.4 GHz can penetrate vegetation layers and shallow soil layers with less atmosphere effects, thus L band has the potential to detect deeper frozen soil information. The Soil Moisture and Ocean Salinity (SMOS) mission and the Soil Moisture Active Passive (SMAP) mission launched recently both include satellite based L band passive microwave radiometer for soil moisture and freeze/thaw state detection. These projects offer

continuous L band regular data which may encourage the deep frozen ground studies. Few permafrost scientists started to shift their attention on the L band to retrieve the freeze thaw/state of soils [*Rautiainen et al.*, 2014; *Rautiainen et al.*, 2016; *Schwank et al.*, 2004], and the L band radiative transfer mechanism is still under exploration. Physical based L band quantitative RTM should be built to numerically describe the long wave radiative transfer process and extend the soil exploration range of satellite observation.

Frozen soil plays a significant role in both climate change and hydrological processes of cryosphere. Therefore, frozen soil model can be widely applied in not only permafrost itself, but also associated climate and hydrology researches. It is highly essential to clarify the interaction mechanism between atmosphere and permafrost, thus to improve the prediction ability of climate models in cold frozen soil regions, and to address the potential impact of permafrost on hydrology, ecology, society and economy, which is closely related to human life. The application of this frozen soil assimilation system can be widely extended to the following aspects, which may greatly contribute to the cryosphere hydrology and climate field:

(1) Permafrost simulation: Changes in permafrost temperature, thickness, timing, duration, and extent can be good indicators of climate change [*V Romanovsky et al., 2002*]. Permafrost has been identified as one of six cryosphere indicators of global climate change within the international framework of the WMO Global Climate Observing System[*Jerry Brown et al.*, 2008]. It is crucially important to simulate permafrost in Arctic, Siberia and Tibet Plateau for past 30 years to investigate the spatial-temporal variation of permafrost and reveal the inside temperature - water profile and active layer thickness change under the recent climate change by using the frozen soil assimilation system based on a frozen soil physical model, a microwave satellite data and reanalysis dataset.

(2) Permafrost prediction: According to the Intergovernmental Panel on Climate Change (IPCC) fifth assessment report, there is high confidence that permafrost temperatures have increased up to 3°C in Northern Alaska (1980s–mid-2000s) and up to 2°C in Russian European North (1971–2010) as a result of the increased Arctic warming [Stocker et al., 2014]. How the permafrost responses to the future climate change is one of hot topics that human concerns more and more. It will be interesting to simulate permafrost under various scenarios, such as three possible scenarios of aggressive, moderate and no emission reductions, proposed by IPCC 2007 [*Parry et al.*, 2007] or using GCM prediction output as forcing data for permafrost model.

(3) Weather forecast: The prediction ability of climate model in cold permafrost region is still undesirable. Viterbo et al.[1999] found that the European Center for Medium Range Forecast model tends to produce cold atmosphere over land surface, which can be attributed to the lack of freezing/ thawing description in land surface model. Currently, in most of climate models and land surface models, heat-water transfer within frozen soil and freeze-thaw cycle are not well described [*V. Koren et al.*, 1999; *Y. Zhang and Lu*, 2002]. It is necessary to introduce the frozen soil model into regional climate model or medium range forecast model to evaluate the impact of frozen ground over climate simulation accuracy from the aspects of surface energy - water fluxes and to improve the prediction performance of weather forecast model in cryosphere.

(4) Formation mechanism of Asian Monsoon: The importance of Tibet Plateau as a heat source for the formation and maintenance of the Asian Monsoon has been discussed by many

researchers, e.g. [*Hermann Flohn*, 1957; *H Flohn*, 1960; *Taniguchi and Koike*, 2007; *Taniguchi et al.*, 2012]. Permafrost and seasonal frozen soil are quite developed in Tibet Plateau. It has been found that winter snow over Tibet Plateau has a clear positive correlation with the subsequent summer rainfall over central and east China [*T-W Wu and Qian*, 2003]. It can be attributed that snow anomalies over the Tibetan Plateau change the soil moisture and the surface temperature through the snowmelt process at first, and subsequently alter heat, moisture and radiation fluxes from the surface to the atmosphere [*Qian et al.*, 2003]. Similarly, permafrost has more water storage than snow and also can change the surface temperature and soil moisture when the active layers thaw. Permafrost can be one of the keys to explore the physical mechanism of Asian Monsoon, which has not been paid enough attention and may contribute to the Asia Monsoon field if permafrost in Tibet Plateau is considered.

(5) Water quality and water resource evaluation: The frozen soil model is able to produce continuous water and soil temperature at hourly time step and basin scale in the cold region, which may allow us to calculate the total water storage (including ice) of permafrost in different seasons in cold basins. As we all known, water temperature is a factor of primary importance for many water physical, chemical and biological processes, which controls soil water transport, solute transport, nutrient fertilizer, microbial activity, root development and seed germination[*Bierhuizen and Wagenvoort*, 1974; *Kramer and Boyer*, 1995]. Our frozen soil model is able to simulate soil water temperature of each layer under surface energy budget. It is possible to solve the river water temperature by accumulating the soil water energy into rivers and adding river surface energy budget. By using the dynamic water temperature-this key parameter, it is able to quantitatively evaluate the biological, chemical and physical properties of the river water in cold regions.

(6) River basin and water resource management in cold region: Snowmelt, glacier water and water in permafrost are the main precious water source for the cold regions. However, most of cold regions are located in the arid or semi-arid regions. How to manage the river and water resources efficiently and effectively in these regions is still a hot topic for the local governments and hydrologists. By using the integrated cold region river model (including permafrost, snow and glacier), it is possible to monitor, to simulate, and to predict the total water amount stored in snow, glacier and permafrost, and the river discharge, river level in the cold region river, which can offer more accurate river and water resource information to river manager and related communities or governments for better river management and policy making.

(7) Snow melt flood and permafrost related disaster: The impermeability of frozen soil generally prohibits snowmelt water infiltration and forces surface runoff to flow downslope, which may result in severe flash floods along with landslides and debris flow after snowmelt or heavy rainfall events in the spring. [*Flerchinger and Saxton*, 1989; *Victor Koren et al.*, 2014; *Storey*, 1955]. It is highly important to monitor, to model and to project the snowmelt flood and permafrost related disasters under climate change. The permafrost regions are very sensitive and vulnerable to global warming. Warm permafrost are structurally weak and prone to be erosion or sudden collapse, which is often accompanied by erosion and other physical changes to the landscape. Therefore, it is necessary to identify cold regions vulnerable to permafrost degradation and within these regions, identify structures, infrastructures and industries at high risk. Moreover, methods for quantifying the mitigation cost and risks associated with permafrost degradation are also crucial. Last but not least, How to develop new engineering

techniques or adapt current building codes to withstand potential risk due to permafrost degradation is also a meaningful topic for civil engineers.

APPENDIX 1: PERMAFROST GLOSSARY

Active layer: the surface soil layer in permafrost regions that thaws each summer and freezes each winter.

Active layer thickness: the annual maximum depth of thaw of the soil in summer.

Closed talik: a talik below the active layer, but above the permafrost table.

Continuous permafrost: regions where permafrost underlies 90-100% of the land area.

Depth of zero annual amplitude: the soil depth where the permafrost temperature has no seasonal variation.

Discontinuous permafrost: regions where permafrost underlies 50-90% of the land area.

Ground ice: bodies of pure ice within permafrost in the form of wedges, lenses, and layers

Ice lens or layer: a horizontal body of ground ice formed when fine grained silt and clay draw liquid water toward ice through surface tension and capillary suction.

Ice wedge: a vertical body of ground ice formed by soil contraction in winter. A vertical crack forms due to contraction in winter. Water flows into the cracks in spring, freezes and expands.

Isolated permafrost patches: regions where permafrost underlies less than 10% of the land area.

Open talik: a talik extending down to the permafrost base. Sometimes called a through talik.

Permafrost: soil or rock remaining at or below 0°C for at least two consecutive years.

Permafrost base: the bottom of the permafrost layer within the soil column.

Permafrost carbon feedback: amplification of surface warming due to the release into the atmosphere of the carbon currently frozen in permafrost

Permafrost degradation: any increase in active layer thickness, melting of ground ice, thinning of permafrost, or decrease in the areal extent of permafrost over time.

Permafrost table: The bottom of the active layer and the top of the permafrost layer in the soil column.

Rock glacier: tongue-shaped bodies of perennially frozen material with interstitial ice and ice lenses that move downslope by creep as a consequence of the ice deformation.

Sporadic permafrost: regions where permafrost underlies 10-50% of the land area.

Talik: a layer or body of permanently unfrozen ground in a region of permafrost.

Thaw bulb: a closed talik under lakes and rivers which do not completely freeze in winter

Thermal erosion: surface erosion triggered by permafrost thaw.

Thermokarst depression: a local subsidence or collapse due to the melting of ground ice.

Thermokarst lake: a thermokarst depression or subsidence that is filled with water.

2: AMSR-E BRIGHTNESS TEMPERATURE TIME SERIES FROM 2003-2011 AT GAIZE, TIBET.

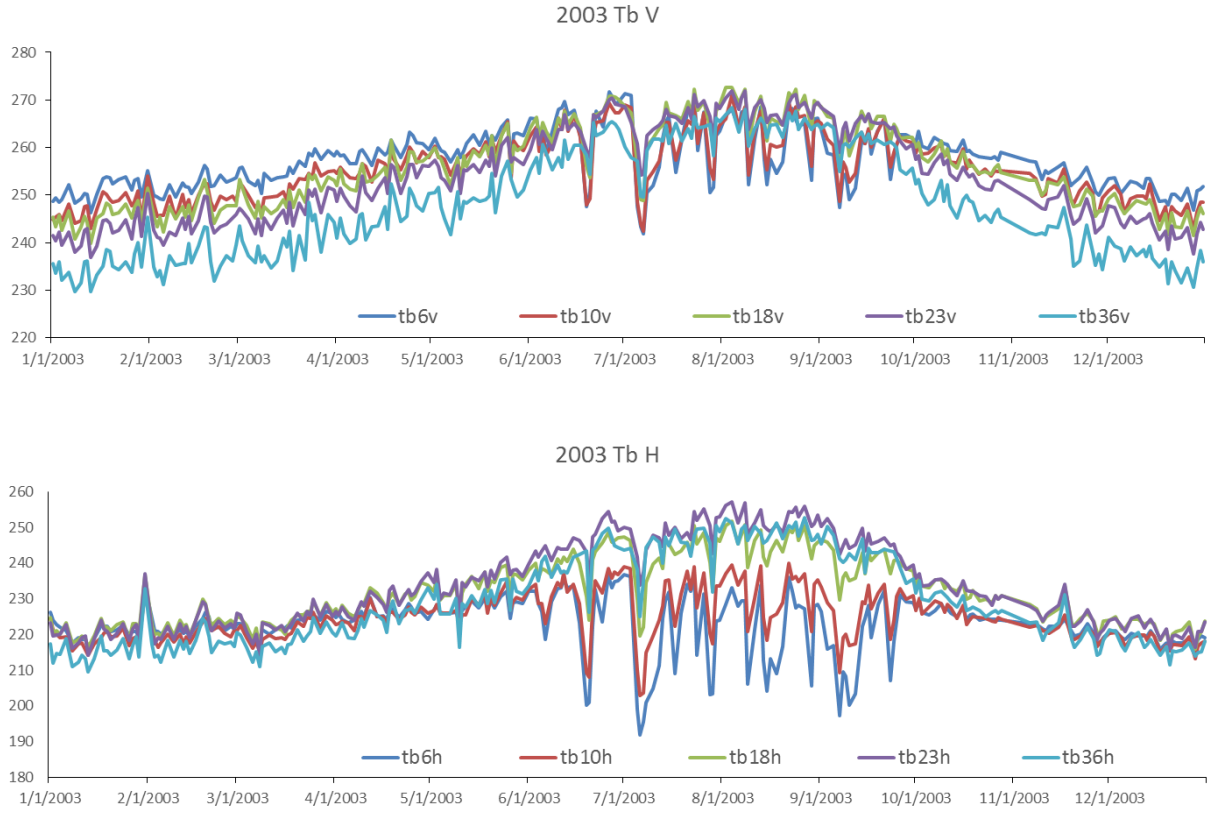

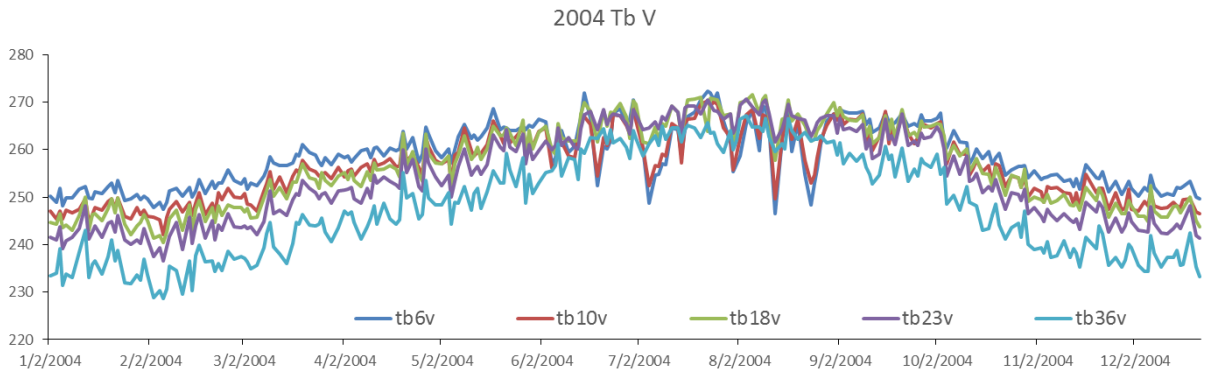
2004 Tb V
280
270
260
250
240
230
220
tb6v
tb10v
tb18v
tb23v
tb36v
1/2/2004
2/2/2004
3/2/2004
4/2/2004
5/2/2004
6/2/2004
7/2/2004
8/2/2004
9/2/2004
10/2/2004
11/2/2004
12/2/2004

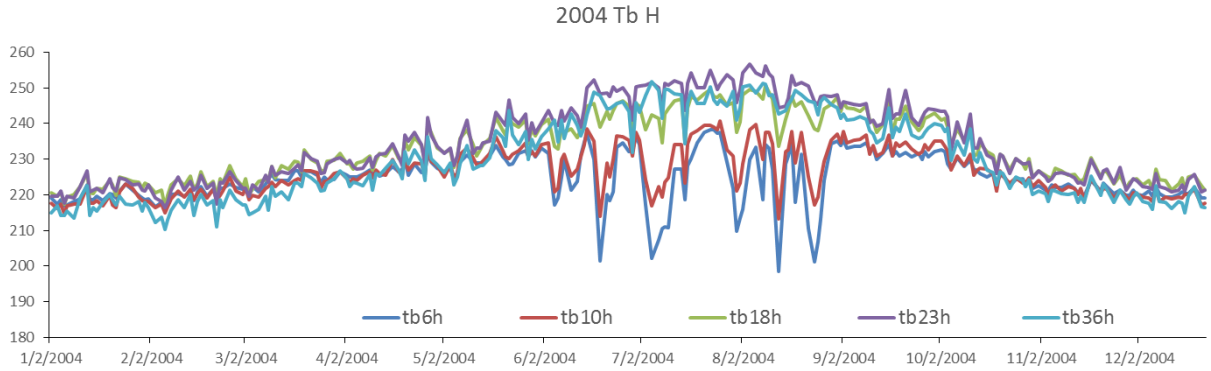
2004 Tb H
260
250
240
230
220
210
200
190
180
tb6h
tb10h
tb18h
tb23h
tb36h
1/2/2004
2/2/2004
3/2/2004
4/2/2004
5/2/2004
6/2/2004
7/2/2004
8/2/2004
9/2/2004
10/2/2004
11/2/2004
12/2/2004

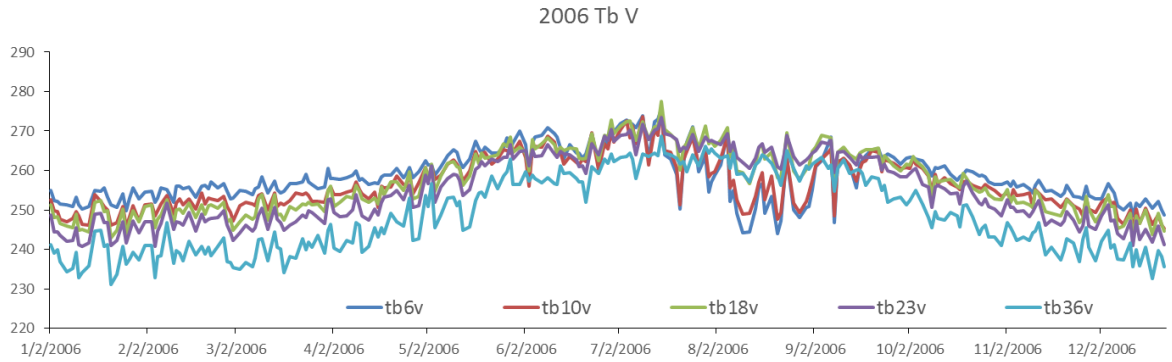
2006 Tb V
290
280
270
260
250
240
230
220
tb6v
tb10v
tb18v
tb23v
tb36v
1/2/2006
2/2/2006
3/2/2006
4/2/2006
5/2/2006
6/2/2006
7/2/2006
8/2/2006
9/2/2006
10/2/2006
11/2/2006
12/2/2006

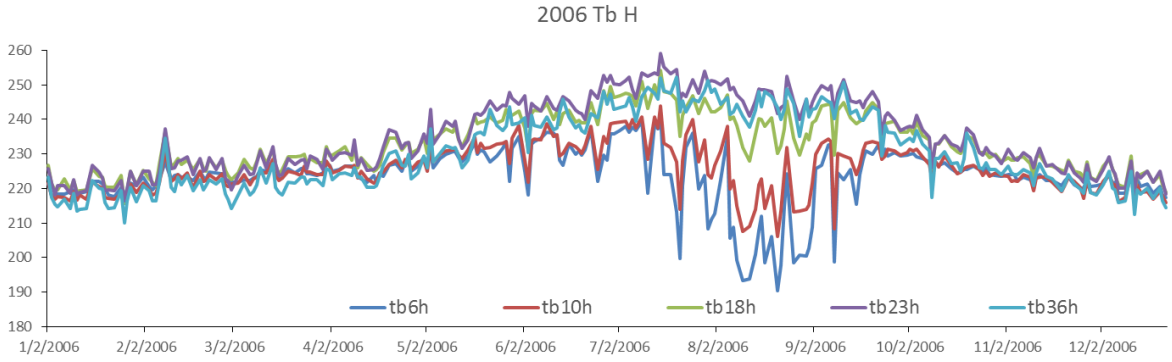
2006 Tb H
260
250
240
230
220
210
200
190
180
tb6h
tb10h
tb18h
tb23h
tb36h
1/2/2006
2/2/2006
3/2/2006
4/2/2006
5/2/2006
6/2/2006
7/2/2006
8/2/2006
9/2/2006
10/2/2006
11/2/2006
12/2/2006

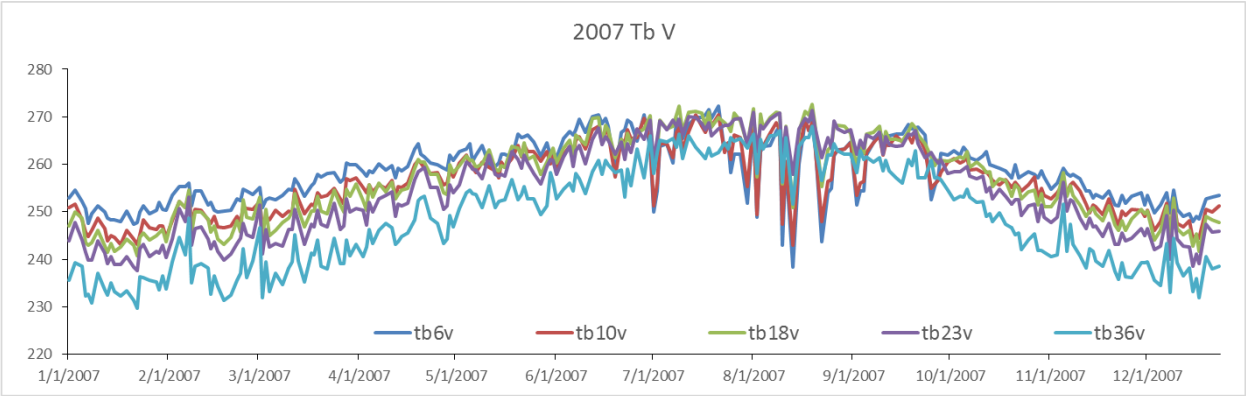
2007 Tb V
280
270
260
250
240
230
220
tb6v
tb10v
tb18v
tb23v
tb36v
1/1/2007
2/1/2007
3/1/2007
4/1/2007
5/1/2007
6/1/2007
7/1/2007
8/1/2007
9/1/2007
10/1/2007
11/1/2007
12/1/2007

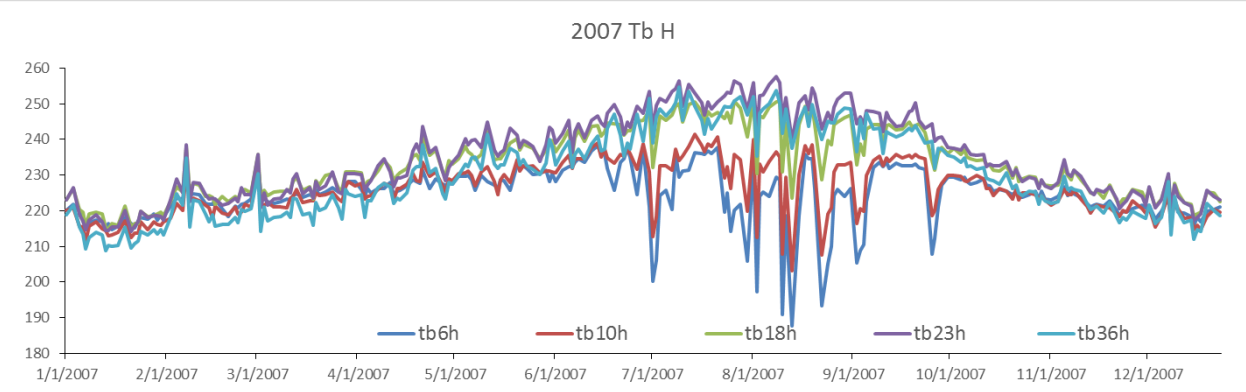
2007 Tb H
260
250
240
230
220
210
200
190
180
tb6h
tb10h
tb18h
tb23h
tb36h
1/1/2007
2/1/2007
3/1/2007
4/1/2007
5/1/2007
6/1/2007
7/1/2007
8/1/2007
9/1/2007
10/1/2007
11/1/2007
12/1/2007

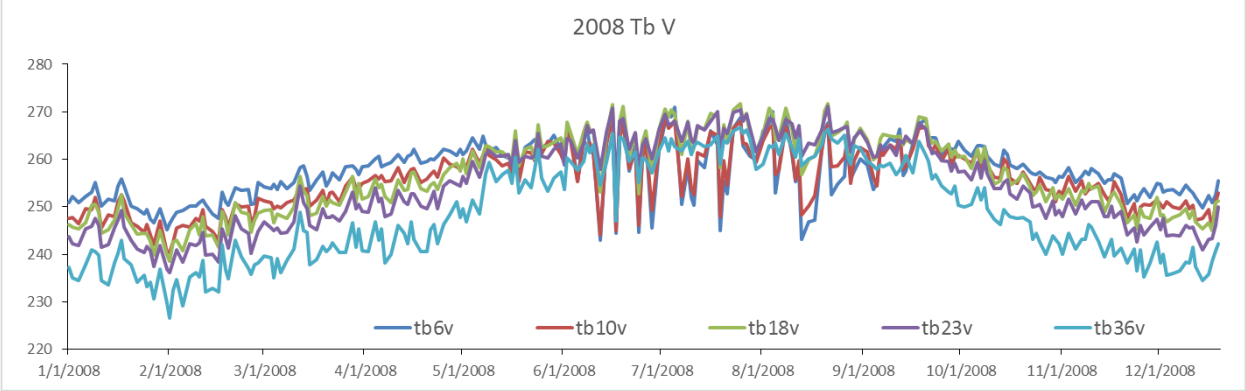
2008 Tb V
280
270
260
250
240
230
220
tb6v
tb10v
tb18v
tb23v
tb36v
1/1/2008
2/1/2008
3/1/2008
4/1/2008
5/1/2008
6/1/2008
7/1/2008
8/1/2008
9/1/2008
10/1/2008
11/1/2008
12/1/2008

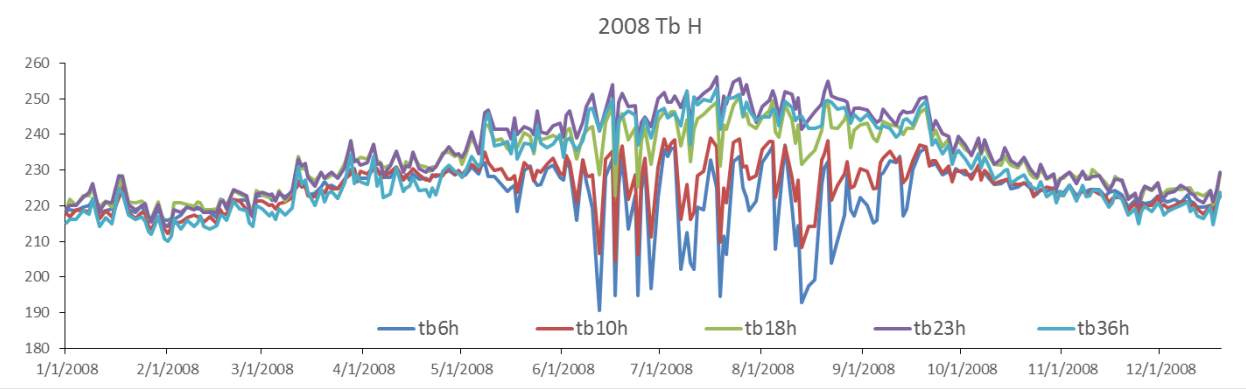
2008 Tb H
260
250
240
230
220
210
200
190
180
tb6h
tb10h
tb18h
tb23h
tb36h
1/1/2008
2/1/2008
3/1/2008
4/1/2008
5/1/2008
6/1/2008
7/1/2008
8/1/2008
9/1/2008
10/1/2008
11/1/2008
12/1/2008

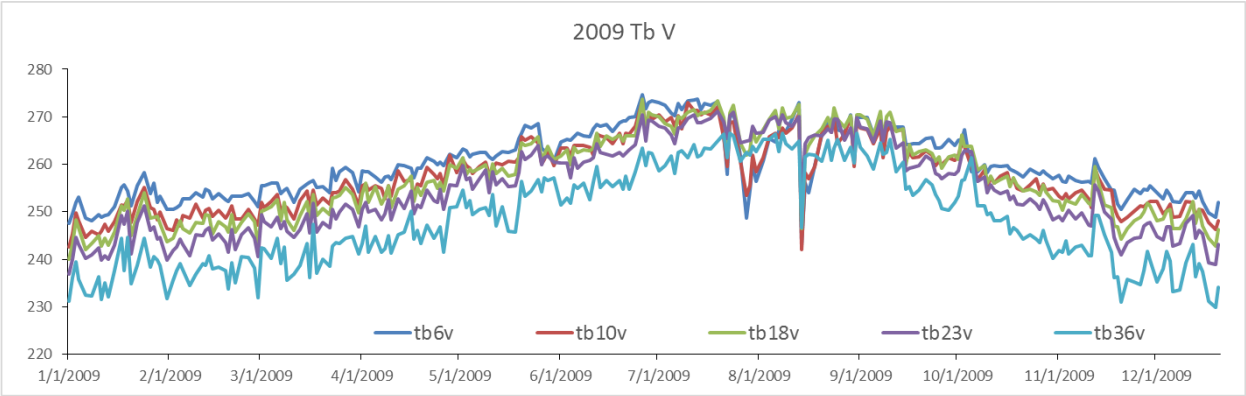
2009 Tb V
280
270
260
250
240
230
220
tb6v
tb10v
tb18v
tb23v
tb36v
1/1/2009
2/1/2009
3/1/2009
4/1/2009
5/1/2009
6/1/2009
7/1/2009
8/1/2009
9/1/2009
10/1/2009
11/1/2009
12/1/2009

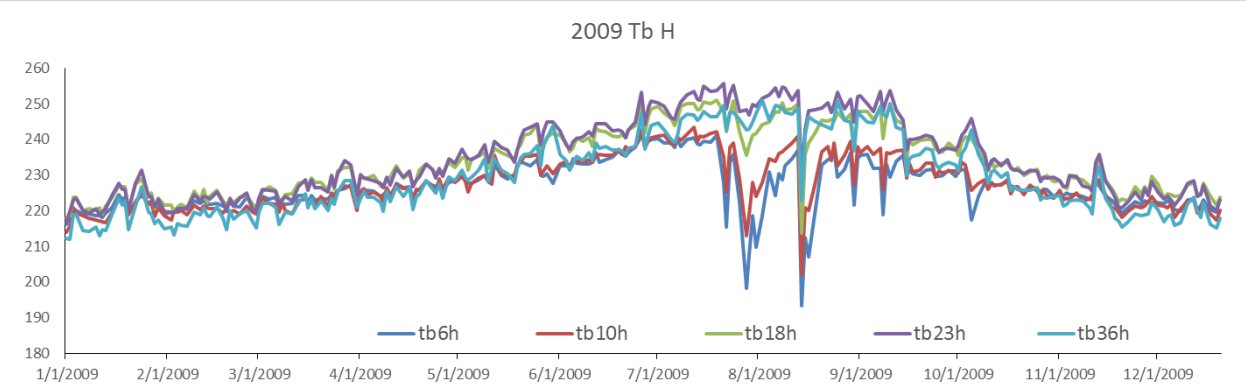
2009 Tb H
260
250
240
230
220
210
200
190
180
tb6h
tb10h
tb18h
tb23h
tb36h
1/1/2009
2/1/2009
3/1/2009
4/1/2009
5/1/2009
6/1/2009
7/1/2009
8/1/2009
9/1/2009
10/1/2009
11/1/2009
12/1/2009

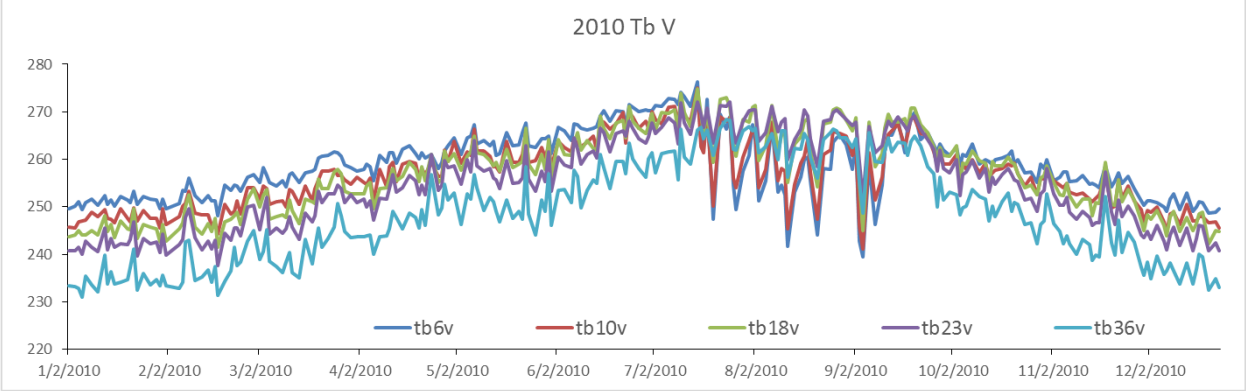
2010 Tb V
280
270
260
250
240
230
220
tb6v
tb10v
tb18v
tb23v
tb36v
1/2/2010
2/2/2010
3/2/2010
4/2/2010
5/2/2010
6/2/2010
7/2/2010
8/2/2010
9/2/2010
10/2/2010
11/2/2010
12/2/2010

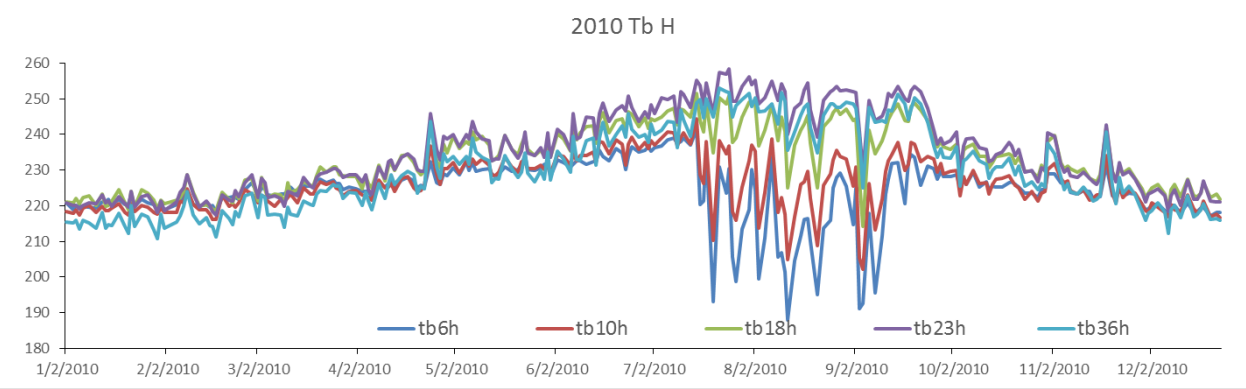
2010 Tb H
260
250
240
230
220
210
200
190
180
tb6h
tb10h
tb18h
tb23h
tb36h
1/2/2010
2/2/2010
3/2/2010
4/2/2010
5/2/2010
6/2/2010
7/2/2010
8/2/2010
9/2/2010
10/2/2010
11/2/2010
12/2/2010

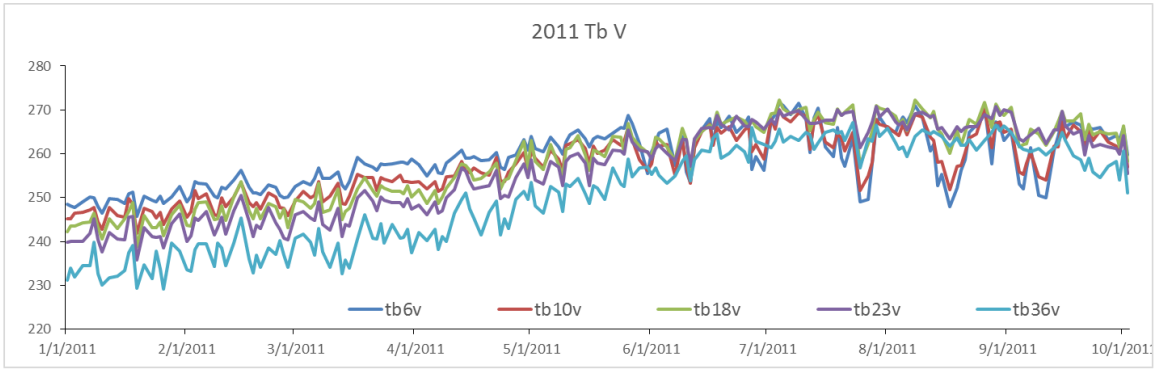

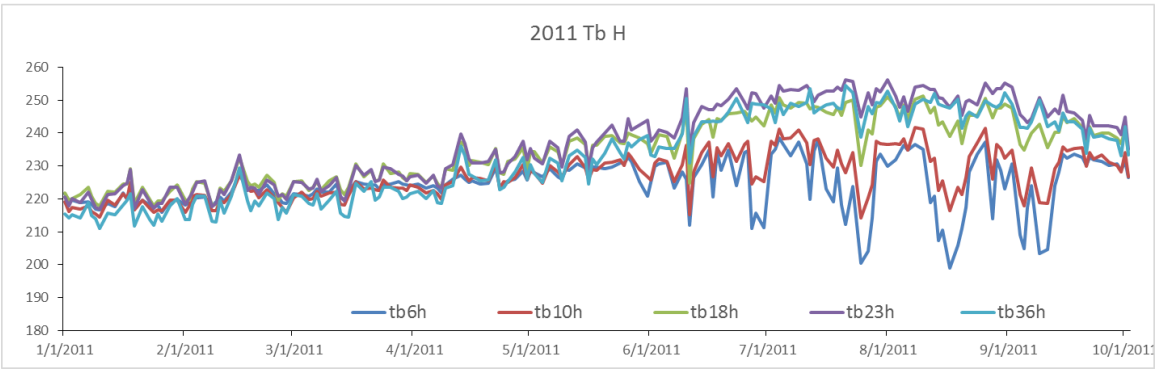

3: CLAUSIUS–CLAPEYRON RELATION

The Clausius–Clapeyron relation, proposed by Rudolf Clausius[*Clausius*, 1850] and Benoît Paul Émile Clapeyron [*Clapeyron*, 1834; *Clausius*, 1850] characterizes a discontinuous phase transition between two phases of matter of a single constituent. On a pressure–temperature (P–T) diagram (Figure A3.1), the line separating the two phases is known as the coexistence curve.

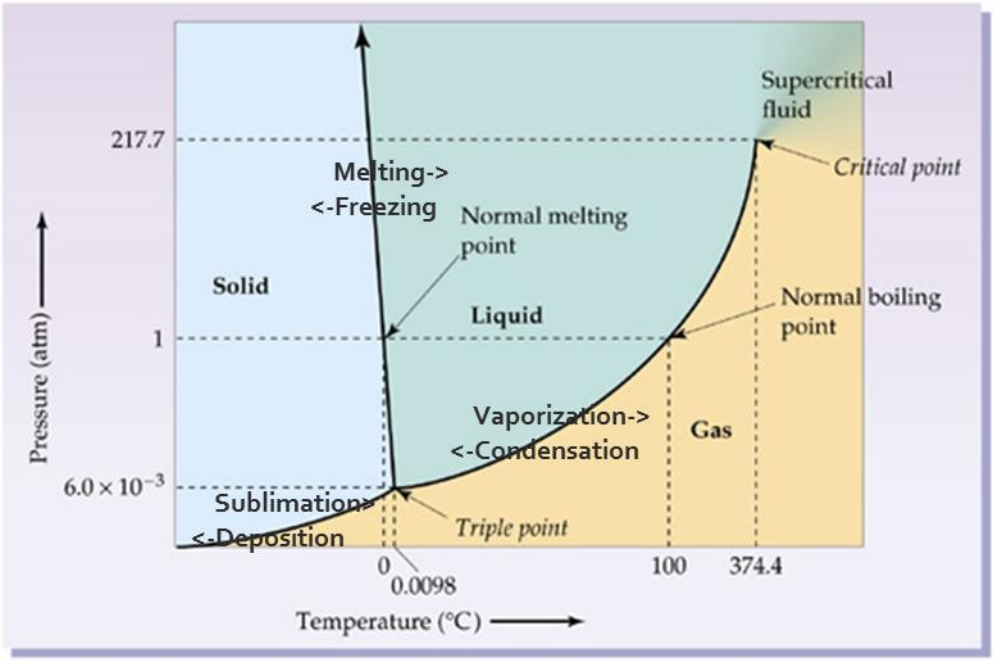

Figure A3.1 Pressure–temperature (P–T) diagram of water phase change.

The Clausius–Clapeyron relation gives the slope of the tangents to this curve, which can be used to find the relationship between pressure and temperature along phase boundaries. The mathematic expression is as follow:

$$\frac{dP}{dT} = \frac{L}{T_0 \Delta v} = \frac{\Delta S}{\Delta v}$$

where dP/dT is the slope of the tangent to the coexistence curve at any point (Pa/K), L is the specific latent heat (J/kg), T_0 is the reference temperature (K), Δv is the specific volume change of phase transition (m^3/kg), ΔS is the entropy change of the phase transition.

From the above graph (Figure A3.1), we can see that the freezing point of water decreases with pressure increasing. At the standard atmosphere pressure, the freezing point of water is 273.15K. While inside of soil, the soil water pressure exerted from capillary force can depress the freezing point, which can be described by the Clausius–Clapeyron equation.

REFERENCES

Bierhuizen, J., and W. Wagenvoort (1974), Some aspects of seed germination in vegetables. 1. The determination and application of heat sums and minimum temperature for germination, *Scientia Horticulturae*, *2*(3), 213-219.

Boyarskii, D., V. Tikhonov, and N. Y. Komarova (2002), Model of dielectric constant of bound water in soil for applications of microwave remote sensing, *Progress In Electromagnetics Research*, *35*, 251-269.

Briggs, M. A., M. A. Walvoord, J. M. McKenzie, C. I. Voss, F. D. Day‐Lewis, and J. W. Lane (2014), New permafrost is forming around shrinking Arctic lakes, but will it last?, *Geophysical Research Letters*, *41*(5), 1585-1592.

Brown, J., O. J. Ferrians Jr, J. A. Heginbottom, and E. S. Melnikov (1997), Circum-Arctic map of permafrost and ground-ice conditions, *Report Rep. 45*.

Brown, J., S. L. Smith, V. Romanovsky, H. H. Christiansen, G. Clow, and F. E. Nelson (2008), Global terrestrial network for permafrost [GTN-P], *Terrestrial Essential Climate Variables for Assessment, Mitigation and Adaptation*, 24-25.

Burt, T., and P. J. Williams (1976), Hydraulic conductivity in frozen soils, *Earth Surface Processes*, *1*(4), 349-360.

Campbell, M. J., and J. Ulrichs (1969), Electrical properties of rocks and their significance for lunar radar observations, *Journal of Geophysical Research*, *74*(25), 5867-5881. Ceop_AP Tibet plateau Map, edited.

Chang, A., and M. Cao (1996), Monitoring soil condition in the northern Tibetan Plateau using SSM/I data, *Hydrology Research*, *27*(3), 175-184.

Che, T., L. Xin, R. Jin, R. Armstrong, and T. Zhang (2008), Snow depth derived from passive microwave remote-sensing data in China, *Annals of Glaciology*, *49*(1), 145-154.

Chen, B., S. Luo, S. Lu, Y. Zhang, and D. Ma (2014), Effects of the soil freeze-thaw process on the regional climate of the Qinghai-Tibet Plateau, *Climate Research*, *59*(3), 243-257, doi:10.3354/cr01217.

Chen, K.-S., T.-D. Wu, L. Tsang, Q. Li, J. Shi, and A. K. Fung (2003), Emission of rough surfaces calculated by the integral equation method with comparison to three-dimensional moment method simulations, *IEEE Transactions on Geoscience and Remote Sensing*, *41*(1), 90-101.

Cherkauer, K. A., and D. P. Lettenmaier (1999a), Hydrologic effects of frozen soils in the upper Mississippi River basin, *Journal of Geophysical Research: Atmospheres (1984-2012), 104*(D16), 19599-19610.

Cherkauer, K. A., and D. P. Lettenmaier (1999b), Hydrologic effects of frozen soils in the upper Mississippi River basin

Journal of Geophysical Research: Atmospheres (1984?2012) Volume 104, Issue D16, *Journal of Geophysical Research: Atmospheres (1984?2012), 104*(D16), 19599-19610.

Christiansen, H. H., B. Etzelmüller, K. Isaksen, H. Juliussen, H. Farbrot, O. Humlum, M. Johansson, T. Ingeman‐Nielsen, L. Kristensen, and J. Hjort (2010), The thermal state of permafrost in the Nordic area during the International Polar Year 2007–2009, *Permafrost and Periglacial Processes*, *21*(2), 156-181.

Clapeyron, É. (1834), *Mémoire sur la puissance motrice de la chaleur*, J. Gabay.

Clausius, R. (1850), Über die bewegende Kraft der Wärme und die Gesetze, welche sich daraus für die Wärmelehre selbst ableiten lassen, *Annalen der Physik*, *155*(3), 368-397.

Cosby, B., G. Hornberger, R. Clapp, and T. Ginn (1984), A statistical exploration of the relationships of soil moisture characteristics to the physical properties of soils, *Water Resources Research*, *20*(6), 682-690.

Deardorff, J. (1978), Efficient prediction of ground surface temperature and moisture, with inclusion of a layer of vegetation, *Journal of Geophysical Research: Oceans*, *83*(C4), 1889-1903.

Dobson, M. C., F. T. Ulaby, M. T. Hallikainen, and M. A. El-Rayes (1985), Microwave dielectric behavior of wet soil—Part II: Dielectric mixing models, *IEEE Trans. Geosci. Remote Sens*, *23*(1), 35-46.

Duguay, C. R., T. Zhang, D. W. Leverington, and V. E. Romanovsky (2005), Satellite remote sensing of permafrost and seasonally frozen ground, *Remote Sensing in Northern Hydrology: Measuring Environmental Change*, 91-118.

England, A., and R. DeRoo (2006), Active layer thickness and moisture content of arctic tundra from SVAT/Radiobrightness models and assimilated 1.4 or 6.9 GHz brightness, *Final Report of NSF Award, ID*, *240747*.

England, A., J. Galantowicz, and B. Zuerndorfer (1991), A volume scattering explanation for the negative spectral gradient of frozen soil, paper presented at Geoscience and Remote Sensing Symposium, 1991. IGARSS'91. Remote Sensing: Global Monitoring for Earth Management., International, IEEE.

England, A. W. (1976), Relative influence upon microwave emissivity of fine-scale stratigraphy, internal scattering, and dielectric properties, *pure and applied geophysics*, *114*(2), 287-299.

Fagerlund, G. (1973), Determination of pore-size distribution from freezing-point depression, *Matériaux et construction*, *6*(3), 215-225.

FAO (2003), Digital Soil Map of the World and Derived Soil Properties, edited by U. N. FAO, http://www.fao.org/ag/agl/lwdms.stm#cd1

Farouki, O. T. (1986), Thermal properties of soils.

Ferrians, O., and G. D. Hobson (1973), Mapping and predicting permafrost in North America: A review, 1963–1973, paper presented at 2nd International Conference on Permafrost. Northamerican Contribution, Yakutsk, USSR.

Flerchinger, G. N., and K. E. Saxton (1989), SIMULTANEOUS HEAT AND WATER MODEL OF A FREEZING SNOW-RESIDUE-SOIL SYSTEM .1. THEORY AND DEVELOPMENT, *Transactions of the Asae*, *32*(2), 565-571.

Flohn, H. (1957), Large-scale aspects of the “summer monsoon” in South and East Asia, *J. Meteor. Soc. Japan*, *75*, 180-186.

Flohn, H. (1960), Recent investigations on the mechanism of the “Summer Monsoon” of Southern and Eastern Asia, paper presented at Proc. Symp. Monsoon of the World.

Gisnås, K., B. Etzelmüller, H. Farbrot, T. Schuler, and S. Westermann (2013), CryoGRID 1.0: Permafrost distribution in Norway estimated by a spatial numerical model, *Permafrost and Periglacial Processes*, *24*(1), 2-19.

Grab, S. (2002), Characteristics and palaeoenvironmental significance of relict sorted patterned ground, Drakensberg plateau, southern Africa, *Quaternary Science Reviews*, *21*(14), 1729-1744.

Grim, R. E. (1968), Clay mineralogy.

Grody, N. C., and A. N. Basist (1996), Global identification of snowcover using SSM/I measurements, *IEEE Transactions on geoscience and remote sensing*, *34*(1), 237-249.

Guo, J., L. Tsang, W. Asher, K.-H. Ding, and C.-T. Chen (2001), Applications of dense media radiative transfer theory for passive microwave remote sensing of foam covered ocean, *IEEE transactions on geoscience and remote sensing*, *39*(5), 1019-1027.

Haeberli, W. (2000), Modern research perspectives relating to permafrost creep and rock glaciers: a discussion, *Permafrost and Periglacial Processes*, *11*(4), 290-293.

Haeberli, W., J. Noetzli, L. Arenson, R. Delaloye, I. Gärtner-Roer, S. Gruber, K. Isaksen, C. Kneisel, M. Krautblatter, and M. Phillips (2010), Mountain permafrost: development and challenges of a young research field, *Journal of Glaciology*, *56*(200), 1043-1058.

Hallikainen, M. T., F. T. Ulaby, M. C. Dobson, M. A. El-Rayes, and L.-K. Wu (1985), Microwave dielectric behavior of wet soil-part 1: empirical models and experimental observations, *IEEE Transactions on Geoscience and Remote Sensing*(1), 25-34.

Hansson, K., J. Šimůnek, M. Mizoguchi, L.-C. Lundin, and M. T. Van Genuchten (2004), Water flow and heat transport in frozen soil, *Vadose Zone Journal*, *3*(2), 693-704.

Hoekstra, P., and A. Delaney (1974), Dielectric properties of soils at UHF and microwave frequencies, *Journal of geophysical research*, *79*(11), 1699-1708.

Humlum, O. (1997), Active layer thermal regime at three rock glaciers in Greenland, *Permafrost and Periglacial Processes*, *8*(4), 383-408.

Humlum, O. (1998), Active layer thermal regime 1991-1996 at Qeqertarsuaq, Disko Island, central west Greenland, *Arctic and Alpine Research*, 295-305.

Ishimaru, A., and Y. Kuga (1982), Attenuation constant of a coherent field in a dense distribution of particles, *JOSA*, *72*(10), 1317-1320.

Jafarov, E., D. Nicolsky, V. Romanovsky, J. Walsh, S. Panda, and M. Serreze (2014), The effect of snow: How to better model ground surface temperatures, *Cold Regions Science and Technology*, *102*, 63-77.

Jin, R., and X. Li (2009), Improving the estimation of hydrothermal state variables in the active layer of frozen ground by assimilating in situ observations and SSM/I data, *Science China D-Earth Science*, *39*(9), 1220-1231, doi:10.1007/s11430-009-0174-0.

Jin, R., X. Li, and T. Che (2009), A decision tree algorithm for surface soil freeze/thaw classification over China using SSM/I brightness temperature, *Remote Sensing of Environment*, *113*(12), 2651-2660.

Johansen, O. (1977), Thermal conductivity of soils*Rep.*, DTIC Document.

Jones, B., G. Grosse, C. Arp, M. Jones, K. Walter Anthony, and V. Romanovsky (2011), Modern thermokarst lake dynamics in the continuous permafrost zone, northern Seward Peninsula, Alaska, *Journal of Geophysical Research: Biogeosciences (2005–2012)*, *116*(G2).

Jorgenson, M. T., V. Romanovsky, J. Harden, Y. Shur, J. O'Donnell, E. A. Schuur, M. Kanevskiy, and S. Marchenko (2010), Resilience and vulnerability of permafrost to climate change This article is one of a selection of papers from The Dynamics of Change in Alaska's Boreal Forests: Resilience and Vulnerability in Response to Climate Warming, *Canadian Journal of Forest Research*, *40*(7), 1219-1236.

Judge, J., J. F. Galantowicz, A. W. England, and P. Dahl (1997), Freeze/thaw classification for prairie soils using SSM/I radiobrightnesses, *Geoscience and Remote Sensing, IEEE Transactions on*, *35*(4), 827-832.

Klein, L., and C. Swift (1977), An improved model for the dielectric constant of sea water at microwave frequencies, *IEEE Transactions on Antennas and Propagation*, *25*(1), 104-111.

Komarov, V., S. Wang, and J. Tang (2005), Permittivity and measurements, *Encyclopedia of RF and microwave engineering*.

Koren, V., J. Schaake, K. Mitchell, Q. Y. Duan, F. Chen, and J. M. Baker (1999), A parameterization of snowpack and frozen ground intended for NCEP weather and climate models, *Journal of Geophysical Research-Atmospheres*, *104*(D16), 19569-19585, doi:10.1029/1999jd900232.

Koren, V., M. Smith, and Z. Cui (2014), Physically-based modifications to the Sacramento Soil Moisture Accounting model. Part A: Modeling the effects of frozen ground on the runoff generation process, *Journal of Hydrology*, *519*, 3475-3491.

Kramer, P. J., and J. S. Boyer (1995), *Water relations of plants and soils*, Academic press.

Kuga, Y., and A. Ishimaru (1984), Retroreflectance from a dense distribution of spherical particles, *JOSA A*, *1*(8), 831-835.

Kulik, V. (1978), Water infiltration into soil, *Gidrometeoizdat, Moscow*, *19878*.

Kurylyk, B. L., K. T. B. MacQuarrie, and J. M. McKenzie (2014), Climate change impacts on groundwater and soil temperatures in cold and temperate regions: Implications, mathematical theory, and emerging simulation tools, *Earth-Science Reviews*, *138*, 313-334, doi:10.1016/ j.earscirev. 2014.06.006.

Lantuit, H., D. Atkinson, P. P. Overduin, M. Grigoriev, V. Rachold, G. Grosse, and H.-W. Hubberten (2011), Coastal erosion dynamics on the permafrost-dominated Bykovsky Peninsula, north Siberia, 1951-2006, *2011*, doi:10.3402/polar.v30i0.7341.

Laurion, I., W. F. Vincent, S. MacIntyre, L. Retamal, C. Dupont, P. Francus, and R. Pienitz (2010), Variability in greenhouse gas emissions from permafrost thaw ponds

Limnology and Oceanography Volume 55, Issue 1, *Limnology and Oceanography, 55*(1), 115-133.

Lawrence, D. M., K. W. Oleson, M. G. Flanner, P. E. Thornton, S. C. Swenson, P. J. Lawrence, X. Zeng, Z. L. Yang, S. Levis, and K. Sakaguchi (2011), Parameterization improvements and functional and structural advances in version 4 of the Community Land Model, *Journal of Advances in Modeling Earth Systems*, *3*(1).

Lawrence, D. M., A. G. Slater, V. E. Romanovsky, and D. J. Nicolsky (2008), Sensitivity of a model projection of near‐surface permafrost degradation to soil column depth and representation of soil organic matter, *Journal of Geophysical Research: Earth Surface*, *113*(F2).

Li, Q., S. Sun, and Q. Dai (2009a), The Numerical Scheme Development of a Simplified Frozen Soil Model, *Advances in Atmospheric Sciences*, *26*(5), 940-950, doi:10.1007/s00376-009-7174-z.

Li, Q., S. Sun, and Y. Xue (2010), Analyses and development of a hierarchy of frozen soil models for cold region study, *Journal of Geophysical Research-Atmospheres*, *115*, doi:10.1029/2009jd012530.

Li, X., X. Li, Z. Li, M. Ma, J. Wang, Q. Xiao, Q. Liu, T. Che, E. Chen, and G. Yan (2009b), Watershed allied telemetry experimental research, *Journal of Geophysical Research: Atmospheres (1984–2012)*, *114*(D22).

Liang, D., K. Tse, Y. Tan, L. Tsang, and K. H. Ding (2006), Scattering and Emission in Snow Based on QCA/DMRT and Numerical Maxwell Model of 3Dimentional Simulations (NMM3D), paper presented at 2006 IEEE MicroRad, IEEE.

Liang, D., X. Xu, L. Tsang, K. M. Andreadis, and E. G. Josberger (2008), The effects of layers in dry snow on its passive microwave emissions using dense media radiative transfer theory based on the quasicrystalline approximation (QCA/DMRT), *IEEE Transactions on Geoscience and Remote Sensing*, *46*(11), 3663-3671.

Liou, K.-n. (1974), Analytic two-stream and four-stream solutions for radiative transfer, *Journal of the Atmospheric Sciences*, *31*(5), 1473-1475.

Liou, Y.-A., and A. W. England (1996), Annual temperature and radiobrightness signatures for bare soils, *Geoscience and Remote Sensing, IEEE Transactions on*, *34*(4), 981-990.

Liu, G. (1998), A fast and accurate model for microwave radiance calculations, *Journal of the Meteorological Society of Japan*, *76*(2), 335-343.

Lu, H., T. Koike, H. Tsutsui, T. Graf, D. Kuria, H. Fujii, and M. Mourita (2006), A radiative transfer model for soil media with considering the volume effects of soil particles: Field observation and numerical simulation, paper presented at 2006 IEEE International Symposium on Geoscience and Remote Sensing, IEEE.

Luo, D., J. HuiJun, S. Marchenko, and V. Romanovsky (2014), Distribution and changes of active layer thickness (ALT) and soil temperature (TTOP) in the source area of the Yellow River using the GIPL model, *Science China Earth Sciences*, *57*(8), 1834-1845.

Luo, L. F., et al. (2003), Effects of frozen soil on soil temperature, spring infiltration, and runoff: Results from the PILPS 2(d) experiment at Valdai, Russia, *Journal of Hydrometeorology*, *4*(2), 334-351, doi:10.1175/1525-7541(2003)4<334:eofsos>2.0.co;2.

Mackay, J. R. (1997), A full-scale field experiment (1978-1995) on the growth of permafrost by means of lake drainage, western Arctic coast: a discussion of the method and some results, *Canadian Journal of Earth Sciences*, *34*(1), 17-33.

Nash, J. E., and J. V. Sutcliffe (1970), River flow forecasting through conceptual models part I—A discussion of principles, *Journal of hydrology*, *10*(3), 282-290.

Neluwala, G., Panduka (2015), High Resolution Soil Moisture Retrieval Using A Satellite-based Data Assimilation System, 80 pp, The University of Tokyo.

Nicolsky, D., V. Romanovsky, and G. Panteleev (2009), Estimation of soil thermal properties using in-situ temperature measurements in the active layer and permafrost, *Cold Regions Science and Technology*, *55*(1), 120-129.

Njoku, E., J. Schieldge, and A. B. Kahle (1980), Joint microwave and infrared studies for soil moisture determination.

O'Neill, K., and R. D. Miller (1985), Exploration of a rigid ice model of frost heave, *Water Resources Research*, *21*(3), 281-296.

Ono, Y., and T. Irino (2004), Southern migration of westerlies in the Northern Hemisphere PEP II transect during the Last Glacial Maximum, *Quaternary International*, *118*, 13-22.

Osterkamp, T., and V. Romanovsky (1999), Evidence for warming and thawing of discontinuous permafrost in Alaska, *Permafrost and Periglacial Processes*, *10*(1), 17-37.

Panda, S. K., S. S. Marchenko, and V. E. Romanovsky (2014), High-resolution permafrost modeling in Denali National Park and Preserve*Rep.*, Natural Resource Technical Report, National Park Service, Fort Collins, Colorado, 1–44, available at: https://irma. nps. gov/App/Reference/Profile/2208990.

Parry, M. L., O. F. Canziani, J. P. Palutikof, P. J. van der Linden, and C. E. Hanson (2007), IPCC, 2007: climate change 2007: impacts, adaptation and vulnerability. Contribution of working group II to the fourth assessment report of the intergovernmental panel on climate change, edited, Cambridge University Press, Cambridge.

Pennock, B. E., and H. P. Schwan (1969), Further observations on the electrical properties of hemoglobin-bound water, *The Journal of physical chemistry*, *73*(8), 2600-2610.

Peters-Lidard, C., E. Blackburn, X. Liang, and E. Wood (1998), The effect of soil thermal conductivity parameterization on surface energy fluxes and temperatures, *Journal of the Atmospheric Sciences*, *55*(7), 1209-1224.

Picard, G., L. Brucker, A. Roy, F. Dupont, M. Fily, A. Royer, and C. Harlow (2013), Simulation of the microwave emission of multi-layered snowpacks using the Dense Media Radiative transfer theory: the DMRT-ML model.

Pomeroy, J. W., D. M. Gray, T. Brown, N. R. Hedstrom, W. L. Quinton, R. J. Granger, and S. K. Carey (2007), The cold regions hydrological process representation and model: a platform for basing model structure on physical evidence, *Hydrological Processes*, *21*(19), 2650-2667, doi:10.1002/hyp.6787.

Poutou, E., G. Krinner, C. Genthon, and N. de Noblet-Ducoudré (2004), Role of soil freezing in future boreal climate change, *Climate Dynamics*, *23*(6), 621-639.

Qian, Y., Y. Zheng, Y. Zhang, and M. Miao (2003), Responses of China's summer monsoon climate to snow anomaly over the Tibetan Plateau, *International Journal of Climatology*, *23*(6), 593-613.

Rautiainen, K., J. Lemmetyinen, M. Schwank, A. Kontu, C. B. Ménard, C. Maetzler, M. Drusch, A. Wiesmann, J. Ikonen, and J. Pulliainen (2014), Detection of soil freezing from L-band passive microwave observations, *Remote Sensing of Environment*, *147*, 206-218.

Rautiainen, K., T. Parkkinen, J. Lemmetyinen, M. Schwank, A. Wiesmann, J. Ikonen, C. Derksen, S. Davydov, A. Davydova, and J. Boike (2016), SMOS prototype algorithm for detecting autumn soil freezing, *Remote Sensing of Environment*, *180*, 346-360.

Rigon, R., G. Bertoldi, and T. M. Over (2006), GEOtop: A distributed hydrological model with coupled water and energy budgets, *Journal of Hydrometeorology*, *7*(3), 371-388, doi:10.1175/jhm497.1.

Riseborough, D., N. Shiklomanov, B. Etzelmüller, S. Gruber, and S. Marchenko (2008), Recent advances in permafrost modelling, *Permafrost and Periglacial Processes*, *19*(2), 137-156.

Romanovsky, V., M. Burgess, S. Smith, K. Yoshikawa, and J. Brown (2002), Permafrost temperature records: indicators of climate change, *EOS, Transactions American Geophysical Union*, *83*(50), 589-594.

Romanovsky, V. E., S. L. Smith, and H. H. Christiansen (2010), Permafrost thermal state in the polar Northern Hemisphere during the international polar year 2007–2009: a synthesis, *Permafrost and Periglacial Processes*, *21*(2), 106-116.

Schaefer, K., H. Lantuit, V. Romanovsky, and E. Schuur (2012), Policy implications of warming permafrost.

Schuur, E. A., J. G. Vogel, K. G. Crummer, H. Lee, J. O. Sickman, and T. E. Osterkamp (2009), The effect of permafrost thaw on old carbon release and net carbon exchange from tundra, *Nature*, *459*(7246), 556-559.

Schwank, M., M. Stahli, H. Wydler, J. Leuenberger, C. Matzler, and H. Fluhler (2004), Microwave L-band emission of freezing soil, *IEEE Transactions on Geoscience and Remote Sensing*, *42*(6), 1252-1261.

Shrestha, M., L. Wang, T. Koike, Y. Xue, and Y. Hirabayashi (2012), Modeling the spatial distribution of snow cover in the Dudhkoshi region of the Nepal Himalayas, *Journal of Hydrometeorology*, *13*(1), 204-222.

Shur, Y., and M. Jorgenson (2007), Patterns of permafrost formation and degradation in relation to climate and ecosystems, *Permafrost and Periglacial Processes*, *18*(1), 7-19.

Sidorchuk, A., O. Borisova, and A. Panin (2001), Fluvial response to the Late Valdai/Holocene environmental change on the East European Plain, *Global and Planetary Change*, *28*(1), 303-318.

Smith, L. C., Y. Sheng, G. MacDonald, and L. Hinzman (2005a), Disappearing arctic lakes, *Science*, *308*(5727), 1429-1429.

Smith, N. V., S. S. Saatchi, and J. T. Randerson (2004), Trends in high northern latitude soil freeze and thaw cycles from 1988 to 2002, *Journal of Geophysical Research: Atmospheres*, *109*(D12).

Smith, S. L., M. M. Burgess, D. Riseborough, and F. Mark Nixon (2005b), Recent trends from Canadian permafrost thermal monitoring network sites, *Permafrost and Periglacial Processes*, *16*(1), 19-30.

Smith, S. L., J. Throop, A. G. Lewkowicz, and C. R. Burn (2012), Recent changes in climate and permafrost temperatures at forested and polar desert sites in northern Canada 1 1 This article is one of a series of papers published in this CJES Special Issue on the theme of Fundamental and applied research on permafrost in Canada, *Canadian Journal of Earth Sciences*, *49*(8), 914-924.

Stocker, T., D. Qin, G.-K. Plattner, M. Tignor, S. K. Allen, J. Boschung, A. Nauels, Y. Xia, V. Bex, and P. M. Midgley (2014), *Climate change 2013: The physical science basis*, Cambridge University Press Cambridge, UK, and New York.

Stocker‐Mittaz, C., M. Hoelzle, and W. Haeberli (2002), Modelling alpine permafrost distribution based on energy‐balance data: a first step, *Permafrost and Periglacial Processes*, *13*(4), 271-282.

Stogryn, D. E. (1971), Higher order interaction energies for systems of asymmetric molecules, *Molecular Physics*, *22*(1), 81-103.

Storey, H. C. (1955), Frozen soil and spring and winter floods, *Water. The Yearbook of Agriculture*, *1955*, 179-184.

Stähli, M., P. E. Jansson, and L. C. Lundin (1999), Soil moisture redistribution and infiltration in frozen sandy soils, *Water Resources Research*, *35*(1), 95-103.

Subcommittee, P. (1988), Glossary of permafrost and related ground-ice terms, *Associate Committee on Geotechnical Research, National Research Council of Canada, Ottawa*, 156.

SUN, S. (2005), *Physical, biochemical mechanism and paramerization of Land surface model*, 307 pp., meterology press, Beijing.

Taniguchi, K., and T. Koike (2007), Increasing atmospheric temperature in the upper troposphere and cumulus convection over the eastern part of the Tibetan Plateau in the pre-monsoon season of 2004, *気象集誌. 第2 輯*, *85*, 271-294.

Taniguchi, K., T. Tamura, T. Koike, K. Ueno, and X. Xu (2012), Atmospheric conditions and increasing temperature over the Tibetan Plateau during early spring and the pre-monsoon season in 2008, *気象集誌. 第2 輯*, *90*(0), 17-32.

Tikhonov, V. (1994), Model of complex dielectric constant of wet and frozen soil in the 1-40 GHz frequency range, paper presented at Geoscience and Remote Sensing Symposium, 1994. IGARSS'94. Surface and Atmospheric Remote Sensing: Technologies, Data Analysis and Interpretation., International, IEEE.

Tsang, L., C. T. Chen, A. T. Chang, J. Guo, and K. H. Ding (2000), Dense media radiative transfer theory based on quasicrystalline approximation with applications to passive microwave remote sensing of snow, *Radio Science*, *35*(3), 731-749.

Tsang, L., K. Ding, and B. Wen (1992), Dense media radiative transfer theory for dense discrete random media with particles of multiple sizes and permittivities, *Progress in Electromagnetic Research*, *6*(5), 181-225.

Tsang, L., D. Liang, X. Xu, and P. Xu (2008), Microwave emission from snowpacks: modeling the effects of volume scattering, surface scattering and layering, paper presented at Microwave Radiometry and Remote Sensing of the Environment, 2008. MICRORAD 2008, IEEE.

Tsutsui, H., and T. Koike (2012), Development of Snow Retrieval Algorithm Using AMSR-E for the BJ Ground-Based Station on Seasonally Frozen Ground at Low Altitude on the Tibetan Plateau, *気象集誌. 第2 輯*, *90*(0), 99-112.

Tsutsui, H., T. Koike, and T. Graf (2007), Development of a dry-snow satellite algorithm and validation at the CEOP Reference Site in Yakutsk, *気象集誌. 第2 輯*, *85*, 417-438.

Ulaby, F., R. Moore, and A. Fung (1986), Microwave remote sensing: Active and passive. Volume 3-From theory to applications.

Ulaby, F. T., R. K. Moore, and A. K. Fung (1982), Microwave Remote Sensing Active and Passive-Volume II: Radar Remote Sensing and Surface Scattering and Enission Theory.

Vafai, K., and S. Whitaker (1986), Simultaneous heat and mass transfer accompanied by phase change in porous insulation, *Journal of heat transfer*, *108*(1), 132-140.

Viterbo, P., A. Beljaars, J. F. Mahfouf, and J. Teixeira (1999), The representation of soil moisture freezing and its impact on the stable boundary layer, *Quarterly Journal of the Royal Meteorological Society*, *125*(559), 2401-2426.

Wang, J., T. Che, H. Li, and X. Hao (2008a), WATER:Dataset of automatic meteorological observations at the Dadongshu mountain pass snow observation station, edited by C. a. A. R. E. and and C. A. o. S. Engineering Research Institute, doi:10.3972/water973.0295.db.

Wang, J., H. Li, Y. Bai, L. , Zhe, Xin, and Bingjie (2008b), WATER: Dataset of intensive runoff

observations in the Binggou watershed foci experimental area, edited by C. a. A. R. E. and and C. A. o. S. Engineering Research Institute, doi:10.3972/water973.0164.db.

Wang, J. R., and T. J. Schmugge (1980), An empirical model for the complex dielectric permittivity of soils as a function of water content, *IEEE Transactions on Geoscience and Remote Sensing*(4), 288-295.

Wang, L., T. Koike, K. Yang, R. Jin, and H. Li (2010), Frozen soil parameterization in a distributed biosphere hydrological model, *Hydrology and Earth System Sciences*, *14*(3), 557-571.

Weng, F., Y. Han, P. van Delst, Q. Liu, and B. Yan (2005), JCSDA community radiative transfer model (CRTM), paper presented at Proc. 14th Int. ATOVS Study Conf.

Westermann, S., T. Østby, K. Gisnås, T. Schuler, and B. Etzelmüller (2015), A ground temperature map of the North Atlantic permafrost region based on remote sensing and reanalysis data, *The Cryosphere*, *9*(3), 1303-1319.

Williams, P. J., and M. W. Smith (1991), *The Frozen Earth: Fundamentals of Geocryology*, Cambridge University Press.

Woo, M.-K., and P. Steer (1979), Measurement of trace rainfall at a high arctic site, *Arctic*, 80-84.

Wu, Q., Y. Hou, H. Yun, and Y. Liu (2015), Changes in active-layer thickness and near-surface permafrost between 2002 and 2012 in alpine ecosystems, Qinghai–Xizang (Tibet) Plateau, China, *Global and Planetary Change*, *124*, 149-155.

Wu, Q., and T. Zhang (2010), Changes in active layer thickness over the Qinghai‐Tibetan Plateau from 1995 to 2007, *Journal of Geophysical Research: Atmospheres*, *115*(D9).

Wu, T.-W., and Z.-A. Qian (2003), The relation between the Tibetan winter snow and the Asian summer monsoon and rainfall: An observational investigation, *Journal of Climate*, *16*(12), 2038-2051.

Xu, X., J. Wang, and L. Zhang (2001), *physics of frozen soils*, 1 ed., 396 pp., science press.

Yang, D., T. Jiang, Y. Zhang, and E. Kang (1988), Analysis and Correction of Errors in Precipitation Measurement at the head of Urumqi, *Journal of Glaciology and Geocryology*, *10*(4), 384-400.

Yang, K., T. Koike, B. Ye, and L. Bastidas (2005), Inverse analysis of the role of soil vertical heterogeneity in controlling surface soil state and energy partition, *Journal of Geophysical Research: Atmospheres (1984–2012)*, *110*(D8).

Yang, Z., Z. Yang, F. Liang, and Q. Wang (1993), Permafrost hydrological processes in Binggou Basin of Qilian Mountains, *Journal of Glaciology and Geocryology 15*, 235-241.

YANG, Z.-p., Y. H. OU, M.-h. SONG, C.-p. ZHOU, W.-b. YANG, and X.-p. LIU (2010), Species diversity and above-ground biomass of alpine vegetation in permafrost region of Qinghai-Tibetan Plateau, *Chinese Journal of Ecology*, *29*(4), 617.

Yoshikawa, K., and L. D. Hinzman (2003), Shrinking thermokarst ponds and groundwater dynamics in discontinuous permafrost near Council, Alaska, *Permafrost and Periglacial Processes*, *14*(2), 151-160.

Zarba, R. L., E. Bouloutas, and M. Celia (1990), General mass-conservative numerical solution for the unsaturated flow equation, *Water Resources Research WRERAQ*, *26*(7), 1483-1496.

Zhang, L. (2010), Research advances in passive microwave remote sensing of freeze-thaw processes over complex landscapes, *Adv. Earth Sci*, *26*(10), 1023-1029.

Zhang, T., and R. Armstrong (2001), Soil freeze/thaw cycles over snow‐free land detected by passive microwave remote sensing, *Geophysical Research Letters*, *28*(5), 763-766.

Zhang, T., R. Armstrong, and J. Smith (2003a), Investigation of the near‐surface soil freeze‐thaw cycle in the contiguous United States: Algorithm development and validation, *Journal of Geophysical Research: Atmospheres*, *108*(D22).

Zhang, T., R. G. Barry, K. Knowles, J. Heginbottom, and J. Brown (1999), Statistics and characteristics of permafrost and ground‐ice distribution in the Northern Hemisphere 1, *Polar Geography*, *23*(2), 132-154.

Zhang, X., S. Sun, and Y. Xue (2007a), Development and testing of a frozen soil parameterization for cold region studies, *Journal of Hydrometeorology*, *8*(4), 690-701, doi:10.1175/jhm605.1.

Zhang, X., S. F. Sun, and Y. Xue (2007b), Development and testing of a frozen soil parameterization for cold region studies, *Journal of Hydrometeorology*, *8*(4), 690-701.

Zhang, Y., G. Cheng, X. Li, X. Han, L. Wang, H. Li, X. Chang, and G. N. Flerchinger (2013), Coupling of a simultaneous heat and water model with a distributed hydrological model and evaluation of the combined model in a cold region watershed, *Hydrological Processes, 27*(25), 3762-3776.

Zhang, Y., and S. H. Lu (2002), Development and validation of a simple frozen soil parameterization scheme used for climate model, *Advances in Atmospheric Sciences*, *19*(3), 513-527.

Zhang, Y., T. Ohata, K. Ersi, and Y. Tandong (2003b), Observation and estimation of evaporation from the ground surface of the cryosphere in eastern Asia, *Hydrological processes*, *17*(6), 1135-1147.

Zhang, Z., D. L. Kane, and L. D. Hinzman (2000), Development and application of a spatially-distributed Arctic hydrological and thermal process model (ARHYTHM), *Hydrological Processes*, *14*(6), 1017-+, doi:10.1002/(sici)1099-1085(20000430)14:6<1017::aid-hyp982>3.0.co;2-g.

Zhao, L., D. M. Gray, and D. H. Male (1997), Numerical analysis of simultaneous heat and mass transfer during infiltration into frozen ground, *Journal of Hydrology*, *200*(1), 345-363.

Zimov, S. A., E. A. Schuur, and F. S. Chapin III (2006), Permafrost and the global carbon budget, *Science(Washington)*, *312*(5780), 1612-1613.

Zuerndorfer, B., and A. W. England (1992), Radiobrightness decision criteria for freeze/thaw boundaries, *Geoscience and Remote Sensing, IEEE Transactions on*, *30*(1), 89-102.

玉川勝徳, 小池俊雄, L. Hui, Y. Kun, 萩野谷成徳, 石川裕彦, X. XiangDe, and W. Shihong (2009), 陸面データ同化手法を用いた Tibet Gaize における土壌水分と地表面フラックスの推定, 水工学論文集第 53 巻, edited, March.